Zoological Journal of the Linnean Society, 2026, **206**(**1**), zlaf064
https://doi.org/10.1093/zoolinnean/zlaf064

OXFORD

Original Article

Unveiling hidden species' diversity within Southern Ocean Iphimediidae (Crustacea: Amphipoda) through DNA and 3D-geometric morphometrics, with the description of 10 new species

Marie L. Verheye[1,2,3,*], Thierry Backeljau[4], Cédric d'Udekem d'Acoz[5], Bruno Frédérich[1], Anthony Herrel[6,7,8,9], Gilles Lepoint[2], Isa Schön[3]

[1]Laboratory of Evolutionary Ecology (LEE), UR FOCUS, University of Liège, 13 allée du six août, B-4000 Liège, Belgium
[2]Laboratory of Trophic and Isotope Ecology (LETIS), UR FOCUS, University of Liège, 13 allée du six août, B-4000 Liège, Belgium
[3]Operational Directorate Natural Environments, Royal Belgian Institute of Natural Sciences (RBINS), Rue Vautier 29, B-1000 Brussels, Belgium
[4]Operational Directorate Taxonomy and Phylogeny, Royal Belgian Institute of Natural Sciences (RBINS), Rue Vautier 29, B-1000 Brussels, Belgium
[5]Operational Directorate Scientific Heritage, Royal Belgian Institute of Natural Sciences (RBINS), Rue Vautier 29, B-1000 Brussels, Belgium
[6]Mécanismes Adaptatifs et Evolution, UMR 7179, Muséum national d'Histoire naturelle (MNHN), Rue Buffon 55, 75105 Paris, France
[7]Department of Biology, Evolutionary Morphology of Vertebrates, Ghent University, K.L. Ledeganckstraat 35, B-9000 Ghent, Belgium
[8]Functional Morphology Laboratory, Department of Biology, University of Antwerp, Universiteitsplein 1, B-2610 Antwerp, Belgium
[9]Naturhistorisches Museum Bern, Bernastrasse 15, 3005 Bern, Switzerland
LSID urn:lsid:zoobank.org:pub:603E0BB1-E63B-472C-93C8-AEF9889458C9

[*]Corresponding author. Laboratory of Evolutionary Ecology (LEE), UR FOCUS, University of Liège, 13 allée du six août, B-4000 Liège; Laboratory of Trophic and Isotope Ecology (LETIS), UR FOCUS, University of Liège, 13 allée du six août, B-4000 Liège, Belgium; Operational Directorate Natural Environments, Royal Belgian Institute of Natural Sciences (RBINS), Rue Vautier 29, B-1000 Brussels, Belgium. E-mail: mverheye@uliege.be

ABSTRACT

The Antarctic shelf benthos is threatened by climate-related environmental changes and anthropogenic stressors. A baseline knowledge of biodiversity and species' distribution ranges is essential for effective monitoring and conservation. Here, we integrate DNA-based species' delimitation methods with morphological analyses to explore species' diversity within Antarctic Iphimediidae. Our results reveal that 10 nominal species are complexes of multiple species, most of which can be distinguished by small but consistent morphological differences. We formally describe 10 of these new species: *Stegopanoploea brevidentata* sp. nov., *Maxilliphimedia acutilobata* sp. nov., *Maxilliphimedia oliveri* sp. nov., *Echiniphimedia spinosior* sp. nov., *Echiniphimedia maxima* sp. nov., *Iphimediella longidentata* sp. nov., *Iphimediella brachyodonta* sp. nov., *Iphimediella longilobata* sp. nov., *Labriphimedia adeliae* sp. nov., and *Labriphimedia anneninae* sp. nov.. Most previously recorded circum-Antarctic iphimediid species are found to consist of regionally distributed species. Furthermore, we apply 3D-geometric morphometrics on the *Gnathiphimedia sexdentata* complex to investigate whether 'cryptic' species can be differentiated by variation in continuous morphological traits. This method provides additional diagnostic characters for the morphological identification of two *G. sexdentata* clades. This integrative taxonomy study increases the number of nominal Antarctic iphimediid species from 39 to 49, with 14 additional putative species requiring further study for formal description.

Keywords: species delineation - taxonomy - morphometrics - molecular phylogeny - Antarctica - COI mtDNA - scanning electron microscopy

INTRODUCTION

As an isolated ocean at the end of the thermal continuum, the Southern Ocean hosts a highly endemic cold-adapted marine fauna (Peck *et al.* 2018). However, this unique biota is now challenged by climate-related changes, as some parts of the continent, particularly the Antarctic Peninsula and Scotia Arc, are among the fastest warming areas on Earth (Turner *et al.* 2009, Convey and Peck 2019). The anticipated consequences on the marine communities are as extensive as diverse, including loss or increased disturbance of habitats, decreased physiological performance in warmer waters, compromised calcium carbonate skeletal maintenance under ocean acidification, competition

Received 7 September 2024; revised 3 April 2025; accepted 7 May 2025

with invasive species, and cascading effects throughout the entire food webs (Trathan and Agnew 2010, Constable *et al.* 2014, Michel *et al.* 2019). In order to monitor and mitigate climate-induced changes in ecological interactions, migrations, distributions, and ecosystem stability, a baseline knowledge of Antarctic biodiversity and species' distributions is imperative (De Broyer *et al.* 2011). However, the actual number of marine Antarctic species is probably greatly underestimated (Gutt *et al.* 2004, De Broyer *et al.* 2011). Moreover, species' distribution ranges are often ill-defined owing to the opportunistic nature of Antarctic sampling (De Broyer *et al.* 2011). As a direct consequence, it is currently impossible to evaluate which and how many species are threatened or endangered by climate change (Griffiths 2010, Constable *et al.* 2014).

In this context, DNA barcoding offers a fast and powerful means to identify species and to provide preliminary estimates of biodiversity (Grant *et al.* 2011). A variety of approaches to delimitate and identify species-level entities based on single-locus genetic data have been developed—including the tree-based Poisson tree process (PTP; Zhang *et al.* 2013, Kapli *et al.* 2017) and general mixed Yule coalescent (GMYC; Pons *et al.* 2006, Fujisawa and Barraclough 2013), and the distance-based automatic barcode gap discovery (ABGD; Puillandre *et al.* 2012) methods—and are widely used in biodiversity assessments (e.g. Monaghan *et al.* 2009, Blanco-Bercial *et al.* 2014). To reduce the risk of errors in the interpretation of any single data type, DNA barcoding is often used in combination with other lines of evidence (e.g. geographical, ecological, behavioural, morphological, and other molecular data) in integrative taxonomic frameworks (Padial *et al.* 2010, Schlick-Steiner *et al.* 2010, Carstens *et al.* 2013). Notably, non-overlapping morphological character variation, as a proxy for reproductive isolation and independently evolving lineages, is commonly used in species' delineation (Wiens 2007, Zapata and Jiménez 2012). For some taxa, however, morphological characters that can be used to discriminate species are scarce or absent (Rannala and Yang 2020), as in the case of species complexes, i.e. sets of genetically distinct but morphologically identical or highly similar species. When the discovery of 'cryptic' species by DNA-based methods triggers closer scrutiny of morphological variation, previously overlooked interspecific differences can often be detected (Sáez and Lozano 2005, d'Udekem d'Acoz and Verheye 2017, Verheye and d'Udekem d'Acoz 2021). Still, in some cases, clear-cut discrete differences may be lacking and species might only differ by subtle variations in continuous traits, such as in the relative size or shape of particular structures (e.g. in amphipods: Riedlecker *et al.* 2009 , King and Leys 2011, Layeghi *et al.* 2022). As a consequence, the visual evaluation of differences between such morphologically very similar species can be ambiguous and subjective (Mutanen and Pretorius 2007). Geometric morphometrics, a method to quantify variation in anatomical shapes using Cartesian coordinates (i.e. landmarks; Adams *et al.* 2013), may offer an objective way to visualize shape differences and to evaluate the extent of interspecific versus intraspecific variation (Mutanen and Pretorius 2007, Ruane 2015).

Molecular and integrative studies uncovered numerous species complexes in Antarctic marine taxa, especially in benthic organisms with limited dispersal abilities (e.g. Linse *et al.* 2007, Mahon *et al.* 2008, Brandão *et al.* 2010, Brasier *et al.* 2016, Verheye *et al.* 2016, d'Udekem d'Acoz and Verheye 2017). Overlooked species' diversity is particularly common in benthic Antarctic peracarids, which are most species-rich in the Southern Ocean (Clarke and Johnston 2003, Held 2003, Raupach *et al.* 2007). Life-history traits, such as brooding lifestyle, sometimes associated with low adult mobility, may limit gene flow over large distances (De Broyer *et al.* 2003, Thatje 2012). For instance, while 22% of all benthic to benthopelagic amphipod species are currently recorded as circum-Antarctic (De Broyer and Jażdżewska 2014), most of the species that have been studied by DNA methods were shown to be complexes of locally restricted species (e.g. Lörz *et al.* 2009, Havermans *et al.* 2011, 2013, Verheye *et al.* 2016), while only a few were confirmed as true circum-Antarctic (e.g. Havermans *et al.* 2011, d'Udekem d'Acoz *et al.* 2018, Verheye and d'Udekem d'Acoz 2021).

With 39 described sub-Antarctic and Antarctic species in 11 genera, the amphipod family Iphimediidae is particularly well represented in the Southern Ocean (https://www.marinespecies.org/; accessed on 19.07.2024). These species typically inhabit the epibenthic assemblages of sessile suspension-feeders (De Broyer *et al.* 2001). Although the ecology of many iphimediid species remains unknown, the family mainly comprises specialized micropredatory browsers of sponges (Coleman 1989b, Dauby *et al.* 2001, Graeve *et al.* 2001, Nyssen *et al.* 2005, Amsler *et al.* 2009), bryozoans (Klages and Gutt 1990), cnidarians (Dauby *et al.* 2001), and holothurians (Nyssen *et al.* 2002). Iphimediids have an 'armoured morphology': acuminate coxae 2–4, a varying number of usually paired dorsal teeth on pereonites 5–7 and pleonites (in *Echiniphimedia,* the whole body is covered by spines), distal margin of peduncular articles 1–2 of antenna 1 with processes, bases of pereipods 5–7 often with posterior cusps or teeth, and epimeral plate 3 with two large posterior cusps. Characters of taxonomic value to discriminate iphimediid species often relate to this armoured morphology: species can be differentiated by the number, length, and/or shape of such teeth, processes, and cusps (Coleman 2007). Despite this wealth of taxonomic characters, several nominal iphimediid species may be complexes of similar species. For instance, *Gnathiphimedia sexdentata* (Schellenberg, 1926) was reported to have a circum-Antarctic distribution (Coleman 2007) and described as morphologically 'extremely variable' (Watling and Holman 1981) with respect to, for example, the length of the spines on the peduncular articles of antenna 1 (Walker 1907, Chevreux 1913, Watling and Holman 1981), coxa shapes (Barnard 1932, Nicholls 1938, De Broyer 1983), and the width of the head sinus (Watling and Holman 1981). A new species was described as *G. incerta* Bellan-Santini, 1972 but it was later argued that because of the overlap in morphology for nearly all characters, *G. incerta* could not be reliably distinguished from *G. sexdentata* other than by its shorter dorsal body processes (Watling and Holman 1981).

In the present study, we reconstructed a novel multigene phylogeny (*COI*, 28S, and *H3*) of the family Iphimediidae to (i) discuss the systematics of the family at genus-level and (ii) explore the species' diversity in Antarctic iphimediids. For the latter objective, we first applied a range of molecular species'

delimitation methods on the *COI* and 28S gene trees and genetic distances, and then screened the delimited putative species for morphological differences. Finally, we explored if morphometric tools could highlight variations that are difficult to detect by simple visual inspection within one suspected species complex (*G. sexdentata*). 3D-geometric morphometrics were applied on micro-CT scans to quantify the shape of selected anatomical traits of potential taxonomic value at the species-level. Exploratory methods were used to characterize patterns of morphological variation within and among clades and DNA-based putative species.

MATERIALS AND METHODS

Taxon sampling

We analysed 29 out of the 39 currently recognized Iphimediidae species from the Antarctic region (south of the Polar Front), along with one species labelled as 'sp. nov'., one sub-Antarctic species (*Iphimedia imparilabia*), one sub-Antarctic/Antarctic species (*Labriphimedia pulchridentata*), and six non-Antarctic iphimediids (out of 47 known species), for a total of 154 specimens. Nine out of the 13 genera are represented (https://www.marinespecies.org/, accessed on 27.03.2024; Supporting Information, Table S1).

Antarctic samples were collected during several expeditions of the R.V. *Polarstern*: ANT-XXIII/8 (2006-2007), ANT-XXIV/2 (2008), ANT-XXVII/3 (2011), and ANT-XXIX/3 (2013) in the Drake Passage, the Bransfield Strait, the eastern coast of the Antarctic Peninsula, and the eastern Weddell Sea. Additional specimens were sampled from the Adélie Coast on board of R.V. *Astrolabe* during the CEAMARC (2007-2009) and REVOLTA (2011-2013) expeditions. Specimens from the Ross Sea were collected during TAN0402 (2004) and TAN0802 (2008) expeditions of R.V. *Tangaroa*. Non-Antarctic specimens were collected during the SANTO (2006) expedition in Vanuatu, the KAVIENG (2014) expedition in Papua New Guinea, with the R.V. *Johan Ruud* in Norway (2002), and by opportunistic sampling in France (2014), Italy (2001), and South Africa (2012).

All specimens were preserved in 96%–100% pure ethanol for DNA analysis. Vouchers are deposited at the Royal Belgian Institute of Natural Sciences (RBINS, Brussels, Belgium), the Muséum national d'Histoire naturelle (MNHN, Paris, France), and the National Institute of Water and Atmospheric Research (NIWA, Wellington, New Zealand; Supporting Information, Table S1).

DNA sequencing

DNA was extracted from the pleopods and abdomen muscles using a NucleoSpin® Tissue kit (Macherey-Nagel) following the manufacturer's protocol for animal tissues. The DNA was eluted in 100 µL of sterile distilled H_2O (RNase free) and stored at –20°C. DNA concentrations were checked with a NanoDrop Spectrophotometer (ThermoFisher Scientific, Waltham, MA, USA).

Fragments of the mitochondrial cytochrome *c* oxidase subunit I (*COI*; ~550 base pairs), the nuclear 28S rDNA region (28S; ~1400 bp), and Histone 3 (*H3*; ~360 bp) genes were amplified by polymerase chain reaction (PCR). Amplifications were performed in a 25 µL reaction mix, which contained 0.15 µL Taq DNA Polymerase (5 U μL^{-1}; Qiagen, Antwerp, Belgium), 2.5 µL 10× CoralLoad PCR Buffer (Quiagen, Antwerp, Belgium), 2.5 µL dNTPs mix (250 µM of each), 11–16 µL RNase-free water, 1.25 µL of each primer (2 µM), and 1–6 µL of DNA extract (about 50–100 ng per reaction).

The *COI* fragment was amplified with the primers Cp-COIF3 (Pilar Cabezas *et al.* 2013) and COI2R (Otto and Wilson 2001). The thermal cycling protocol used for the *COI* amplification followed Pilar Cabezas *et al.* (2013), except that the annealing temperature was set at 51°C. The 28S fragment was amplified with the primers 28S-3311F (Witt *et al.* 2006) and 28R (Hou *et al.* 2007), modified as follows: 5′-GGGACTACCCGCTGAACTTAAGCAT-3′ and 5′-GTCTTTCGCCCCTATGCCCAACTG-3′. PCR amplification conditions for 28S consisted of an initial denaturation for 3 min at 94°C, followed by 40 cycles of denaturation at 94°C for 40 s, annealing at 45°C for 40 s, extension at 72°C for 90 s, and a final extension at 72°C for 10 min. The *H3* fragment was amplified using the primers HisH3f and HisH3r and conditions of Corrigan *et al.* (2014) but with the annealing temperature set to 48°C.

The size of the PCR products was checked on 1.2% agarose gel stained with SYBR Safe (ThermoFisher Scientific, Waltham, MA, USA). Prior to sequencing, PCR products were purified with Exonuclease I (20 U μL^{-1}) and FastAP Thermosensitive alkaline phosphatase (1 U μL^{-1}) (ThermoFisher Scientific, Waltham, MA, USA), following the manufacturer's protocol. Forward and reverse strands were sequenced with fluorescent-labelled dideoxynucleotide terminators (BigDye v.3.1; Applied Biosystems, Foster City, CA, USA) on an automated ABI 3130xl DNA analyser (Applied Biosystems, Foster City, CA, USA) using the PCR primers.

Phylogenetic analyses

Sequence chromatograms were manually checked, and forward and reverse sequence fragments were assembled with CODONCODE ALIGNER v.3.7.1 (CodonCode Corporation, available from http://www.codoncode.com/aligner/). All sequences are novel and have been deposited in GenBank (Supporting Information, Table S1).

28S sequences were aligned with MAFFT v.7 (Katoh and Standley 2013) (available from http://mafft.cbrc.jp/alignment/server/), using the structural alignment strategy Q-INS-i under default settings. As some regions of the 28S sequences were too divergent to be confidently aligned, the program ALISCORE v.2.0 (Misof and Misof 2009) was used to identify poorly aligned regions for removal with ALICUT v.2.3, prior to further analysis. Protein-coding genes *COI* and *H3* were aligned with CLUSTALW in MEGA6 (Tamura *et al.* 2013). To prevent inclusion of pseudogenes, amino acid translations of both fragments were checked for stop codons. The identity of sequences was confirmed by BLASTN searches (Chen *et al.* 2015) on NCBI (https://blast.ncbi.nlm.nih.gov/) to check for contamination.

The best-fit DNA substitution models were selected based on the Bayesian information criterion on the concatenated dataset, which was partitioned by gene and by codon position (for *COI* and *H3*) in PartitionFinder (Lanfear *et al.* 2012).

Preliminary phylogenetic trees were first constructed using Bayesian inference (BI) for the separate gene datasets in order to check for congruence between gene trees. A concatenated dataset including *COI*, 28S, and *H3* sequences was also assembled with SequenceMatrix (Vaidya *et al.* 2011) and both BI and maximum likelihood (ML) were used to reconstruct phylogenetic relationships from the concatenated dataset.

BI trees were reconstructed with MrBayes v.3.2 (Ronquist and Huelsenbeck 2003) in the CIPRES portal (Miller *et al.* 2010). BI analysis of all datasets included two runs of 10^7 generations. Trees were sampled every 1000 generations using four Markov chains, and default heating values. Convergence was assessed by the standard deviation of split-frequencies (<0.01) and by examining the trace plots of log-likelihood scores in TRACER 1.7 (Rambaut and Drummond 2018). The first 10% trees were discarded as burn-in, while the remaining trees were used to construct a 50% majority rule consensus tree and estimate posterior probabilities (PP). Nodes with PP ≥ 0.95 were considered as significantly supported.

ML trees of the concatenated dataset were constructed with GARLI v.2.0 (Zwickl 2006) in the CIPRES portal (Miller *et al.* 2010). For each dataset, 10 separate ML searches were run independently from different stepwise-reconstructed trees. The tree with the highest log-likelihood across runs was considered for further analyses. Confidence levels of branches were estimated by 1000 bootstrap replicates. Nodes with bootstrap values (BV) ≥70 were considered as well-supported.

We reconstructed an ultrametric tree with BEAST v.2.4, required to run the GMYC algorithm. Identical sequences (haplotypes) were pruned to a single copy before implementation, because zero-length terminal branches can influence likelihood estimations (Monaghan *et al.* 2009, Fujisawa and Barraclough 2013). The phylogenetic analysis was performed under a relaxed log-normal clock set to an evolutionary rate of 1.0 (i.e. no attempt to estimate divergence time) and a speciation Yule tree model, using a random starting tree. Analyses were run for 10^8 MCMC generations, sampled every 1000th generations, and the first 10% of the samples were discarded as burn-in. TRACER v1.7 (Rambaut and Drummond 2018) was used to check for minimum effective sample size (ESS) of 200 and to visually inspect stationarity and convergence by plotting likelihood values (Rambaut *et al.* 2018). The resulting trees were summarized into a target maximum clade credibility tree with TreeAnnotator v.1.8.0.

Species' delimitation

Methodology

Specimens were first identified to the morphologically most similar described species using the handbook of Coleman (2007). Based on the *COI* and 28S trees and genetic distances, the putative species status of well-supported clades was evaluated with three different species' delimitation methods (see below). However, the results suggested that the 28S gene evolves too slowly relative to the rate of speciation: 28S-based species delimitation methods lumped together morphologically well-defined and generally accepted species. We, therefore, did not rely on the 28S-based species' delimitation results, but rather used the nuclear data to confirm that there were no incongruences between the *COI* and 28S gene trees, caused by, e.g., introgression or incomplete lineage sorting (Funk and Omland 2003). Specimens were then re-examined with a (Leica M80) Stereo Zoom Microscope to determine if consistent morphological differences could be found between the putative species of a complex. To define a best-supported delimitation scheme, we identified splits that were congruent among all methods. As ABGD and bPTP/GMYC return different types of errors, a congruent split is most likely to be correct (Dellicour and Flot 2018). It has been shown by simulations that ABGD has a tendency to overlump, while tree-based methods (bPTP and GMYC) tend to oversplit (Dellicour and Flot 2018, Luo *et al.* 2018). Therefore, splits that were defined only by either ABGD or any or both tree-based methods (bPTP, GMYC) were not considered unless they were also supported by consistent morphological differences. We also did not take weakly supported splits (AIC-based support values or PP < 0.7) into account nor ABGD-delimited species that were not monophyletic in the concatenated tree. Lastly, we investigated whether the species delimited as such also exhibited distinct 28S haplotypes based on a haplotype network.

We followed a generalized lineage concept, defining species as separately evolving metapopulation lineages. The species' delimitation methods used here represent multiple lines of evidence (operational criteria) that are relevant to assess lineage separation, i.e. the different properties acquired during lineage divergence (e.g. proxies for reproductive isolation, morphological diagnosability, and monophyly; de Queiroz 2007). *COI* clades delimited as species through the methodology described above were regarded as 'putative species' and, when congruent with morphology, were formally described and named. The description format is concise, aiming at providing sufficient information for morphological identification, and substantiated by *COI* barcodes and 3D models of the type specimens.

DNA-based species' delimitation

We applied three different methods for species delimitations on the Antarctic iphimediid clade. First, we used the bPTP method (Zhang *et al.* 2013), which implements two independent classes of Poisson processes (for intra- and interspecific branching events). It assumes that the number of substitutions between species is significantly higher than the number of substitutions within species, resulting in two different classes of branch lengths. For each possible species' delimitation, the Poisson processes are fitted to the two branch length classes. In the Bayesian implementation, a Markov chain Monte Carlo (MCMC) sampler is used to produce posterior probabilities (PP) for these species' delimitations. A PP ≥ 0.95 was considered significant support for a particular species. The analyses were conducted on the web-server for bPTP (available at http://species.h-its.org/ptp/) using the maximum credibility BI topology with 500 000 generations, thinning set to 100 and burn-in at 10%.

Second, we used the GMYC (Pons *et al.* 2006, Fujisawa and Barraclough 2013) method, which models speciation via a pure birth process and within-species branching events as neutral coalescent processes. It identifies the transition points between inter- and intraspecific branching rates on a time-calibrated ultrametric tree by maximizing the likelihood score of the model. All lineages leading from the root to the transition point

are then considered as different species. The GMYC analysis was carried out in R v.3.0.1 using the SPLITS (Ezard *et al.* 2009) and APE (Paradis *et al.* 2004) packages under the single-threshold method and excluding the outgroup (Fujisawa and Barraclough 2013). The AIC-based support values were calculated for the delimited species to account for delineation uncertainty (Powell 2011) .

Lastly, the ABGD method (Puillandre *et al.* 2012) aims to identify the 'barcode gap' that separates intraspecific and interspecific genetic distances, even when the two distributions overlap. The pairwise genetic distances are first ranked from smallest to largest. A local slope function is computed for a given window size to detect peaks of slope values, the significantly highest peak being the barcoding gap. A primary partition is defined based on this barcoding gap. The procedure is then recursively repeated for each group of the primary partition to obtain secondary partitions until no further gaps can be detected (Puillandre *et al.* 2012). The analysis was performed on the ABGD webserver at https://bioinfo.mnhn.fr/abi/public/abgd/abgdold.html. Tamura-Nei+G distances were computed with MEGA6 (Tamura *et al.* 2013). The latter model was the best-fit for the *COI* dataset among the models available in MEGA, according to the results of the model selection analysis with JModelTest v.0.1.1 (GTR+G, gamma shape = 0.196). As the genus *Echiniphimedia* was lumped together as one putative species when ABGD was applied to the whole dataset, this genus was also analysed separately from the remaining iphimediid taxa. The parameters were set to default (X = 1.5, Pmin = 0.001, Pmax = 0.100, Steps = 10, Number of bins = 20). Results obtained using the recursive partition were examined, and only the putative species detected using the largest *P*-value (maximal prior intraspecific distance) were considered to limit oversplitting. ABGD was not performed on the 28S, as each putative species was represented by one or very few haplotypes and ABGD performs poorly when the number of sequences per species is too small (Puillandre *et al.* 2012). Additionally, a 28S haplotype network was reconstructed and examined to investigate whether the delimited species also exhibit distinct 28S haplotypes. PopART (popart.otago.ac.nz) was used to create a TCS statistical parsimony network (Clement *et al.* 2000) of the 28S gene fragment. Missing data can lead to misleading statistical parsimony networks (Joly *et al.* 2007). Therefore, sequences including too many ambiguous sites, and then the remaining positions of the alignment including ambiguous sites or gaps, were deleted before analysis.

Morphological analyses

Specimens from each species complex were immobilized in 15 and 50 mL polypropylene tubes using 4% agarose gel, and sequentially scanned by high resolution X-ray microcomputed tomography (micro-CT; see Supporting Information, Table S2). Specimens from RBINS and NIWA were scanned at RBINS using a RX EasyTom (RX Solutions, Chavanod, France; https://www.rx-solutions.com), and XRE UniTom (TESCAN, Kohoutovice, Czech Republic; https://www.tescan.com). Specimens from MNHN were scanned on the AST-RX platform of the MNHN (Garcia Sanz *et al.* 2013) in a Phoenix v|tome|x L240-180 (GE Sensing and Inspection Technologies, New York, USA, https://www.ge.com) using the microfocus X-ray tube (1 µm detail detectability). Voltage and amperage were adjusted depending on the specimen's size and density, within the ranges of 60–110 kV and 107–829 µA, resulting in a final voxel size of 5.7–30 µm. AVIZO v.8.1 (Thermo Scientific) was used to produce 3D-surface models of the habitus. Morphological analyses were performed on the habitus only, without any dissections.

When morphological differences were observed between putative species, additional specimens for which no molecular data were available were also examined to evaluate the extent of trait variation and the consistency of the inferred morphological differences across a larger number of specimens. Morphological analyses were performed on the 3D-model whenever a micro-CT scan was available. Otherwise, the specimen was examined under a Leica M80 Stereo Zoom Microscope. Within a species complex, the species that did not comply with the original description were labelled 'aff.' in reference to the most similar nominal species and numbered (material examined in Supporting Information, Table S2).

3D-geometric morphometrics of the *Gnathiphimedia sexdentata* complex

Selection of specimens

To explore if quantitative morphological methods are more powerful in detecting small variations than visual inspection under a stereomicroscope (to differentiate 'cryptic' species), we selected the *Gnathiphimedia sexdentata* complex as a case study. *Gnathiphimedia sexdentata* was selected because of its high morphological variability and taxonomic uncertainties (e.g. Nicholls 1938, Watling and Holman 1981), suggesting that it may include multiple species. A total of 43 specimens were investigated (Supporting Information, Table S3). Although no sexual dimorphism was previously reported in Iphimediidae (except in the width of the pereion; Barnard 1930), the possibility was reassessed by including both females and males in the dataset, when available. No ontogenetic allometry in the studied characters was previously reported (only in the width of the mandible incisor; Watling and Holman 1981). Most specimens identified as *G. sexdentata* in the current study were larger than 1.1 cm (as measured on the 3D models from the tip of the rostrum to the base of the telson; Asochakov 1994), the smallest size reported in the literature for mature and/or ovigerous females (Schellenberg 1926, Barnard 1932, Nicholls 1938, Ren and Huang 1991). There were only three smaller specimens (GNA-SEX-D, 0.79 cm; GNA-SEX-30, 1.05 cm; and GNA-SEX-C, 0.95 cm; see Supporting Information, Table S3), which are most likely subadults. *Gnathiphimedia* aff. *sexdentata* appears to reach a larger size (maximal size 2.85 cm) than what is known for *G. sexdentata*. All included specimens were females with fully developed oostegites, a feature typical for adult females, except for GNA-AFF-SEX-A (1.55 cm). As removing subadult specimens did not change the interpretation of results, they were kept in the final datasets (Supporting Information, Fig. S4).

Acquisition of shape data

Specimens of the *G. sexdentata* complex were scanned on RBINS and MNHN micro-CT scanning platforms (see Morphological analyses). Voltage and amperage were adjusted depending on the specimen's size and density, in the ranges of

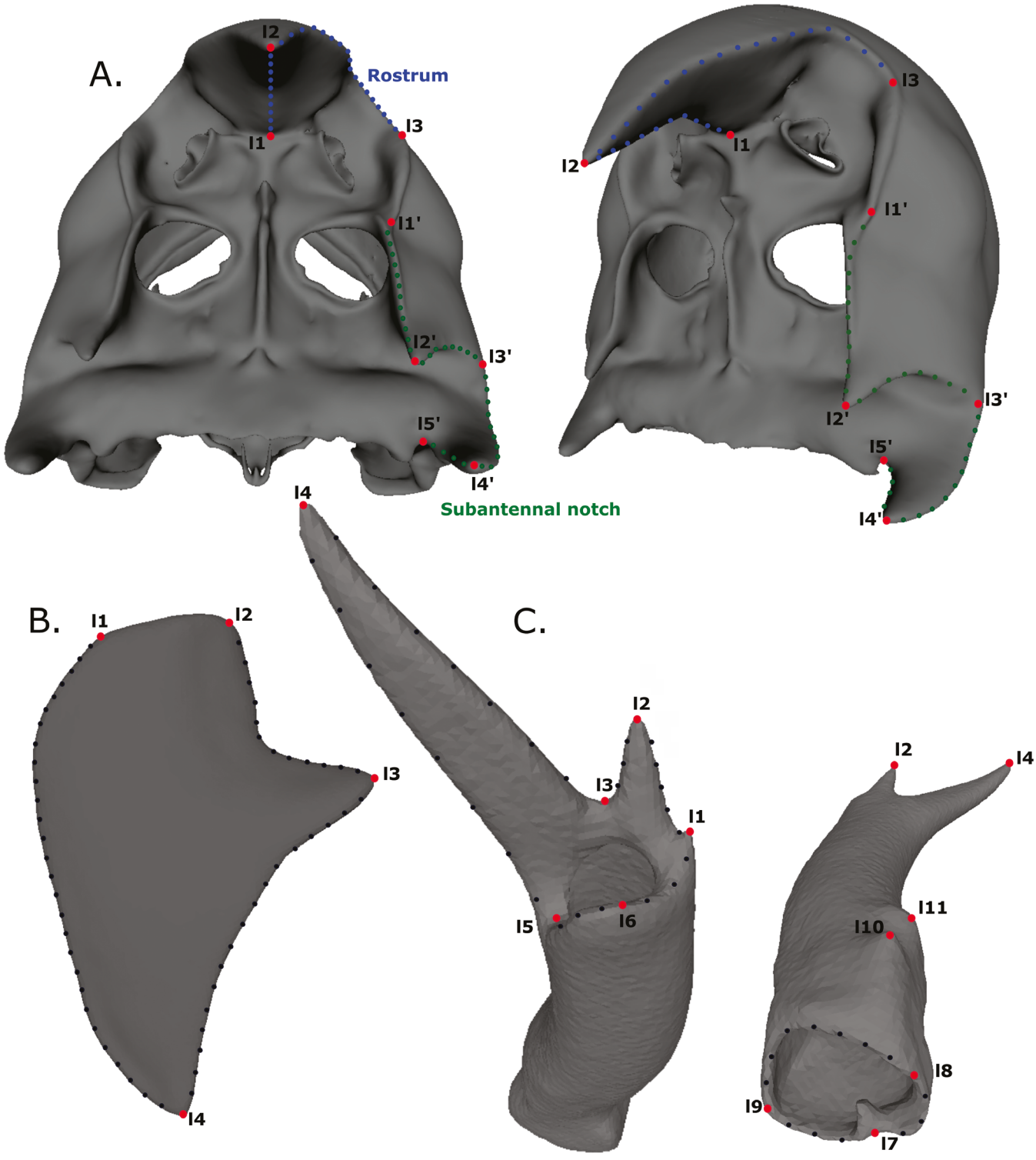

Figure 1. Landmarks (indicated by red dots and "l" followed by a number) and semilandmarks (in between landmarks, indicated by blue/green dots for the head and black dots for other structures) defining the outline of the (A) head, including rostrum and subantennal notch, (B) coxa 4, and (C) first article of the antenna 1 peduncle in *Gnathiphimedia sexdentata* complex.

60–130 kV and 107–829 µA and resulting in a final voxel size of 5.74–14 µm. AVIZO v.8.1 (Thermo Scientific) was used to segment and export 3D surface models of the following structures: (i) head, (ii) coxa 4, and (iii) first article of peduncle antenna 1. These structures were selected because they are variable within the *G. sexdentata* complex (Watling and Holman 1981, De Broyer 1983). Specimens with damage to these structures were discarded to avoid missing data.

Fixed homologous landmarks (LMs) were placed on each of these 3D models with LANDMARK EDITOR v.3.6 (UC Davis).

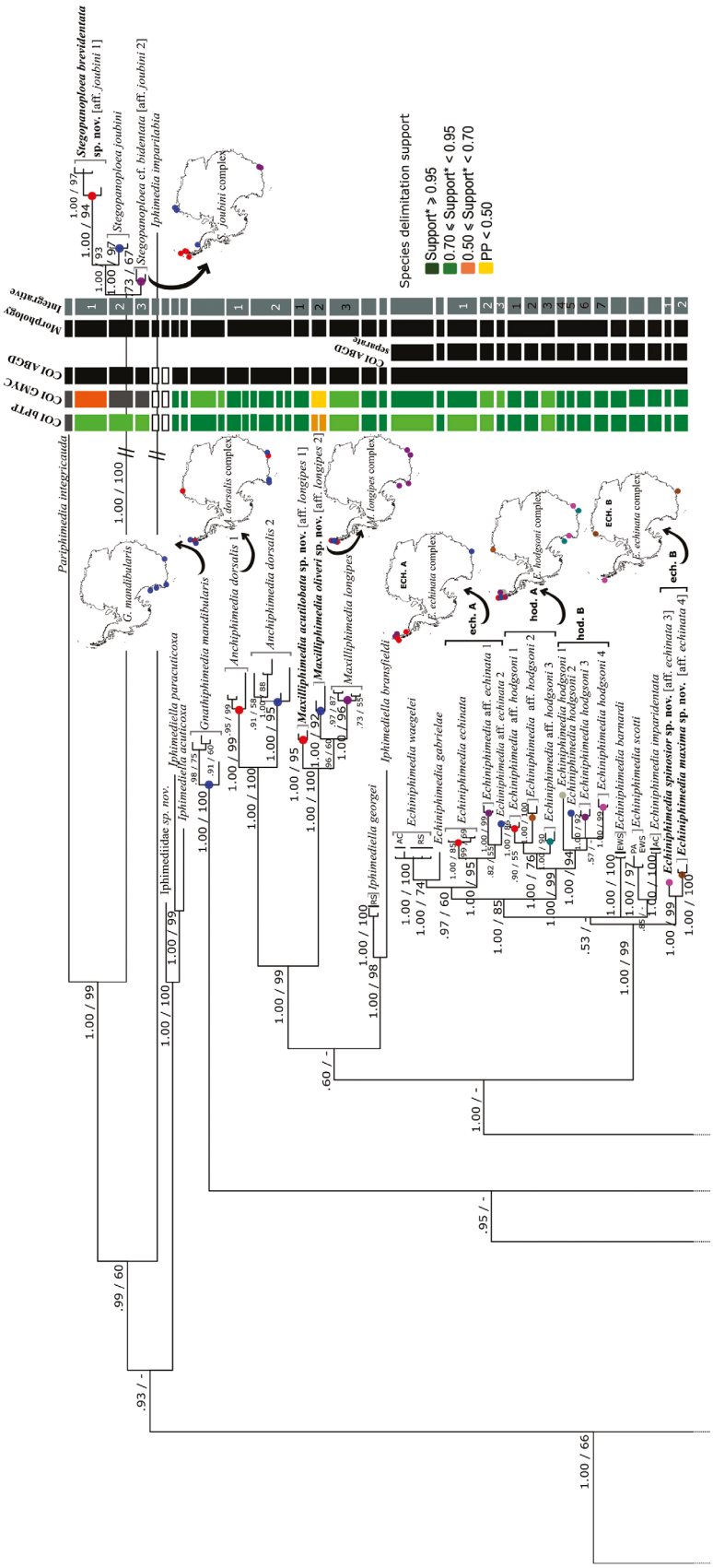

Figure 2. Phylogenetic tree obtained by Bayesian analysis of the concatenated *COI*, 28S, and *H3* sequences. Bayesian PP and BV (1000 replicates) from the ML analysis are indicated besides the nodes of interest. Bootstrap values below 50 are not shown. Geographical distributions of putative species are indicated with coloured dots on maps and corresponding nodes or with the abbreviations PA (Peninsula area), EWS (Eastern Weddell Sea), AC (Adélie Coast), RS (Ross Sea) and Bouv. (Bouvet Island). Species' delimitation results of the DNA-based methods applied separately on *COI* (bPTP, GMYC, and ABGD) and 28S (bPTP only) datasets are indicated besides the concatenated tree. *Boxes are coloured according to the posterior probability (bPTP) or the AIC-based GMYC support values (GMYC) of the inferred delimitation.

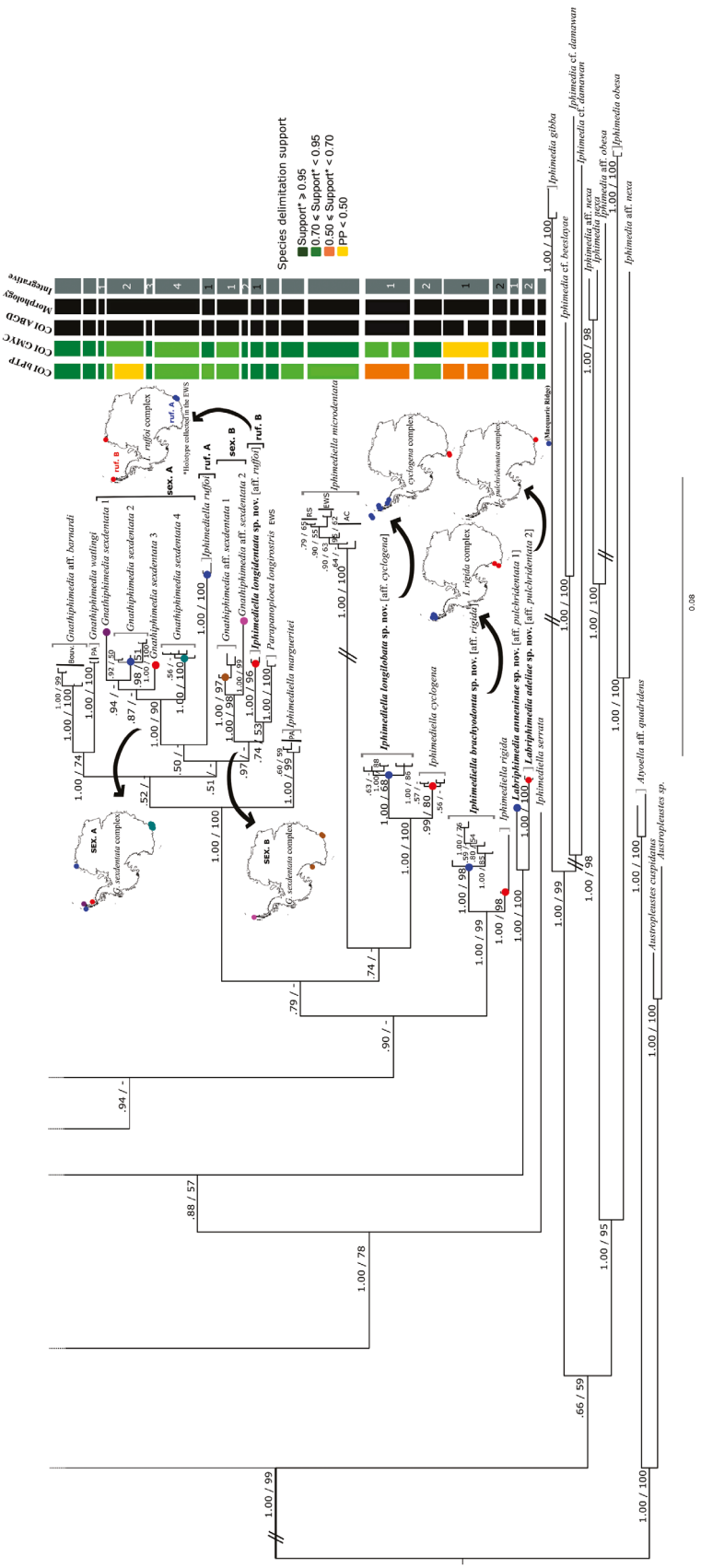

Figure 2. Continued

Table 1. Differences in morphological character states within the *Stegopanoploea joubini* complex. Between brackets are the links to the 3D-models.

***Stegopanoploea joubini* complex (Fig. 3)**	***Stegopanoploea joubini* (Chevreux 1912) [Model 1]**	***Stegopanoploea brevidentata* sp. nov. (*S.* aff. *joubini* 1) [Model 2]**	***Stegopanoploea* cf. *bidentata* (Nicholls 1938) (*S.* aff. *joubini* 2) [Model 3]**
1. Coxa 4 shape	Narrow : strongly excavate posteriorly	Broad : moderately excavate posteriorly	Narrow : strongly excavate posteriorly
2. Coxa 5 posterior process	Subequal to coxa 5 width, pointed	Shorter than coxa 5 width, pointed	Subequal to coxa 5 width, subdistally expanded
3. Postero-lateral process on epimeral plates 1-2	Long, reaching more than half of the following segment	Shorter, length variable but not reaching half of the following segment	Shorter, not reaching half of the following segment
4. Teeth on postero-ventral corner of pereonites 1-7	Strongly produced, on pereonites 5–7 projecting postero-laterally	Weakly produced, on pereonites 5–7 projecting posteriorly (alongside the body axis)	Weakly produced, on pereonites 5–7 projecting posteriorly (alongside the body axis)

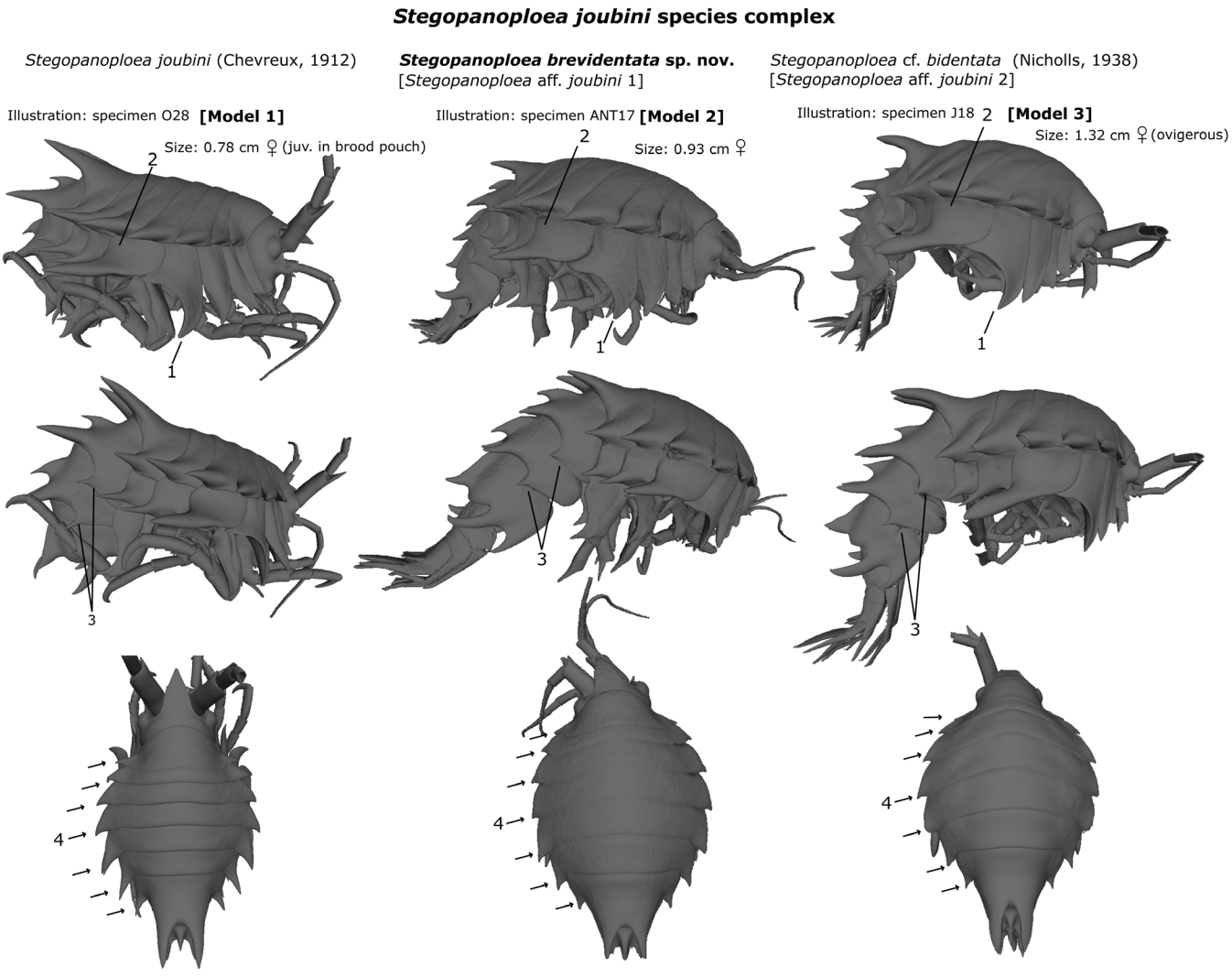

Figure 3. Plate illustrating morphological differences among species of the *Stegopanoploea joubini* complex.

Landmarks were selected at the junction of different structures (LM Type I; Bookstein 1991) and at points where homology is defined by geometry (e.g. the maximal curvature or the tip of a structure, Type II). Semi-landmarks (semi-LMs) were defined as initially very densely sampled curves constrained on each side by LMs, as recommended by Gunz *et al.* (2005).

Table 2. Differences in morphological character states within the *Maxilliphimedia longipes* complex. Between brackets are the links to the 3D models.

***Maxilliphimedia longipes* complex (Fig. 4)**	***Maxilliphimedia longipes* (Walker 1906) [Model 4]**	***Maxilliphimedia acutilobata* sp. nov. (*M.* aff. *longipes* 1) [Model 5]**	***Maxilliphimedia oliveri* sp. nov. (*M.* aff. *longipes* 2) [Model 6]**
1. Subantennal notch	Posterior lobe margins straight, small V-shaped notch between the two lobes	Posterior lobe margins straight, small V-shaped notch between the two lobes	Posterior lobe margins not straight: ventral margin sigmoid and proximally slightly concave, anterior margin slightly convex, narrow slit between the two lobes (the lobes are in contact with each other)
2. Coxa 7	Posterior margin forming a pointed right angle	Posterior margin forming a blunt right angle	Posterior margin forming a distinctly pointed acute (nearly right) angle
3. Dorsal tooth on pleonite 2	Reaching more than half of pleonite 3	Reaching about half of pleonite 3	Reaching about a third of pleonite 3
4. Postero-lateral process on epimeral plate 2	Pointed	Rounded	Rounded to slightly angular
5. Postero-ventral process on epimeral plate 3	Pointed tooth	Angular (acute angle), slightly crenulated ventro-distally	Pointed tooth
6. Shape of the telson lobes	Apically rounded	Apically pointed	Apically rounded

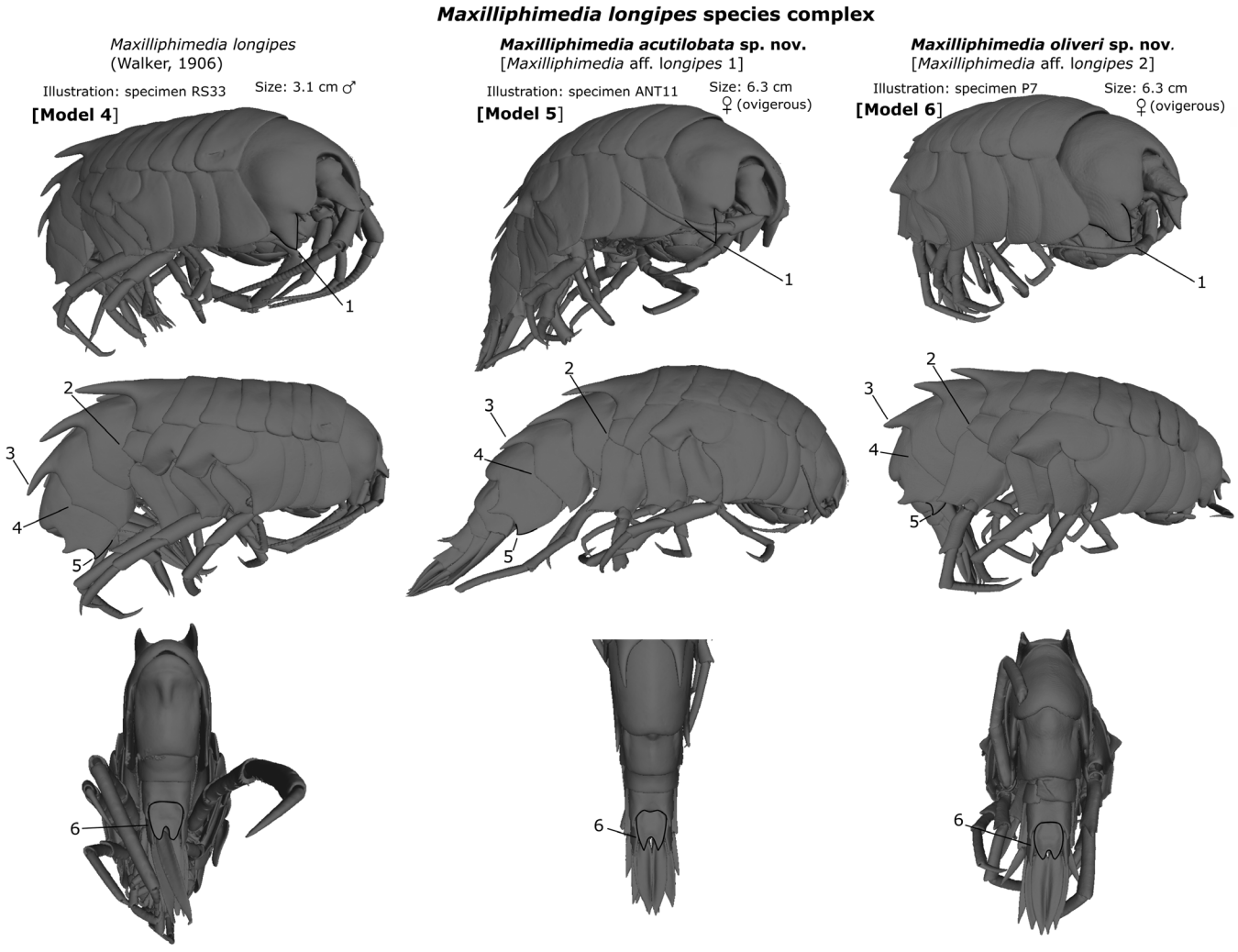

Figure 4. Plate illustrating morphological differences among species of the *Maxilliphimedia longipes* complex.

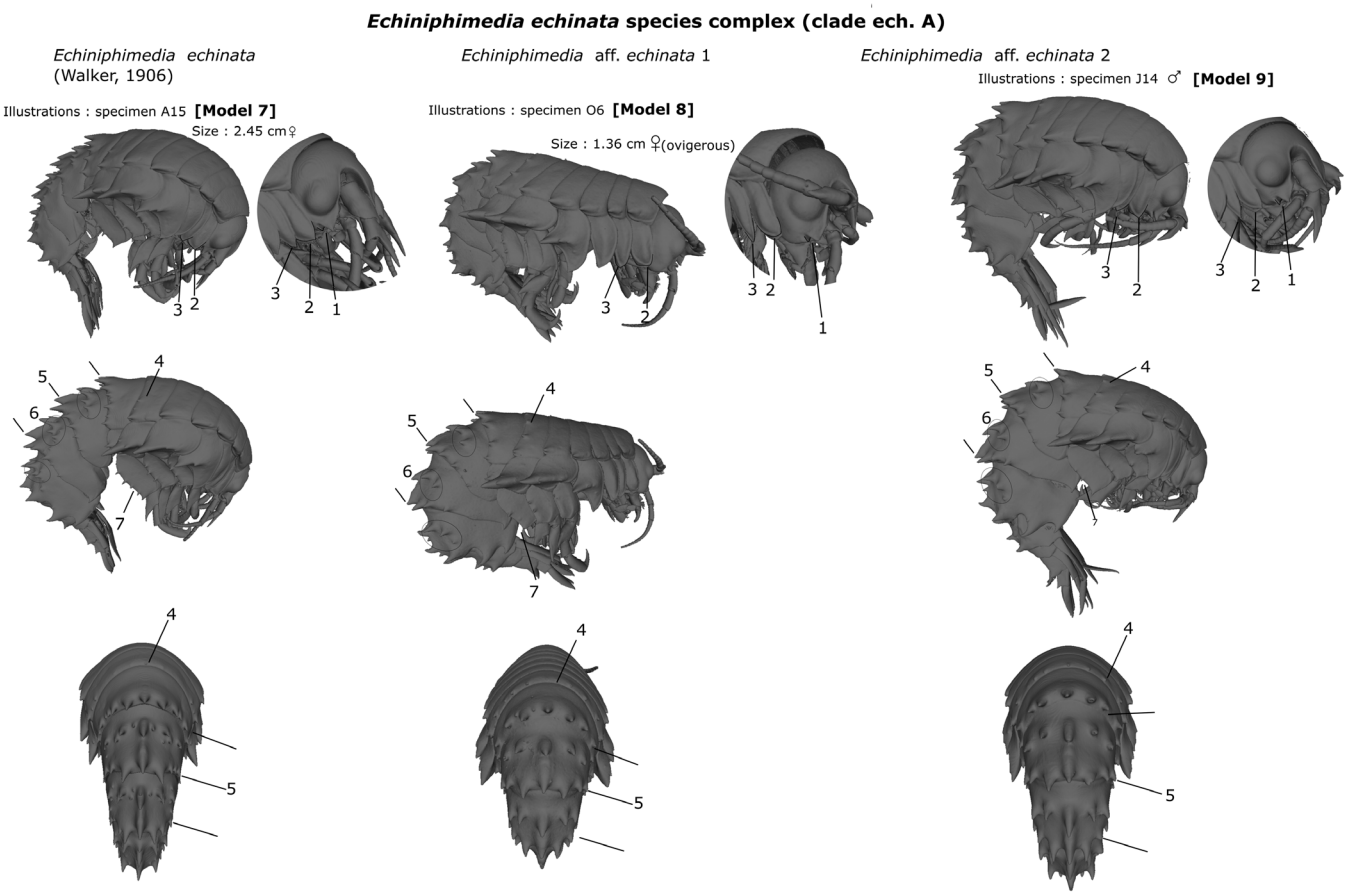

Figure 5. Plate illustrating morphological differences among species of the *Echiniphimedia echinata* complex, clade 'ech. A'.

Prior to sliding, semi-LMs were equidistantly resampled in R using the 'subsampl.inter' function of Botton-Divet *et al.* (2016). In order to transform these semi-LMs into geometrically homologous LMs, semi-LMs were slid along the tangent direction of curves on the surfaces of the meshes by minimizing bending energy, using the R function 'slider3D' [*Morpho*] (Schlager 2017).

To reduce redundancy (oversampling) on the configuration, the latter curves were subsequently downsampled based on a landmark sampling evaluation curve, which was obtained with the R function 'LaSEC' [*LaMBDA*] (Watanabe 2018). This function includes a generalized Procrustes' analysis (GPA; Rohlf and Slice 1990) performed on raw coordinates, followed by a principal component analysis (PCA). Then, three (semi-)LMs are randomly subsampled from the original dataset with subsequent GPA and PCA. By ordinary Procrustes' alignment, the distances between the subsampled coordinates and the corresponding coordinates in the parent data are minimized. The sum of the squared distances is then recorded as a measure of fit. By successively adding additional randomly sampled (semi-)LMs, the procedure is repeated until the entire set of (semi-)LMs in the parent dataset has been sampled. The number of semi-LMs required to accurately describe curve shapes was determined by visual examination of the LaSEC plot: when the fit trajectory reaches a plateau, it indicates that the fit is not improved by adding additional (semi-)LMs. Median fit values were calculated based on 500 iterations. The number of semi-LMs was adjusted to reach a median fit value of 0.99, then the sliding procedure was repeated on this new dataset.

A GPA was then performed in R using the function 'gpagen' [*geomorph*] (Adams and Otárola-Castillo 2013). GPA removes the effects of rotation, translation, and scaling to obtain new coordinates containing only information about the geometric shape of the set of landmarks.

In order to evaluate and mitigate measurement errors in the landmarking procedure, all datasets were digitized twice, and a Procrustes' ANOVA was performed using the function 'Procd. lm' [*geomorph*] to compare whether the mean squares (MS) values for each individual were lower than the error and calculated repeatability. The coordinates' mean between the two replicates was used for further analyses.

LMs and curves were collected only on the left side to avoid redundant information in bilaterally symmetric structures. When the left side was damaged, MESHLAB v.2016.12 was used to produce a mirror image of the structure, and LMs and curves were collected on the right side.

Rostrum: In total, the shape of the rostrum was measured on 34 specimens [3D models]. Three LMs and 79 semi-LMs were placed across the outline of the rostrum, further downsampled to 28 semi-LMs after examination of the LaSEC curve (Fig. 1A; Supporting Information, Table S5A).

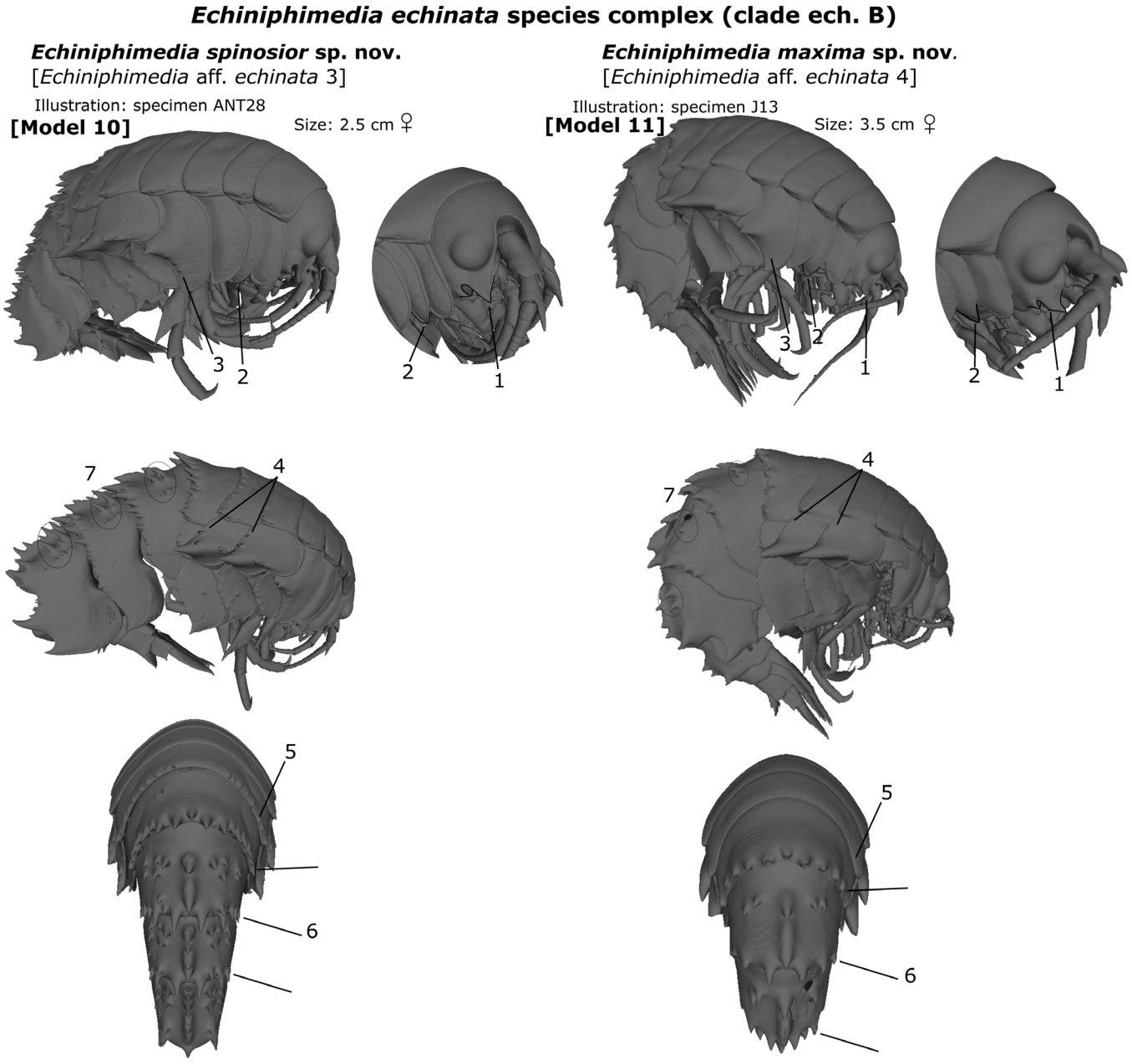

Figure 6. Plate illustrating morphological differences among species of the *Echiniphimedia echinata* complex, clade 'ech. B'.

Subantennal notch: In total, the shape of the subantennal notch was measured on 34 specimens [3D models]. Five LMs and 96 semi-LMs were placed across its outline, further downsampled to 34 semi-LMs after using LasEC (Fig. 1A; Supporting Information, Table S5B).

Coxa 4: The shape of the coxa 4 was measured on 37 specimens [3D models]. Four LMs and 170 semi-LMs were placed across the outline of the coxa 4, and downsampled to 58 semi-LMs (Fig. 1B; Supporting Information, Table S5C) with LasEC.

Antenna 1 peduncle article 1: The shape of the first article of the peduncle of antenna 1 was measured on 35 specimens [3D models]. Eleven LMs and 119 semi-LMs, downsampled to 38 after using LasEC, were placed on the latter structure (Fig. 1C; Supporting Information, Table S5D).

Analyses of shape data

Exploratory methods were employed to characterize patterns of shape variation across *a priori* defined morphospecies (see Morphological analysis), candidate species, and the two sexes.

A PCA on the Procrustes' shape coordinates was performed for each separate morphological dataset, using the variance–covariance matrices to derive a new set of dimensions that maximizes the amount of shape variance explained. The resulting principal components (PCs) were plotted and the distributions of shapes examined. To visualize shape changes

Table 3. Differences of morphological character state differences within the *Echiniphimedia echinata* complex, clade 'ech. A'. Between brackets are the links to the 3D models.

***Echiniphimedia echinata* complex—ech.A (Fig. 5)**	***Echiniphimedia echinata* (Walker 1906) [Model 7]**	***Echiniphimedia* aff. *echinata* 1 [Model 8]**	***Echiniphimedia* aff. *echinata* 2 [Model 9]**
1. Subantennal notch	Anterior lobe pointed, posterior lobe pointed, lobes of subequal length	Anterior lobe angular, posterior lobe rounded, lobes of subequal length	Anterior lobe pointed, posterior lobe pointed, lobes of subequal length
2. Coxa 1	Truncate, antero-ventral corner pointed	Truncate, antero-ventral corner rounded	Truncate, antero-ventral corner usually pointed
3. Coxa 2	Truncate	Truncate, antero-ventral corner rounded	Truncate, antero-ventral corner usually pointed
4. Spines on the posterior margin of pereon 6	9–13	10	7–9
5. Spines on on the posterior margin of pereon 7 and pleon 1–2	13–15	9–11	8–10 (usually 9)
6. Dorso-lateral teeth on pleonites 1–3* *not counting mid-dorsal spines nor spines on (or close to) the posterior margin	More than 5 antero-lateral spines on each side of the segments	2 antero-lateral spines on each side of pleonites 1–2, 2 antero-lateral longer spines on pleonite 3 (sometimes additional 1–3 tubercles)	2 antero-lateral spines on each side of pleonites 1–2, 2 antero-lateral longer spines on pleonite 3 (sometimes additional 1–3 tubercles)
7. Basis of pereiopod 5–7	Posterior margin with 4–7 cusps	Posterior margin with 2-3 cusps	Posterior margin with 2–3 cusps

Table 4. Differences of morphological character states within the *Echiniphimedia echinata* complex, 'clade ech. B'. Between brackets are the links to the 3D models.

***Echiniphimedia echinata* complex—ech.B (Fig. 6)**	***Echiniphimedia spinosior* sp. nov. (*E.* aff. *echinata* 3) [Model 10]**	***Echiniphimedia maxima* sp. nov. (*E.* aff. *echinata* 4) [Model 11]**
1. Subantennal notch	Anterior lobe produced ventrally and pointed, posterior rounded, anterior lobe twice as long or less than posterior.	Anterior lobe produced antero-ventrally and pointed, posterior rounded to slightly angular, anterior lobe more than twice longer than posterior.
2. Coxa 2	Antero-ventral corner rounded, postero-ventral angular	Pointed
3. Coxa 4	1–3 tubercules aligned vertically, below the posterior process	No tubercule below the posterior process
4. Coxa 5-6	1–3 small spines aligned vertically above the dorsal process	No spines above the dorsal process
5. Spines on the posterior margin of pereonite 6	Present, small 15–20	Absent
6. Spines on on the posterior margin of pereonite 7 and pleonite 1–2	15–20	9–13
7. Dorso-lateral teeth on pleonites 1–3* *not counting mid-dorsal spines nor spines on (or close to) the posterior margin	3–5 antero-lateral spines on each side of the segments (sometimes additional 1–3 tubercles)	2 antero-lateral spines on each side of the pleonites 1–2, 2 antero-lateral longer spines on pleonite 3 (sometimes additional 1 smaller)

along the two first PCs, the theoretical shape of the consensus of each GPA shape dataset was obtained by deforming a reference mesh through thin-plate splines into a mean mesh, using the R function 'tps3d' [*geomorph*]. The latter mean mesh was then deformed by the same method into the shapes at the minimum and maximum of the first two PCs. The R function 'deformGrid3d' [*geomorph*] was used to visualize differences between the mean shape and the shapes at the minimum and maximum of the two first PCs. The number of statistically significant principal components was estimated with the broken stick model (Jackson 1993). PCs variances with overlayed broken stick distributions were plotted in R using the functions 'screeplot' and 'bstick' [*vegan*].

In order to inspect the density patterns of the projection of specimens on pairs of PCs, we superimposed kernel density estimates on the PCA biplots. Kernel density estimation (KDE) is a non-parametric method for estimating the probability density function, using a smooth peak function called kernel to fit the observed data points (Parzen 1962). In this specific context, KDE is used to visually infer multiple density clusters, if multiple

Table 5. Differences in morphological character states within the *Echiniphimedia hodgsoni* complex. Between brackets are the links to the 3D models.

***Echiniphimedia hodgsoni* complex (Fig. 7)**	***Echiniphimedia hodgsoni* (clade hod.A) (Walker 1906) [Model 12]**	***Echiniphimedia* aff. *hodgsoni* (clade hod.B) [Model 13]**
1. Spine on the antero-dorsal side of the eye	Present	Absent
2. Coxa 1 and 2	Coxa 1 shorter than 2	Of subequal length
3. Armature over the whole body surface	Short and robust spines	Long and slender spines
4. Dorsal armature on urosomite 1	Usually 2 spines on each side postero-laterally, sometimes just one	2 spines on each side postero-laterally and 2 additional spines medially on the posterior margin, (sometimes additional spines above)
5. Dorsal armature on urosomite 2	1 spine on each side postero-laterally	1 spine on each side postero-laterally (sometimes with additional bud laterally) and 2 additional spines medially close to the posterior margin (sometimes additional spines in between)
6. Rami of uropod 3	As long as urosomite 2, 3 and telson combined	Longer than urosomite 2, 3 and telson combined

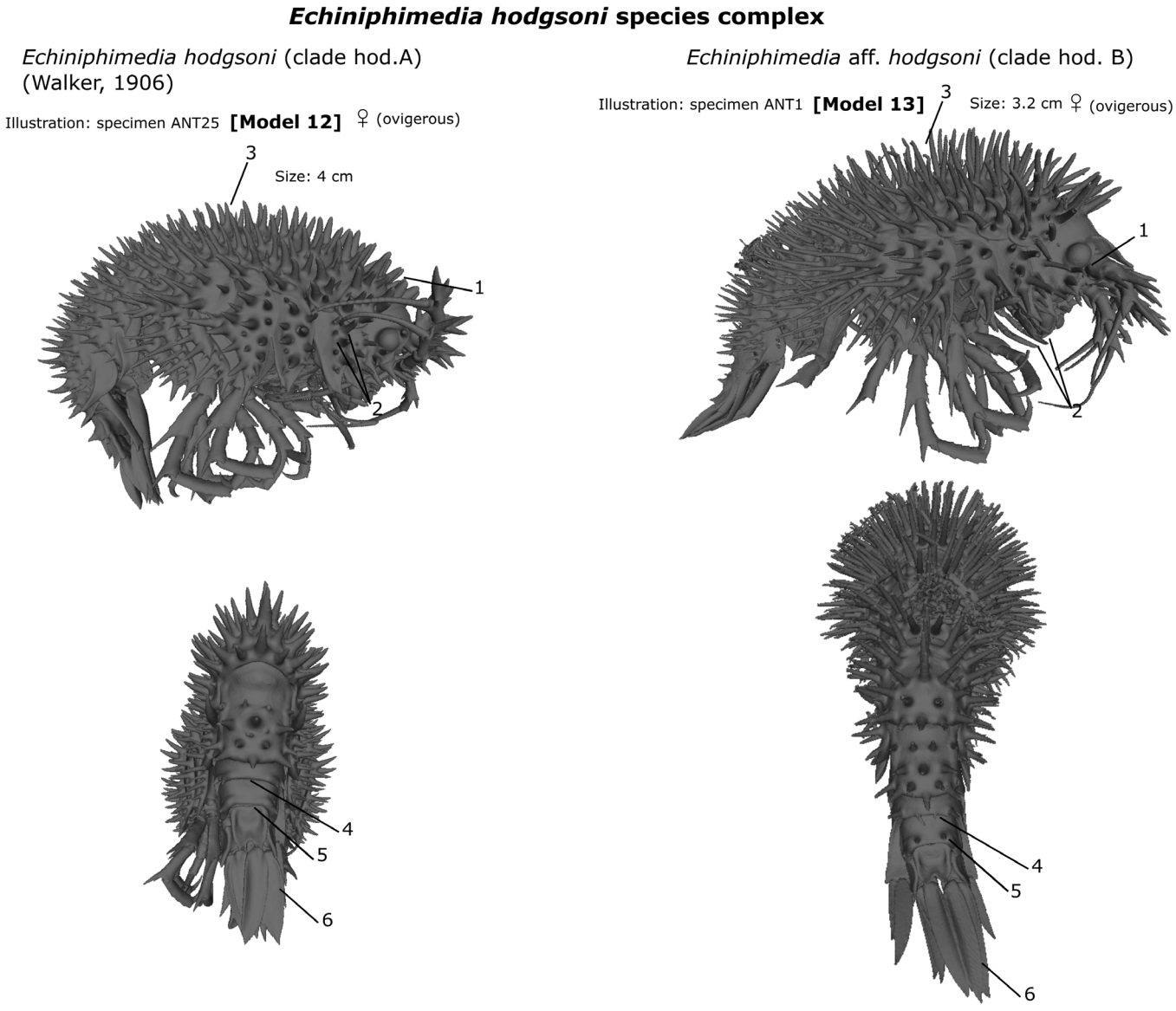

Figure 7. Plate illustrating morphological differences among species of the *Echiniphimedia hodgsoni* complex.

Table 6. Differences of morphological character states within the *Iphimediella ruffoi* complex. Between brackets are the links to the 3D models.

Iphimediella ruffoi **complex** (Fig. 8)	***Iphimediella ruffoi*** **Coleman 1996** [Model 14]	***Iphimediella longidentata* sp. nov.** **(*I.* aff. *ruffoi*)** [Model 15]
1. Subantennal notch	Inferior process twice longer than superior one	Inferior process 1/4th longer than superior one
2. Longer process of article 1 peduncle Antenna 1	Reaching end of 1st flagellar article	Reaching end of 4th flagellar article
3. Rostrum	As long as Antenna 1 peduncular article 1	Reaching about 2/3rd of Antenna 1 peduncular article 1
4. Coxa 1	Apex truncate and oblique anterodistally, with a small tooth on the posteroventral corner	Apex bifid, with two small teeth subequal in length
5. Coxa 5-7	Very small tooth posteroventrally, almost inconspicuous	Produced into a well-developed posteroventral tooth
6. Dorsal teeth on pereonite 7 and pleonites 1–2	Reaching end of following segment	Reaching well beyond end of following segment
7. Basis of pereiopod 7	Length about 1.2× width, posteroventral corner moderately produced	Length about 1.5× width, posteroventral corner strongly produced
8. Postero-lateral process on epimeral plate 2	Weak	Well-developed

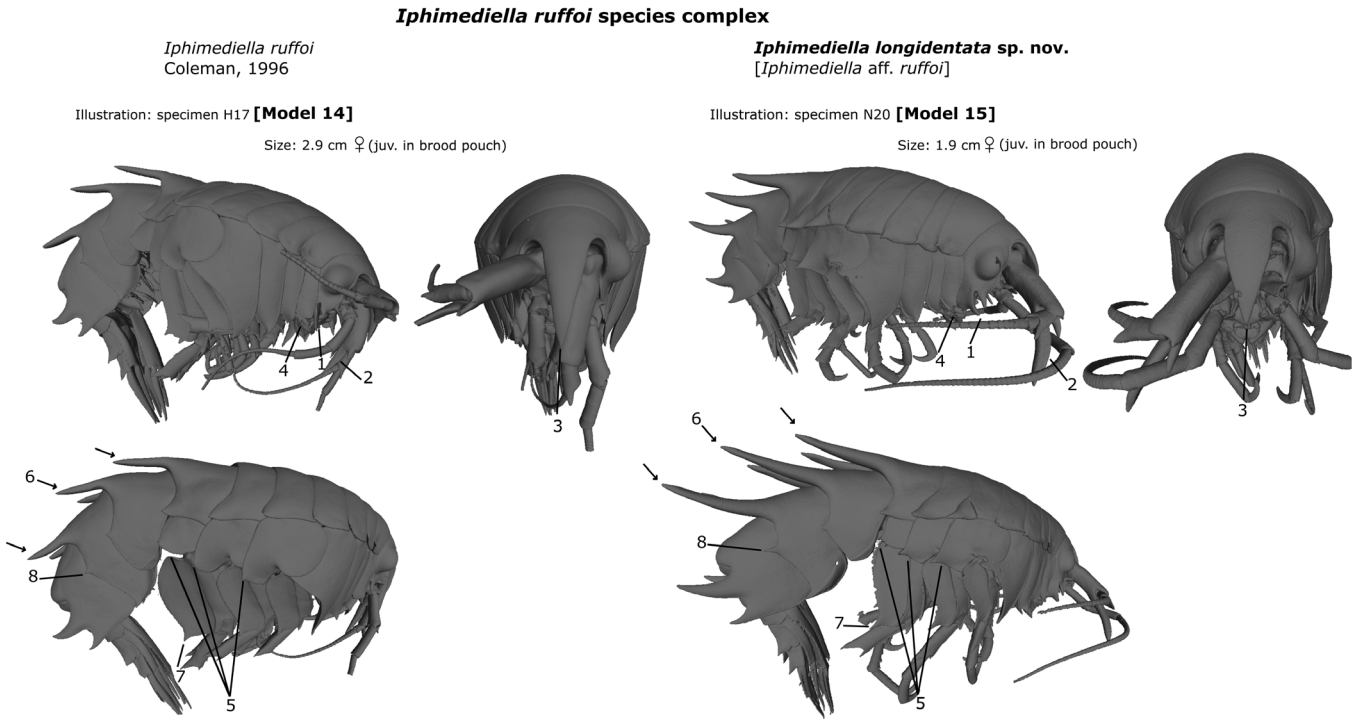

Figure 8. Plate illustrating morphological differences among species of the *Iphimediella ruffoi* complex.

groups are present in the data set. The KDE was generated in R using the KernSur function [*GenKern*], a Gaussian kernel and Sheather and Jones' (1991) plug-in method of bandwidth (smoothing parameter) selection.

We performed MANOVAs to test for differences in the three studied traits among a priori defined morphospecies (*G. sexdentata* and *G.* aff. *sexdentata*; see Morphological analyses) and sexes (within *G. sexdentata* only). We used the function procD.lm [*geomorph*] with 999 permutations to evaluate if the different factors have a significant effect on shape.

RESULTS

Data overview

The concatenated alignment of *COI*, 28S, and *H3* includes 2727 bp. The 28S gene fragment is 2196 bp long, and 1787 bp

after removal of poorly aligned regions, with 1033 variable sites. The best model of nucleotide substitution selected for 28S is SYM+G. The *COI* gene fragment is 584 bp long with 325 variable sites, and models selected for each codon position are as follows: SYM+I+G for the first, HKY+I+G for the second, and GTR+I+G for the third. The *H3* gene fragment is 356 bp long with 112 variable sites, and models selected for each codon position are as follows: HKY+I+G for the first, JC+I for the second, and GTR+G for the third.

Phylogenetic trees

For each dataset, topological discrepancies between the three gene trees only concern statistically unsupported nodes. Topological differences between the ML and BI trees are minimal and, in all cases, only found in unsupported nodes. The topologies of the BEAST ultrametric trees used as input for the GMYC analyses are the same as the topologies of the BI trees obtained with MrBayes, using the separate *COI* and 28S datasets.

The phylogeny based on the concatenated dataset (*COI*, 28S, and *H3*) is presented in Figure 2, while a detailed version of this phylogeny, including all individual names, is provided in the Supporting Information, Figure S6. The clade that includes all Antarctic iphimediid species and the two sub-Antarctic species is supported by both BI and ML analyses (PP = 1.00; BV = 78), although only six non-(sub-)Antarctic iphimediid species are included in the phylogeny. The clade including the latter non-(sub-)Antarctic iphimediids is not supported (PP = 0.66, BV = 59; Fig. 2).

The genera *Iphimediella* and *Gnathiphimedia* are polyphyletic. The genus *Iphimedia* [including mainly non-(sub)Antarctic species] is polyphyletic, as the only investigated sub-Antarctic species (*Iphimedia imparilabia*) is nested among Antarctic species of other genera. The remaining genera (*Echiniphimedia*, *Stegopanoploea*, *Labriphimedia*, *Pariphimedia*, *Anchiphimedia*, and *Maxilliphimedia*) are monophyletic or their monophyly could not be tested because they are only represented by a single species/species complex in the tree. The monophyly of most species/species complexes is supported, except for the species complexes *Gnathiphimedia sexdentata*, *Echiniphimedia echinata*, and *Iphimediella ruffoi* (Fig. 2).

Table 7. Differences in morphological character states within the *Iphimediella rigida* complex. Between brackets are the links to the 3D models.

Iphimediella rigida **complex** (Fig. 9)	***Iphimediella rigida*** Barnard 1930 [Model 16]	***Iphimediella brachyodonta*** **sp. nov.** (***I.*** **aff.** ***rigida***) [Model 17]
1. Dorsal teeth on pleonite 7 and pleonites 1–3	Reaching more than half of the following segment	Not reaching half of the following segment
2. Postero-lateral margin of epimeral plate 1	Produced into a small cusp (pointed)	Rounded to slightly angular (obtuse angle)
3. Postero-lateral margin of epimeral plate 2	Produced into a small cusp (pointed)	Angular (obtuse angle)

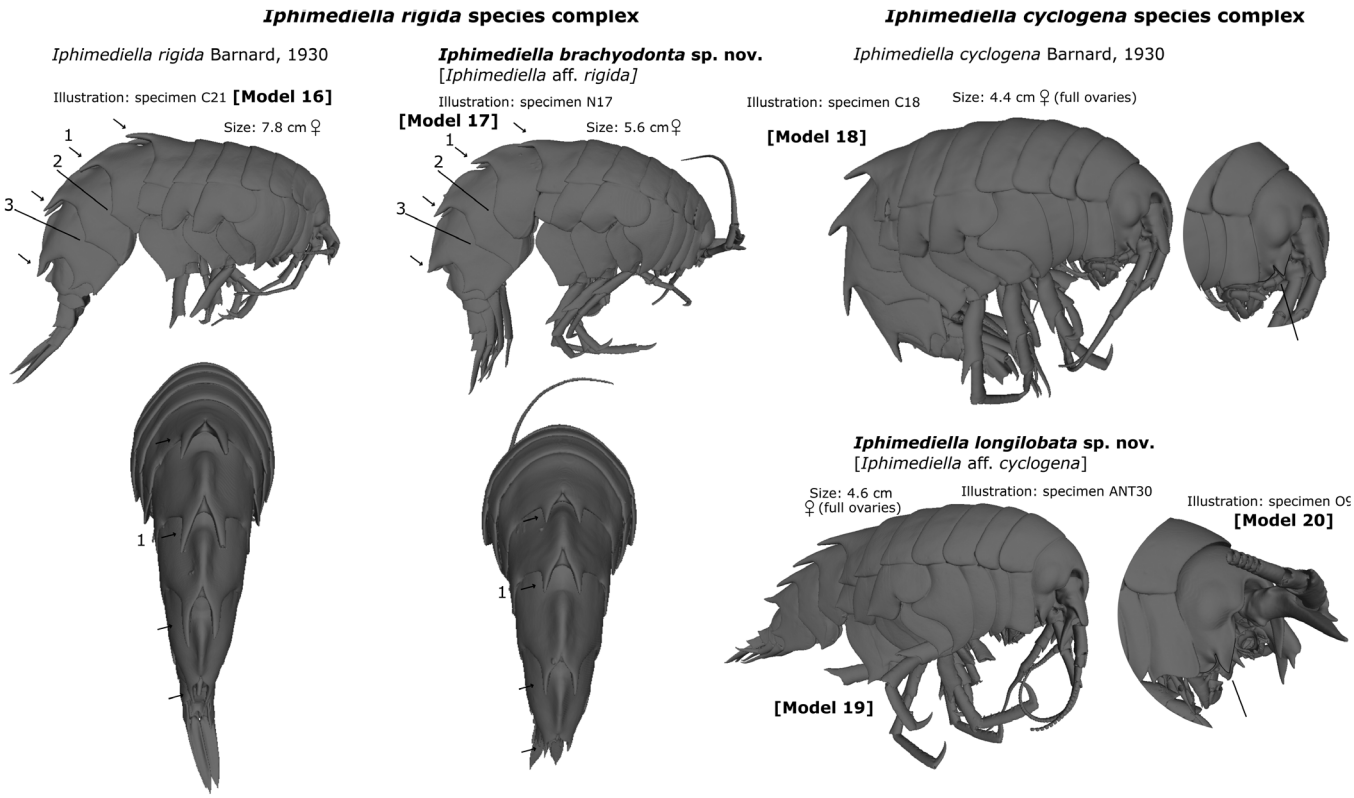

Figure 9. Plate illustrating morphological differences among species of the *Iphimediella rigida and Iphimediella cyclogena* complexes.

Table 8. Differences in morphological character states within the *Labriphimedia pulchridentata* complex. Between brackets are the links to the 3D models.

***Labriphimedia pulchridentata* complex (Fig. 10)**	***Labriphimedia pulchridentata* (Stebbing 1883) Based on Stebbing (1883, 1888) and Coleman (2007)**	***Labriphimedia adeliae* sp. nov. (*L.* aff. *pulchridentata* 1) [Model 21]**	***Labriphimedia anneninae* sp. nov. (*L.* aff. *pulchridentata* 2) [Model 22]**
1. Subantennal notch	Superior process much longer than broad	Superior process much longer than broad	Superior process as large as broad
2. 2d article of peduncle Antenna 1	Two processes of subequal length	Two processes of subequal length	Two processes, one much longer than the other
3. Coxa 1	Bifid, two lobes of similar width	Bifid, two lobes of similar width	Bifid, anterior lobe much broader than posterior one
4. Coxa 2-3	Bifid, strongly concave	Bifid, strongly concave	Bifid, moderately concave
5. Coxa 4	Very narrow and deeply concave posteriorly	Very narrow and deeply concave posteriorly	Broader and weakly concave posteriorly
6. Dorsal teeth on pereonite 5	Absent	Present	Absent
7. Dorsal teeth on pleonites 1–3	Low bidentate carinae	Long bidentate teeth	Low bidentate carinae
8. Teeth on postero-ventral corner of pereonites	On pereonites 1–7	On pereonites 1–7	On pereonites 6–7 only* *unknown for pereonite 5 as broken
9. Lateral processes on pleonite 1	3	3	2
10. Dorso-lateral process on pleonite 2	Long, reaches more than half of following segment	Long, reaches more than half of following segment	Short, does not reach half of the following segment

Species delimitation

The bPTP analysis of the *COI* Bayesian phylogeny suggests 59 putative species within the Antarctic iphimediid clade. The GMYC analysis of the *COI* ultrametric tree returns 60 ML entities (i.e. 'putative species', with a confidence interval of 56–66). The log-likelihood ratio test suggests that this model is a better fit for the data than the single-species' model (likelihood ratio = 32.79, $P = 7.5\ 10^{-8}$). Both methods are mostly congruent regarding the delimited putative species and incongruent delimitations are weakly supported by PP (bPTP) < 0.7. The ABGD method is more conservative in the number of delimited species with a total of 34 (Fig. 2). For example, the entire genus *Echiniphimedia* is lumped together as one putative species by ABGD. The bPTP analysis of the 28S Bayesian phylogeny returns only 20 putative species (as compared to the 59 putative species based on the *COI* tree). Generally accepted morphological species are lumped together by the bPTP analysis of the 28S tree, i.e. the genus *Echiniphimedia* and the clade *Gnathiphimedia–Iphimediella–Parapanoploea* (Supporting Information, Fig. S7). The GMYC analysis of the 28S ultrametric tree estimates 16 ML entities ('putative species'), with a very large confidence interval of 1–26. However, the log-likelihood ratio test suggests that this model is not a significantly better fit for the data than the single-species' model (likelihood ratio = 3.48, $P = .13$).

Stegopanoploea joubini complex

Three putative species were identified within the *Stegopanoploea joubini* complex by all methods of species delimitations. Different combinations of morphological character states are found for each of the three putative species, as well as distinct 28S haplotypes (Table 1; Fig. 3; material examined in the Supporting Information, Table S2A, Fig. S8). While *Stegopanoploea joubini* is distributed both in the Eastern Weddell Sea and the Peninsula area (Larsen B) in the current study, *S.* aff. *joubini* 1 is only found in the Peninsula area (Bransfield Strait and Joinville Island). *Stegopanoploea* aff. *joubini* 2 is only known from the Adélie Coast (Fig. 2).

Gnathiphimedia mandibularis

One (ABGD) to two (bPTP and GMYC) putative species are found within *Gnathiphimedia mandibularis*. No consistent morphological differences are observed across the two putative species. The geographic distribution of the two putative species is limited to the Ross Sea and the Adélie Coast, respectively (Fig. 2).

Anchiphimedia dorsalis complex

Two (ABGD) to six (bPTP and GMYC) putative species are found within the *Anchiphimedia dorsalis* complex. Nuclear 28S sequence data are only available for four of the six bPTP/GMYC-delimited species, which all show distinct haplotypes (Supporting Information, Fig. S8). No consistent morphological differences are observed across the delimited putative species. However, two colour morphs are observed on photographs (see Supporting Information, Table S2B), which could correspond to the two (ABGD) putative species, although additional photographs of more specimens are needed for confirmation. The two groups identified as putative species by the ABGD method (*A. dorsalis* 1 and 2, see Fig. 2) are geographically widespread and both are present at different localities of the Peninsula area (88 km apart), and the Adélie Coast (102 km apart). *Anchiphimedia dorsalis* 1 additionally occurs in the Eastern Weddell Sea and

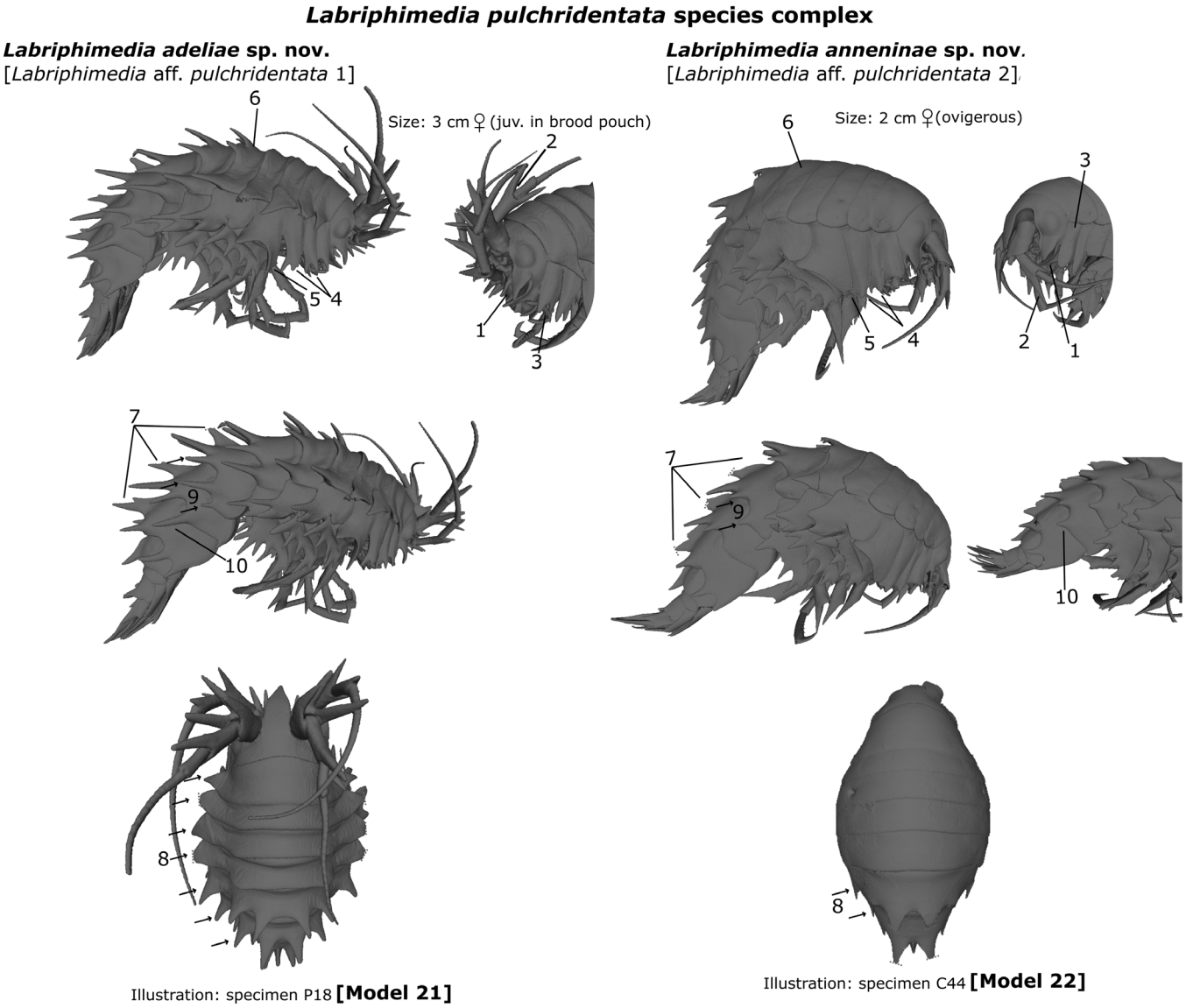

Figure 10. Plate illustrating morphological differences among species of the *Labriphimedia pulchridentata* complex.

A. dorsalis 2 in the Ross Sea. bPTP and GMYC further split *A. dorsalis* 1 into two additional putative species, one on both sides of the Weddell Sea, and the other one in the Adélie Coast. *Anchiphimedia dorsalis* 2 is further split by the latter methods into four putative species, two being found in close localities in the Ross Sea (48 km apart), one occurring at the Peninsula and one at the Adélie Coast (Fig. 2).

Maxilliphimedia longipes complex

Three (GMYC and ABGD) to four (bPTP) putative species are found within the *Maxilliphimedia longipes* complex. The additional splitting of *Maxilliphimedia* aff. *longipes* 2 into two putative species by bPTP is statistically poorly supported (PP < 0.7). Different combinations of morphological character states are found for each of the three (GMYC and ABGD) putative species, as well as distinct 28S haplotypes (Table 2; Figure 4; material examined in Supporting Information, Table S2C, Fig. S8). *Maxilliphimedia* aff. *longipes* 1 and 2 are found in close localities in the Peninsula area (40 km apart), while *M. longipes* is allopatric to its sister-species, found in the Ross Sea and the Adélie Coast (Fig. 2).

Echiniphimedia echinata complex

The *Echiniphimedia echinata* complex appears polyphyletic in the tree (Fig. 2), as clade 'ech. A' is part of a larger clade, including *E. waegelei*, *E. gabrielae*, and *E. hodgsoni* complex (PP = 1.00, BV = 85), but not clade 'ech. B'. Within clade 'ech. A', three putative species and within 'clade ech. B', two putative species are found by GMYC, bPTP, and ABGD (applied on the genus *Echiniphimedia*). The main morphological difference between clades 'ech. A' and 'ech. B' is in the shape of the subantennal notch: while the two lobes of the subantennal notch are of subequal length in all specimens of clade 'ech. A', the anterior lobe is much longer than the posterior in specimens of clade 'ech. B' (see Figures 5 and 6). Within clade 'ech. A', different combinations of morphological character states are found between the three putative species (Table 3 and Figure 5; material examined in Supporting Information, Table S2D). Two of those species

Table 9. Character state differences within the *Gnathiphimedia sexdentata* complex. Between brackets are the links

***Gnathiphimedia sexdentata* complex (Fig. 11)**	***Gnathiphimedia sexdentata* (Schellenberg 1926) [Model 23]**	***Gnathiphimedia* aff. *sexdentata* (Model 24, 25)**
1. Size	Adult specimens <2 cm (max. size observed = 1.8 cm)	Adult specimens >2 cm (max. size observed = 2.6 cm)
1. Subantennal notch	Wide, posterior process curved, directed antero-ventrally	Very wide, posterior process straight on most of its length (sometimes slightly curved distally), directed ventrally
2. Coxa 1 and 2	Bifid	Pointed
3. Postero-lateral margin of epimeral plates 1 and 2	Angular or bearing a very small cusp to rounded	Distinctively pointed
4. Postero-ventral corner basis pereopods 5–7	Produced into a very small cusp	Produced into a tooth
5. Postero-ventral corner of pereonites	Produced into a small cusp, sometimes inconspicuous 5–7 slightly produced posteriorly	Produced laterally into a pointed tooth, longer in pereonites 5–7 and directed postero-laterally

(*Echiniphimedia echinata* and *E.* aff. *echinata* 1), for which we have 28S sequence data, show distinct haplotypes (Supporting Information, Fig. S8). The latter two species are sampled in close proximity in the Peninsula area (58 km apart), while *E.* aff. *echinata* 2 is only found at the Adélie Coast (Fig. 2).

Within clade 'ech. B', several differences in morphological character states are observed between the two putative species, which also show distinct 28S haplotypes (Table 4 and Figure 6; material examined in Supporting Information, Table S2E, Fig. S8). These putative species appear to be allopatric, as *E.* aff. *echinata* 3 was collected west of the South Shetland Islands in the Peninsula area and *E.* aff. *echinata* 4 both in the Eastern Weddell Sea and the Adélie Coast (Fig. 2).

Echiniphimedia hodgsoni complex

Seven putative species are observed within the *Echiniphimedia hodgsoni* complex with GMYC and bPTP, and six with ABGD (applied on the genus *Echiniphimedia*). However, no consistent morphological differences can be detected among these delimited putative species. Two larger clades, 'hod. A' and 'hod. B' (Fig. 2), show consistent differences in morphological character states and distinct 28S haplotypes (Table 5; Figure 7 ; material examined in Supporting Information, Table S2F, Fig. S8). The three putative species within 'hod. A' are allopatrically sampled, viz. in the Peninsula area, in the Eastern Weddell Sea and the Adélie Coast and in the Ross Sea. Within 'hod. B', three of the four putative species (GMYC and bPTP) are collected from closely located stations at the tip of the Peninsula area (the closest ones being 42 km apart). The fourth putative species is allopatric to the others, and found at the Adélie Coast and in the Ross Sea (Fig. 2).

Iphimediella ruffoi complex

The *Iphimediella ruffoi* complex is polyphyletic in the BI tree, as clade 'ruf. B' is nested within a larger, well-supported clade (PP = 0.97, BV < 50) including *Gnathiphimedia* aff. *sexdentata* and *Parapanoploea longirostris* but excluding clade 'ruf. A' from the same species complex. The clades 'ruf. A' and 'ruf. B' are identified as putative species by all species delimitation methods. Details of morphological differences between these two putative species are shown in Table 6 (Fig. 8; material examined in Supporting Information, Table S2G). The specimens identified as *I. ruffoi* (ruf. A) are collected on the Adélie Coast (noting that the type specimen of *I. ruffoi* originated from the Eastern Weddell Sea; Coleman 1996) , whereas *I.* aff. *ruffoi* (ruf. B) is found on both sides of the Weddell Sea (Fig. 2).

Iphimediella rigida complex

Two (GMYC) to three (bPTP and ABGD) putative species are detected within the *Iphimediella rigida* complex. However, the monophyly of the two putative species identified by bPTP and ABGD within *I.* aff. *rigida* is not supported in the *COI* phylogeny (not shown), and they did not form well-supported clades in the trees based on *COI*, 28S, and *H3* (Fig. 2). Differences in morphological character states are found between the two GMYC-delimited putative species, as well as distinct 28S haplotypes (Table 7 and Figure 9; material examined in Supporting Information, Table S2H, Fig. S8). The latter two delimited species, *Iphimediella rigida* and *I.* aff. *rigida*, appear to be allopatric, the first being distributed at the tip of the Peninsula area and the latter, on the eastern side of the Ross Sea (Fig. 2).

Iphimediella cyclogena complex

Two (bPTP and ABGD) to three (GMYC) putative species are found within *I. cyclogena*. One consistent morphological difference in the shape of the subantennal notch is observed between the two putative species identified by bPTP and ABGD: In *I. cyclogena* [Model 18], the anterior lobe is pointed and shorter than the posterior lobe. In *I.* aff. *cyclogena* (***I. longilobata* sp. nov.**; Models 19, 20), the anterior lobe is rounded to bluntly pointed and is as long as or slightly longer than the posterior lobe (Fig. 9; material examined in Supporting Information, Table S2I). These two sister-species appear to be allopatric. *Iphimediella cyclogena* is found on the eastern side of the Ross Sea, whereas *I.* aff. *cyclogena* is collected at both sides of the Weddell Sea (Fig. 2).

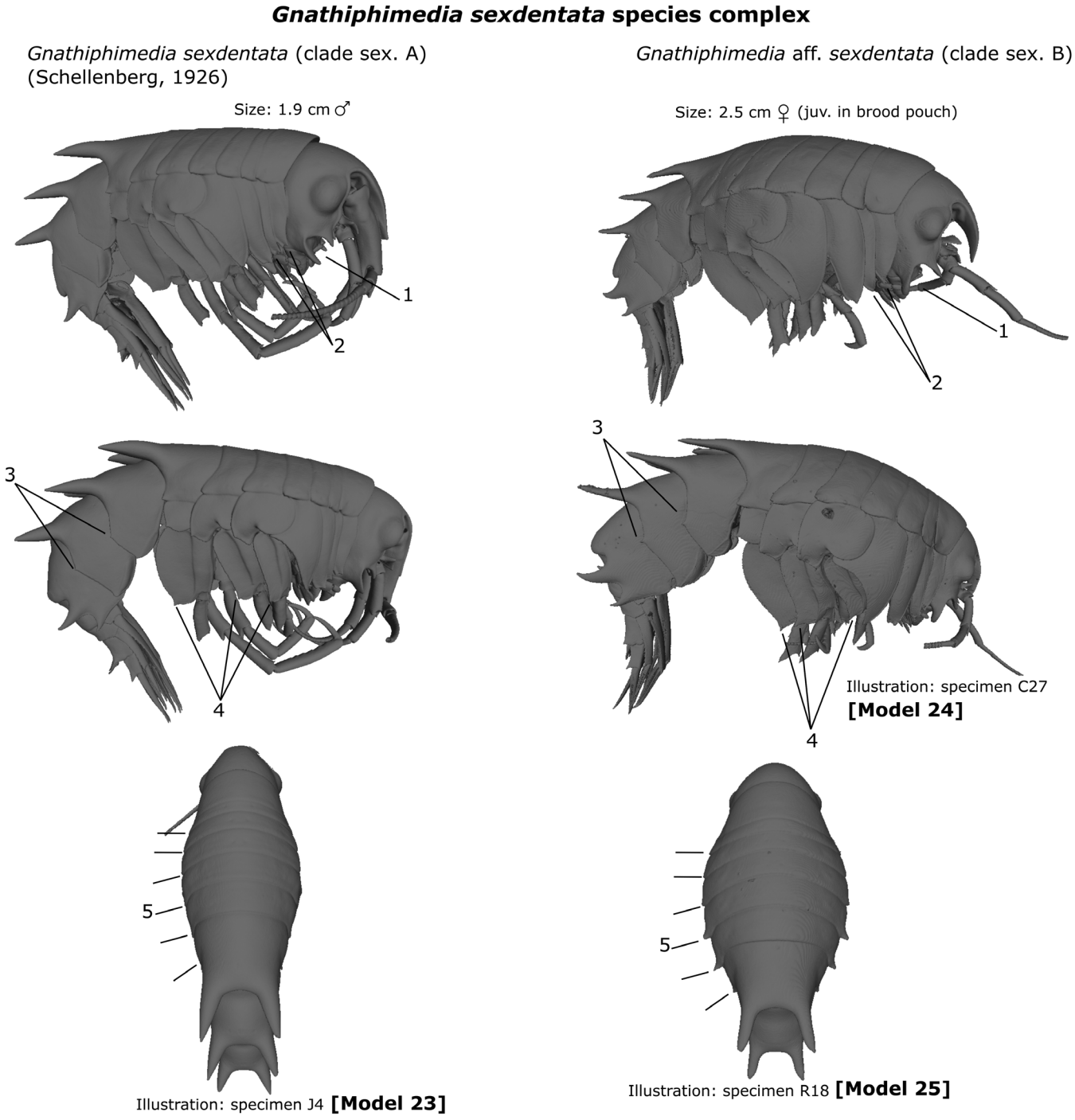

Figure 11. Plate illustrating morphological differences among species of the *Gnathiphimedia sexdentata* complex.

Labriphimedia pulchridentata complex

One (ABGD) to two (bPTP and GMYC) putative species are delimited within the *Labriphimedia pulchridentata* complex. Differences in morphological character states are found between the two (bPTP and GMYC) putative species and as compared to the original description of *L. pulchridentata* Stebbing, 1883 (Table 8 and Figure 10; material examined in Supporting Information, Table S2J). *Labriphimedia* aff. *pulchridentata* 1 is sampled at the Adélie Coast, and *L.* aff. *pulchridentata* 2 on the Macquarie ridge (south of New Zealand), while the type locality of *L. pulchridentata* is at the sub-Antarctic Heard Island (Stebbing 1883).

Gnathiphimedia sexdentata complex

The *Gnathiphimedia sexdentata* complex is polyphyletic in the BI tree, as clade 'sex. B' is part of a larger clade comprising *Iphimediella* aff. *ruffoi* and *Parapanoploea longirostris*, but not the clade 'sex. A' (Fig. 2). Clade 'sex. A' included four (GMYC and ABGD) or five (bPTP) putative species, although the additional split into a fifth putative species (bPTP) is statistically

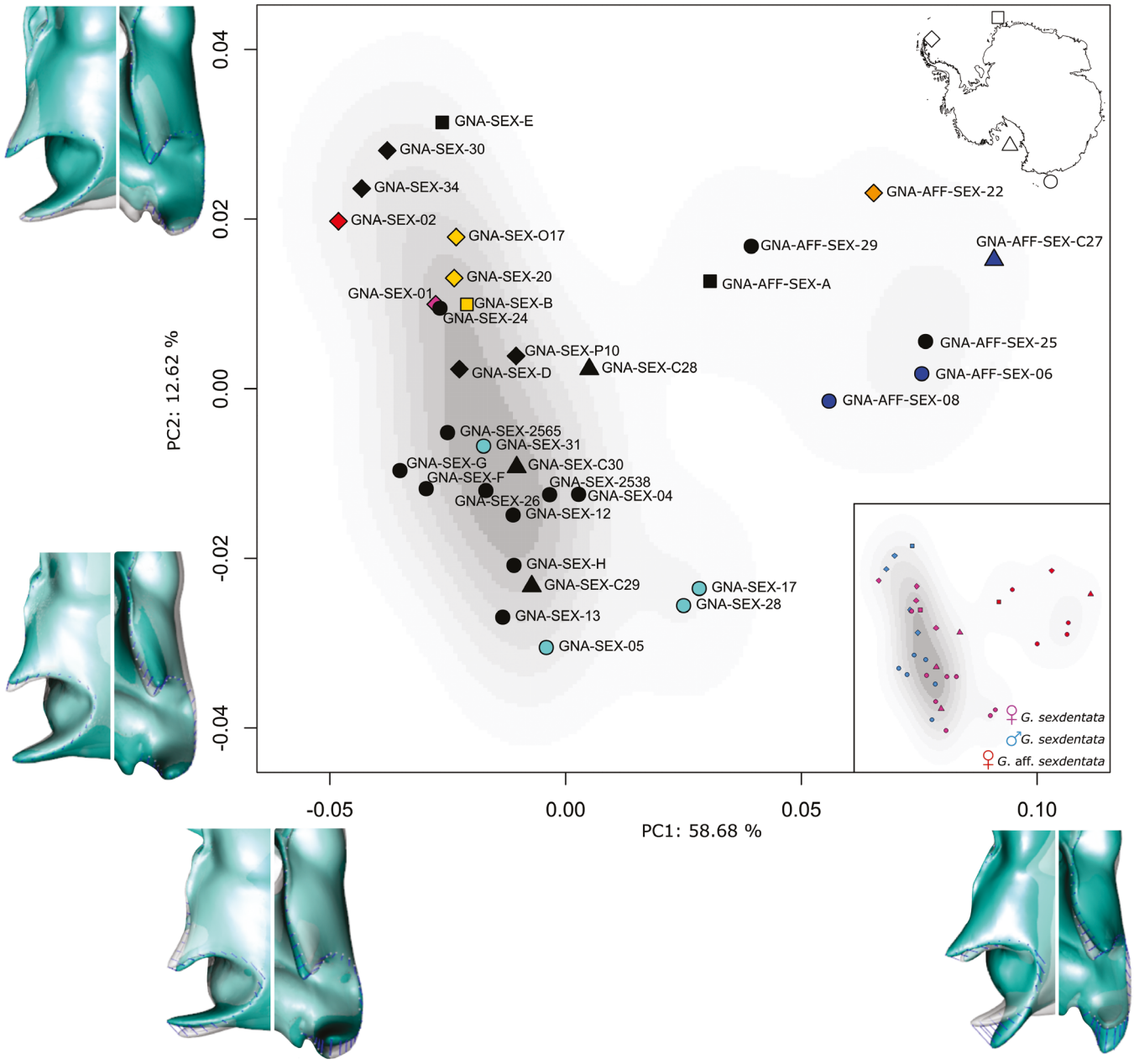

Figure 12. PCA of the morphological shape variation of the subantennal notch in the *Gnathiphimedia sexdentata* complex. Kernel density contours are displayed in the background. Colours represent putative species identified by different species delimitation methods, while black symbols correspond to individuals for which no DNA data were obtained. The shapes of the symbols indicate the region of origin of the sampled specimens: diamond for the Peninsula area, square for the Eastern Weddell Sea, triangle for the Ross Sea and circle for the Adélie Coast (see map in the upper right corner). Shape changes are displayed in both lateral and facial views along each axis as a difference between the mean 3D shape (light grey) and the 3D shapes at the negative and positive extremes of the principal component (turquoise). In the lower right corner, the PCA is represented with specimens colored according to sex: blue, males of *G. sexdentata*; pink, females of *G. sexdentata;* red, females of *G.* aff. *sexdentata.*

not supported (PP < 0.7). The four supported putative species also show distinct 28S haplotypes (Supporting Information, Fig. S8). Clade 'sex. B' comprises two putative species as delimited by all methods. No consistent morphological differences can be found between the putative species, although clades 'sex. A' and 'sex. B' show consistent differences in morphological character states and distinct 28S haplotypes (Table 9; Fig. 11; material examined in Supporting Information, Table S3, Fig. S8). Both putative species have widespread geographical distributions in the current study, ranging from the tip of the Peninsula area to the Adélie Coast, and additionally including the Ross Sea for *Gnathiphimedia* aff. *sexdentata* (Fig. 2).

3D-geometric morphometrics of the *Gnathiphimedia sexdentata* complex

Procrustes' ANOVAs show that the measurement error is small relative to the variation among individuals for all three datasets (Supporting Information, Table S9). This result is confirmed by

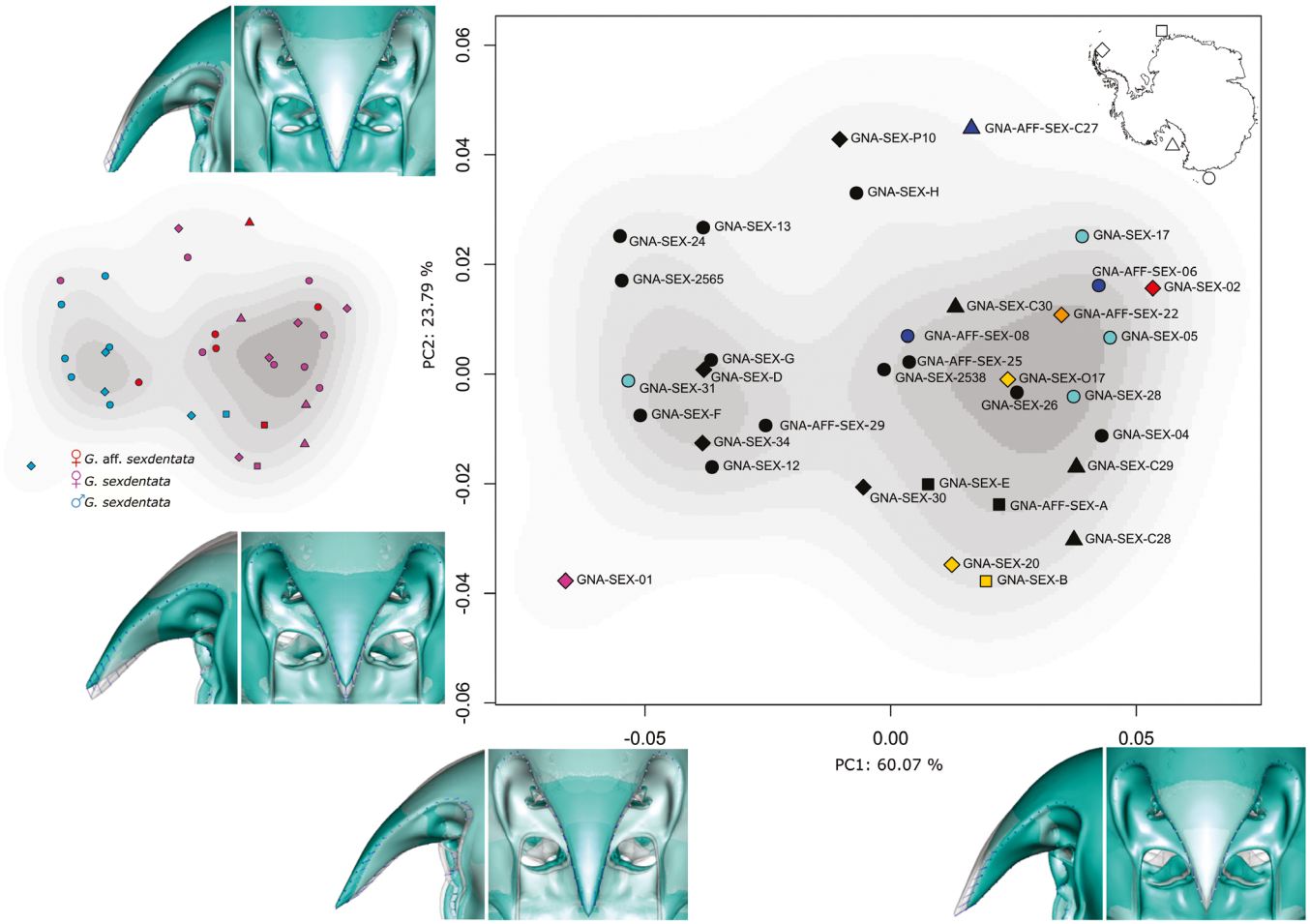

Figure 13. PCA of the rostrum shape variation in the *Gnathiphimedia sexdentata* complex. Kernel density contours are displayed in the background. Colours represent putative species identified by different delimitation methods, while black symbols correspond to individuals for which no DNA data were obtained. The shapes of the symbols indicate the region of origin of the sampled specimens: diamond for the Peninsula area, square for the Eastern Weddell Sea, triangle for the Ross Sea and circle for the Adélie Coast (see map in the upper right corner). Shape changes along each axis are displayed in both lateral and facial views along each axis as a difference between the mean 3D shape (light grey) and the 3D shapes at the negative and positive extremes of the principal component (turquoise). On the left side, the PCA shows specimens coloured according to sex: blue, males of *G. sexdentata*; pink, females of *G. sexdentata;* red, females of *G.* aff. *sexdentata.*

the repeatability scores of, respectively, 96% (head and coxa 4) and 98% (antenna 1 peduncle article 1).

Subantennal notch

The broken-stick method identifies the first four PCs (87.9% variability) as meaningful axes (Supporting Information, Fig. S10). The first two PC axes explain 71.3% of the variance. Kernel density analyses indicate two main density peaks corresponding to *G. sexdentata* and *G.* aff. *sexdentata*. The two morphospecies are morphologically discriminated along PC1, with *G. sexdentata* having a narrower subantennal notch with curved lobes and *G.* aff. *sexdentata* a wider notch with straight lobes. The MANOVA confirms a significant difference in subantennal notch shape between *G. sexdentata* and *G.* aff. *sexdentata* ($P = .001^{***}$; see Supporting Information, Table S11). Both morphospecies show some variability in notch width along PC1, while PC2 explains most of the variability within *G. sexdentata*. Within *G. sexdentata*, this variation is partly due to sexual dimorphism, as females generally show slightly wider notches than males, with some overlap between sexes. The MANOVA indicates that males and females of *G. sexdentata* significantly differ in their notch shape ($P = .004^{**}$; see Supporting Information, Table S11). PC2 explains most of the variability within *G. sexdentata*. Although the latter variability appears continuous, some differences in notch shape are observed among the putative species based on *COI* data along this axis. The anterior lobe of the subantennal notch is shorter and anteriorly directed in the putative species indicated in green in Figure 12, whilst in other putative species, it is longer and more medio-ventrally directed relative to the body axis (Fig. 12). As PCA plots using the third and fourth axes do not provide additional information, they are not shown here.

Rostrum

The broken-stick method identifies the first two PC axes (representing 83.86% of the overall variability) as meaningful axes (Supporting Information, Fig. S10). Kernel density analyses show two main density peaks corresponding to sexual dimorphism (Fig. 13). Within *G. sexdentata*, sexes are discriminated

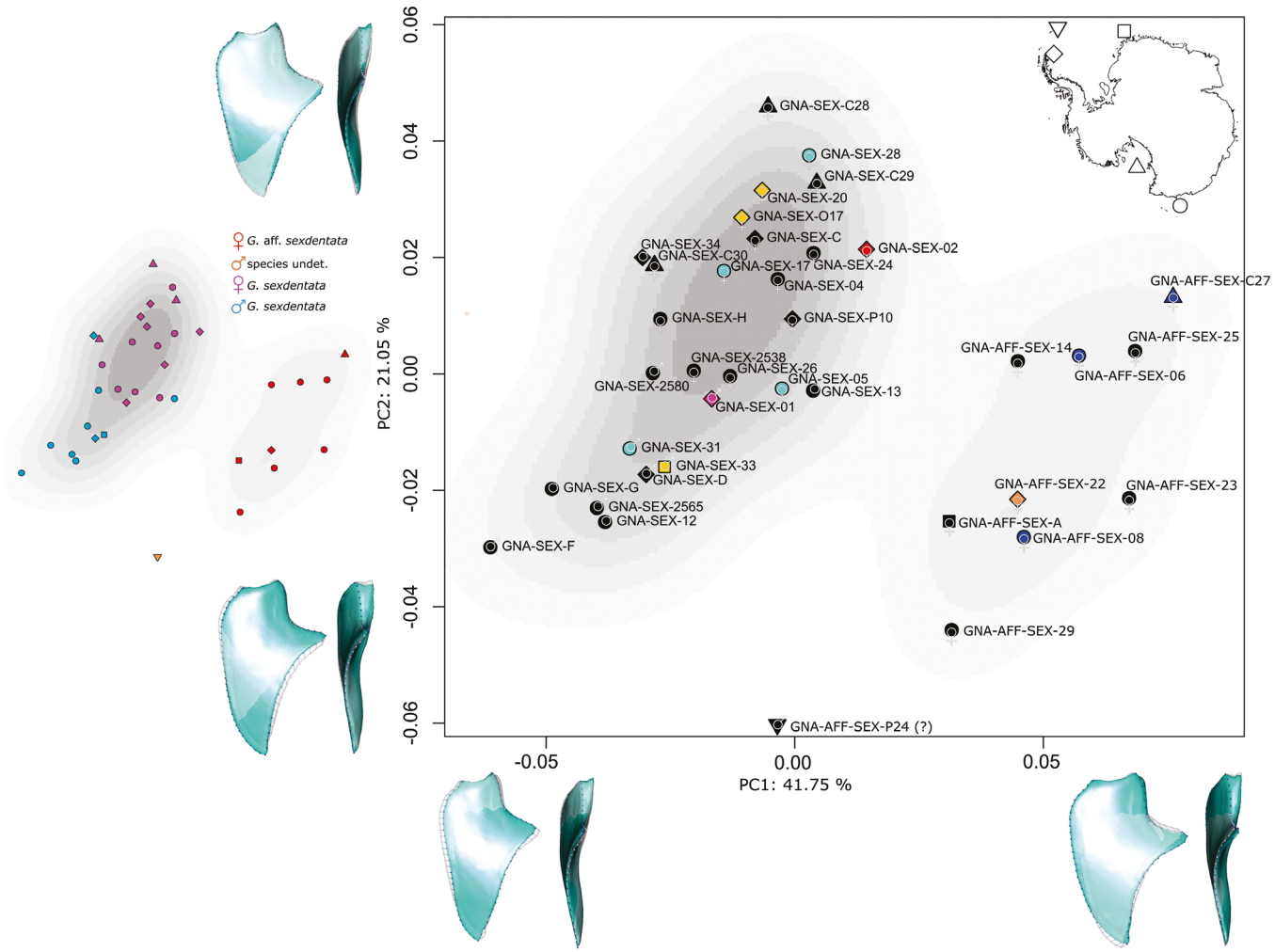

Figure 14. PCA of the shape variation of the coxa 4 in the *Gnathiphimedia sexdentata* complex. Kernel density contours are displayed in the background. Colours represent putative species identified by different delimitation methods, while black symbols correspond to individuals for which no DNA data were obtained. The shapes of the symbols indicate the region of origin of the sampled specimens: diamond for the Peninsula area, square for the Eastern Weddell Sea, inverted triangle for the South Orkneys Islands, triangle for the Ross Sea and circle for the Adélie Coast (see map in the upper right corner). Shape changes displayed along each axis in both facial and lateral views are as a difference between the mean 3D shape (light grey) and the 3D shapes at the negative and positive extremes of the principal component (turquoise). On the left side, the PCA is represented with specimens colored according to sex: blue, males of *G. sexdentata*; orange, male of an undetermined species; pink, females of *G. sexdentata;* red, females of *G.* aff. *sexdentata.*

along PC1, with some overlap. The MANOVA confirms a significant difference in rostrum shape between males and females of *G. sexdentata* ($P = .001^{***}$; see Supporting Information, Table S11). Females generally have shorter and distally tapering rostrums, while most males have longer rostrums with straighter margins. PC2 explains variation in the orientation of the rostrum between individuals, being directed upwards (minimum PC2) to downwards (maximum PC2). *Gnathiphimedia sexdentata* and *G.* aff. *sexdentata* do not significantly differ in rostrum shape (MANOVA: $P = .17$; see Supporting Information, Table S11). Furthermore, the putative species based on *COI* data do not show any clear differences in the rostrum shape (Fig. 13).

Coxa 4

The broken-stick method identifies the first four axes of the PC as meaningful, representing 82.18% of the total variability (Supporting Information, Fig. S10). The first two PCA axes extracted from the covariance matrix explain 62.8% of the shape variance of coxa 4. Kernel density analyses show that two large density peaks could be distinguished, corresponding to the two morphospecies (Fig. 14). *Gnathiphimedia sexdentata* and *G.* aff. *sexdentata* are mainly discriminated along PC1. Indeed, the length of the posterior lobe is shorter in *G. sexdentata* than in *G.* aff. *sexdentata* (Fig. 14). The curvature of the postero-distal margin, going from the tip of the posterior lobe to the tip of the coxa, is almost straight in *G. sexdentata* with a downward-directed tip to concave in *G.* aff. *sexdentata* with a posteriorly directed tip. The MANOVA confirms a significant difference in the 3D-shape of the coxa 4 between *G. sexdentata* and *G.* aff. *sexdentata* ($P = .001^{***}$; see Supporting Information, Table S11). The variability within those two morphospecies is mainly described by PC2 and to a lesser extent by PC1. Within *G. sexdentata,* this variation along both axes appears to mainly correspond to a continuous trend in sexual dimorphism. The MANOVA indicates that males and

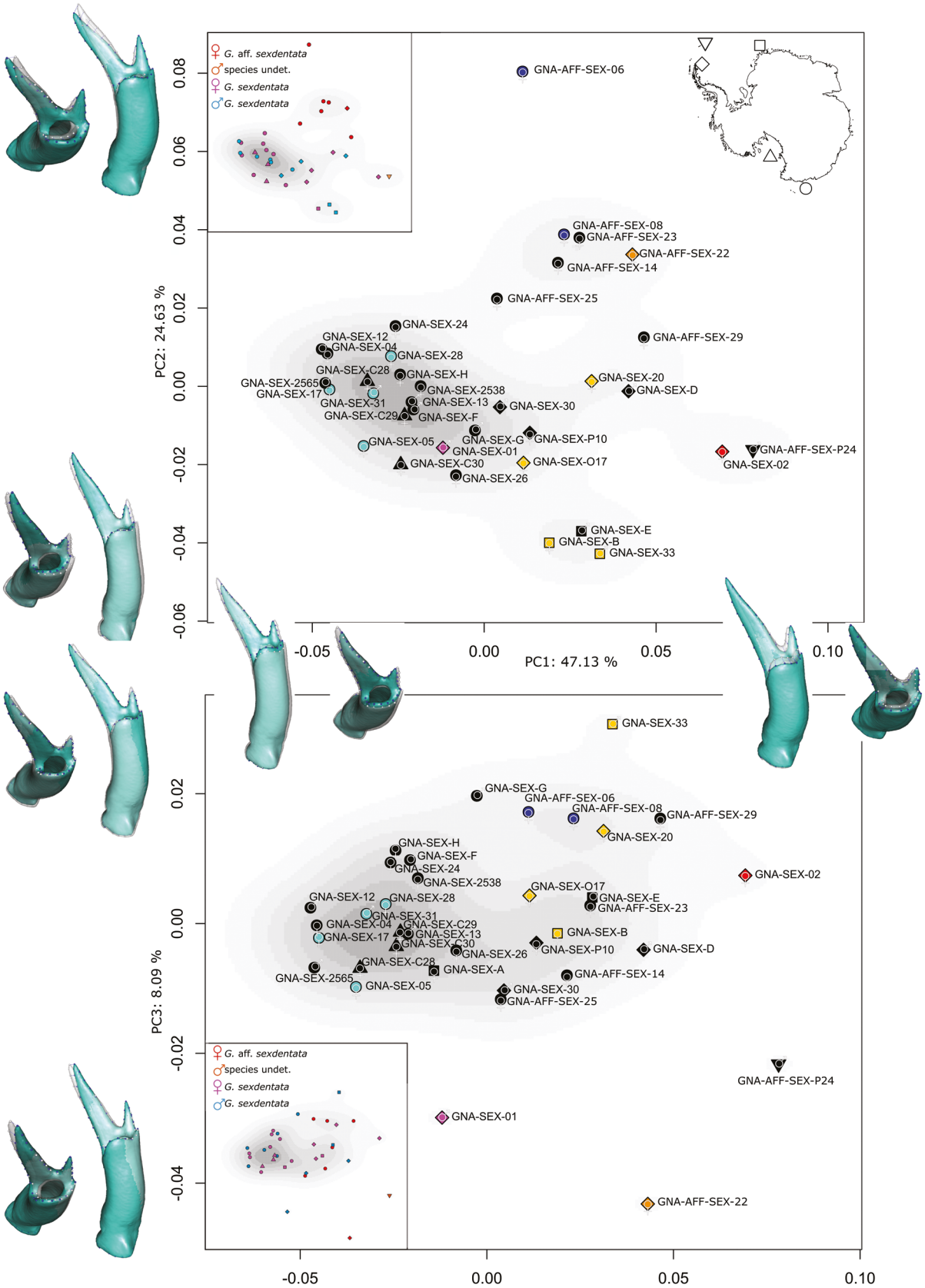

Figure 15. PCA of the shape variation of the first article of the peduncle of Antenna 1 in the *Gnathiphimedia sexdentata* complex. Kernel density contours are displayed in the background. Colours represent putative species identified by different delimitation methods, while black symbols correspond to individuals for which no DNA data were obtained. The shapes of the symbols indicate the region of origin of the sampled specimens: diamond for the Peninsula area, inverted triangle for the South Orkneys Islands, square for the Eastern Weddell Sea, triangle for the Ross Sea and circle for the Adélie Coast. Shape changes along each axis are displayed in two views along each axis as the difference between the mean 3D shape (light grey) and the 3D shapes at the negative and positive extremes of the principal component (turquoise). On the left side, the PCA is represented with specimens colored according to sex: blue, males of *G. sexdentata*; orange, male of an undetermined species; pink, females of *G. sexdentata;* red, females of *G.* aff. *sexdentata.*

females of *G. sexdentata* significantly differed in the 3D-shape of coxa 4 ($P = .001^{***}$; see Supporting Information, Table S11). Female specimens show a wider and slightly longer posterior lobe and larger coxa 4 with a slightly more curved postero-distal margin. Males show a narrower and slightly shorter posterior lobe, a narrower coxa 4 with a straighter postero-distal margin. Variation along PC2 and to a lesser extent along PC1 is also observed within *G.* aff. *sexdentata*. However, potential sexual dimorphism in the variability of *G.* aff. *sexdentata* cannot be tested, as only females of this morphospecies are sampled. No differences in coxa 4 shape are observed between the putative species based on *COI* data within both morphospecies. PC2 also explains the difference between the two morphospecies and GNA-AFF-SEX-P24, which falls outside the kernel density distribution. That individual has a narrower coxa 4 and posterior lobe than all other investigated specimens (Fig. 14). As PCA plots using third and fourth axes do not provide any additional information, they are not shown here.

Antenna 1 peduncle article 1

Following the broken-stick method, the first three PCs (explaining 79.85% variability) are identified as meaningful axes (Supporting Information, Fig. S10). The two first PCs explained 71.76% of the variance in the shape of the first article of the antenna 1's peduncle (ant.1 art.1). Within *G. sexdentata*, a large variability in ant.1 art.1 shape along PC1 is observed. Although this variability appears to be continuous, some differences in shape are observed among the putative species based on *COI* data. A gradient of variation is visible along PC1, from an ant.1 art.1 with a longer body and shorter processes 1 and 2, with a narrower gap between them (in the putative species shown in green; Fig. 15) to an ant.1 art. 1 with progressively shorter bodies and longer processes 1 and 2 with a slightly wider gap between them (in the putative species shown in red; Fig. 15). PC2 allows for some discrimination between *G. sexdentata* and *G.* aff. *sexdentata*, as the MANOVA indicated that there is a significant difference in the shape of ant.1 art.1 between *G. sexdentata* and *G.* aff. *sexdentata* ($P = .001^{***}$; see Supporting Information, Table S11). On the one hand, ant.1 art.1 of *G.* aff. *sexdentata* generally has a larger body, a more laterally oriented process 1 relative to the body axis, and a longer process 2 towards the positive side of PC2. On the other hand, ant.1 art.1 of *G. sexdentata* generally has a narrower body, a less laterally oriented process 1, and a shorter process 2. A lot of variability along PC2 is observed within both morphospecies, as well as within putative species. The MANOVA reveals that males and females of *G. sexdentata* do not significantly differ in the shape of ant.1 art.1 (*P*-value = .274; see Supporting Information, Table S11). Three outlier specimens (GNA-SEX-01, GNA-AFF-SEX-22, and GNA-AFF-SEX-P24) are separated from all other specimens along PC3 (explaining 8.09% of the variance) due to an oblique shift in the orientation of their process 1 towards the peduncular body axis (Fig. 15).

Taxonomy

Stegopanoploea joubini complex

Stegopanoploea joubini (Chevreux, 1912)

(Fig. 3)

Material examined: Five specimens from ANTXXIV-2, stn 48, Eastern Weddell Sea, 70° 23.94′ S, 08° 19.14′ W: (1) RBINS INV.325005, *COI* GenBank PV738842 (O28), SCAN STE-JOU-O28, Model 1, (2) RBINS INV.325006, SCAN STE-JOU-O28b, (3) RBINS INV.325007, SCAN STE-JOU-O28bb, (4) RBINS INV.325008, SCAN STE-JOU-O28bbb, and (5) RBINS INV.325009, *COI* GenBank PV738843 (O29), SCAN STE-JOU-O29. One specimen from ANTXXIVII-3, stn 248-2, Larsen B, 65° 57.51′ S, 60° 28.15′ W: RBINS INV.325010, *COI* GenBank PV738845 (O30). One specimen from ANTXXIX-3, stn 116-6, Bransfield Strait North of Joinville, 62° 33.80′ S, 56° 23.86′ W: RBINS INV. 122911. One specimen from JR144, stn PB-EBS-4-5, South Orkneys Islands, 60° 49.18′ S, 46° 29.06′ W: RBINS INV.325011. One specimen from JR144, stn PB-EBS-4-E, South Orkneys Islands, 60° 49.18′ S, 46° 29.06′ W: RBINS INV.325012.

Distribution: Bransfield Strait, Peninsula (Larsen B), South Orkneys Islands, Eastern Weddell Sea.

Depth range: 190–602 m (present material).

Stegopanoploea brevidentata sp. nov.

(Fig. 3)

urn:lsid:zoobank.org:act:BE1A59B3-1FC8-4EA2-B51E-DBD3F35BA2DB

Type material: Holotype: Female, 9.3 mm, ANT-XXIX/3, stn 164-4, Antarctic Peninsula, off Dundee Island, 63° 37.28′ S, 56° 9.11' W: RBINS INV-325001, *COI* GenBank PV738765 (ANT17), SCAN STE-JOU-ANT17, Model 2. Paratypes: Two specimens from ANT-XXIII/8, stn 689-5, Peninsula Joinville Island, 62° 27.20' S, 55°25.93' W: (1) RBINS INV-325013, *COI* GenBank PV738854 (P1), SCAN STE-JOU-P1 and (2) RBINS INV-325014. Two specimens from ANT-XXIX/3, stn 185-4, Peninsula South of Dundee, 63° 51.53‘ S, 55° 40.74' W: (1) RBINS INV-325000, *COI* GenBank PV738769 (ANT22), SCAN STE-JOU-ANT22 and (2) RBINS INV-325002, SCAN STE-JOU-ANT23. One specimen from KGI Exp. 2011, 20110128-18 (Isla Ardley), King George Island, 62° 12.58' S, 58° 55.55' W: RBINS INV-325015, COI GenBank PV738846 (O39).

Diagnosis: ***Stegopanoploea brevidentata* sp. nov.** conforms to the description of *S. joubini* (Chevreux, 1912) by Coleman (2007), but differs from the specimens interpreted as the true *S. joubini* and *S.* cf. *bidentata* Nicholls, 1938 in the following characters: broader and moderately excavate coxa 4, posterior process on coxa 5 shorter than coxa 5 width and pointed, postero-lateral process on epimeral plates 1–2 of variable length but not reaching half of the following segment, weakly produced teeth on the postero-ventral corner of pereonites 1–7; on pereonites 5–7, projecting posteriorly, alongside the body axis (see Table 1).

Remarks: All specimens of the *S. joubini* complex, including ***S. brevidentata* sp. nov.,** examined here differ from the original description of Chevreux (1912) and are similar to Nicholls (1938) and Bellan-Santini (1972) in the following characters: bidentate basis of both pereiopods 5 and 6, not only the basis of pereiopod 5, and no small obtuse tooth between the carina on pleonite 3 and the superior tooth of epimeral plate 3. The telson is also notched on much less than a fourth of the length (about a tenth).

Distribution: Peninsula: off Joinville and Dundee Islands; King George Island.

Depth range: 102–255 m.

Etymology: The species name (adjective *brevidentatus, -a, -um*) refers to the shorter dorsal teeth and coxa 5 process, as compared to other species of the *S. joubini* complex.

Stegopanoploea cf. *bidentata* Nicholls, 1938

(Fig. 3)

Material examined: Ovigerous female, 13.2 mm, CEAMARC, stn 11/2519, Adélie Coast, 66° 33.71′ S, 141° 15.72′ E: MNHN-IU-2023-670, *COI* GenBank PV738812 (J18), SCAN STE-JOU-J18, Model 3. One specimen from REVOLTA III, stn 449, Adélie Coast, 66° 38′ S, 140° 42′ E: MNHN-IU-2023-671, *COI* GenBank PV738811 (J17). One specimen from REVOLTA IV, stn 015/ 806, Adélie Coast, 66° 37.9′ S, 139° 57.2′ E: MNHN-IU-2019-2170.

Diagnosis: Stegopanoploeae cf. *bidentata* conforms to the description of *S. joubini* (Chevreux, 1912) by Coleman (2007), but differs from the specimens examined here that were interpreted as the true *S. joubini* and ***S. brevidentata* sp. nov.** in the following characters: narrower and strongly excavate coxa 4, posterior process on coxa 5 subequal than coxa 5 width and distally enlarged, postero-lateral process on epimeral plates 1–2 not reaching half of the following segment, weakly produced teeth on the postero-ventral corner of pereonites 1–7; on pereonites 5–7, projecting posteriorly, alongside the body axis (see Table 1).

Remarks: Nicholls (1938) gave a short account on specimens from Commonwealth Bay (Adélie Coast) that he described as *S. joubini* var. *bidentata*, and that differed from the original description of Chevreux (1912) in two characters: bidentate basis of both pereiopods 5 and 6, not only the basis of pereiopod 5, and no small obtuse tooth between the carina on pleonite 3 and the superior tooth of epimeral plate 3. As the species described here was sampled in the same region as the variety described by Nicholls (1938), it is very probable that they are conspecific. However, the illustrations of Nicholls (1938) are not sufficient to verify the diagnostic characters described above, except for the shape of the coxa 4, which fits the present description. Therefore, the name *Stegopanoploea* cf. *bidentata* is used for the specimens examined here. The varietal name *bidentata* introduced by Nicholls (1938) is nomenclaturally valid because it was published before 1961 (ICZN 1999: article 45.6.4).

Distribution: Adélie Coast.

Depth range: 176–199 m.

Maxilliphimedia longipes complex

Maxilliphimedia longipes (Walker, 1906)

(Fig. 4)

Material examined: One specimen from CEAMARC, stn 54/2200, Adélie Coast, 65° 54.74' S, 143° 58.02' E: MNHN-IU-2018-1732, *COI* GenBank PV738807 (J1), SCAN-MAX-LON-03. Three specimens from TAN802, stn 17, Ross Sea, 73° 07.47′ S, 174° 19.23′ E: (1) NIWA 173688, SCAN-MAX-LON-RS33, Model 4, (2) NIWA 173689, *COI* GenBank PV738798 (C7), SCAN-MAX-LON-C7, and (3) NIWA 35558, SCAN-MAX-LON-RS32. Four specimens from MD42, stn 22 CP73, 66° 57.42′ S, 72° 41.41′ E: (1) MNHN-IU-2014-4257, (2) MNHN-IU-2023-699, (3) MNHN-IU-2014-4255, and (4) MNHN-IU-2023-698. One specimen from TAN0802, stn 94, 76° 11.58′ S, 176°17.77′ E: NIWA 36793, *COI* GenBank PV738799 (C8), SCAN-MAX-LON-C8.

Distribution: Ross Sea, Adélie Coast.

Depth range: 321–530 m (present material).

Maxilliphimedia acutilobata sp. nov.

(Fig. 4)

urn:lsid:zoobank.org:act:75C3B7F4-A9F7-4087-B271-45C2C00E5B9E

Maxilliphimedia longipes, Ren and Huang 1991: 194, fig. 3.

Type material: Holotype: Ovigerous female, 63 mm, ANTXXIX-3, stn 204-2, Bransfield Strait Central, 62° 56.07‘ S, 57° 58.14' W, RBINS INV.325017, *COI* GenBank PV738759 (ANT11), SCAN-MAX-LON-06, Model 5. Paratypes: One specimen from ANTXXIII-8, stn 611-1, West Antarctic Peninsula, 60° 58.90' S, 55° 11.31’ W: RBINS INV.325018, *COI* GenBank PV738855 (P13). One juvenile from ANTXXIII-8, stn 680-5, South Shetland Island, 62° 23.37′ S, 61° 25.58′ W: RBINS INV.325019, SCAN-MAX-LON-08. One specimen from ANTXXVII-3, stn 222-5, King George Island, 62° 18.21′ S, 58° 39.90′ W: RBINS INV.325020, SCAN-MAX-LON-05.

Distribution: Bransfield Strait, South Shetland Island, King George Island, West Antarctic Peninsula

Depth range: 215–781 m.

Diagnosis: ***Maxilliphimedia acutilobata* sp. nov.** conforms to the description of *M. longipes* (Walker, 1906) by Coleman (2007), but differs from the examined specimens interpreted as the true *M. longipes* and ***M. oliveri* sp. nov.** in the following combination of characters: the posterior lobe of the subantennal notch is straight, with a small V-shaped notch between the two lobes, the posterior margin of the coxa 7 forms a blunt right angle, the dorsal tooth on pleonite 2 reaches about half of pleonite 3, the postero-lateral process on epimeral plate 2 is rounded, the postero-ventral process on epimeral plate 3 is angular (acute angle) and slightly crenulated ventro-distally, the telson lobes are apically pointed (see Table 2).

Etymology: The name (adjective *acutilobatus, -a, -um*) refers to the acute, apically pointed, telson lobes, as compared to the rounded lobes in the other two species of the *M. longipes* complex.

Maxilliphimedia oliveri sp. nov.

(Fig. 4)

urn:lsid:zoobank.org:act:57217EBC-17CB-4D2B-8597-2F33723C62B

Type material: Holotype: Ovigerous female, 63 mm, ANTXXIII-8, stn 605-5, Elephant Island, 61° 20.27′ S, 55° 30.92′ W, RBINS INV.325022, *COI* GenBank PV738866 (P7), SCAN-MAX-LON-02, Model 6. Paratype: One specimen from ANTXXIX-3, stn 197-5, Bransfield Strait East, 62° 44.73‘ S, 57° 26.79‘ W: RBINS INV.325021, *COI* GenBank PV738760 (ANT12), SCAN-MAX-LON-07.

Distribution: Bransfield Strait, Elephant Island.

Depth range: 152–273 m.

Diagnosis: ***Maxilliphimedia oliveri* sp. nov.** conforms to the description of *M. longipes* (Walker, 1906) by Coleman (2007), but differs from the examined specimens interpreted as the true *M. longipes* and ***M. acutilobata* sp. nov.** in the following combination of characters: the posterior lobe of the subantennal notch is not straight, with a ventral margin sigmoid and proximally slightly concave, the anterior margin slightly convex and a narrow slit between the two lobes (the lobes are in contact with each other), the posterior margin of the coxa 7 forms a distinctively pointed acute (nearly right) angle, the dorsal tooth on pleonite 2 reaches about a third of pleonite 3, the postero-lateral process on epimeral plate 2 is rounded to slightly angular, the postero-ventral corner of epimeral plate 3 is a pointed tooth, the telson lobes are apically rounded (see Table 2).

Etymology: This large species is dedicated to Dr Oliver Coleman, for his extensive work on Antarctic Iphimediidae and, notably, in the genus *Maxilliphimedia*. The species' name is the genitive of the noun *oliverus, -i*.

Echiniphimedia echinata complex

Echiniphimedia echinata (Walker, 1906)

(Fig. 5)

Material examined: One specimen from ANTXXIX-3, stn 197-5, Bransfield Strait East, 62° 44.73' S, 57° 26.79' W: RBINS INV.325025, *COI* GenBank PV738777 (ANT9), SCAN-ECH-ECH-01. One specimen from ANTXXVII-3, stn 228-4, Peninsula Larsen A, 64° 55.58' S, 60° 33.37' W: RBINS INV.325026, *COI* GenBank PV738849 (O5), SCAN-ECH-ECH-29. One specimen from KGI Exp. 2011, 20110204-02 (Fildes Bay), King George Island, 62° 13.17′ S, 58° 53.80′ W: RBINS INV.325024, *COI* GenBank PV738750 (A15), SCAN-ECH-ECH-A15, Model 7. Two specimens from KGI Exp. 2011, 20110217-19 (Fildes Bay), King George Island, 62° 12.11′ S, 58° 56.36′ W: (1) RBINS INV.325027, SCAN-ECH-ECH-12 and (2) RBINS INV.325028, SCAN-ECH-ECH-13. One specimen from CEAMARC, stn 50A/1384, Adélie Coast, 66° 45.20′ S, 145° 12.51′ E: MNHN-IU-2023-672, SCAN-ECH-ECH-05.

Distribution: King George Island, Bransfield Strait, Peninsula (Larsen A), Adélie Coast, Ross Sea.

Depth range: 258–597 m (present material).

Remarks: There are probably more species in the *Echiniphimedia echinata* complex (see Figs 2 and 5 and Table 3). However, it remains unclear which specimens in our material correspond to the true *E. echinata*. Descriptions and illustrations of *E. echinata* of Walker (1906, 1907) and Coleman (2007) better fit this morphotype (see Fig. 5) regarding the number of antero-lateral spines on each side of pleonites and the number of cusps on the posterior margins of pereiopods 5–7 basis, but with some differences in the length of antenna 1 peduncle article 2 longer process, which appears shorter in the description of the type specimen (reaching the end of the first flagellar article) and the pointed antero-ventral corner of coxa 1, appearing rounded in Walker (1907: pl. 10) but, however, pointed in Coleman (2007: 76). Moreover, the specimens examined here corresponding to this morphotype were sampled in the Peninsula area, while the type specimens were collected in the Ross Sea. Because of these uncertainties, and the fact that allometric changes in the number of spines are not fully understood, we described here only two species in this complex.

Echiniphimedia spinosior sp. nov.

(Fig. 6)

urn:lsid:zoobank.org:act:BA95FFAD-F8EB-4568-88DF-8806BC10C6C0

Type material: Holotype: Female, 25 mm, ANTXXIX-3, stn 246-3, Drake Passage East, 62° 44.73′ S, 57° 26.79′ W: RBINS INV.325030, *COI* GenBank PV738771 (ANT28), SCAN-ECH-ECH-02, Model 10. Paratypes: Two specimens from ANTXXIX-3, stn 116-9, Bransfield Strait North of Joinville, 62° 33.79′ S, 56° 27.81′ W: (1) RBINS INV-122916, SCAN-ECH-ECH-07 and (2) RBINS INV.325130.

Distribution: Drake Passage, Bransfield Strait, Eastern Weddell Sea.

Depth range: 260-602 m.

Diagnosis: ***Echiniphimedia spinosior* sp. nov.** generally conforms to the description of *E. echinata* (Walker, 1906) by Coleman (2007), but differs from related species of the *E. echinata* complex in the following characters. It differs from the specimens tentatively interpreted as the true *E. echinata*, *E.* aff. *echinata* 1, *E.* aff. *echinata* 2 in the shape of the subantennal notch with the anterior lobe longer (about 2×) than the posterior, while the two lobes are subequal in the latter three species. It differs from ***E. maxima* sp. nov.** in the following combination of characters: the anterior lobe of the subantennal notch is produced ventrally and pointed, the posterior is rounded, the antero-ventral corner of coxa 2 is rounded, and its postero-ventral corner is angular, 1–3 tubercles aligned vertically below the posterior process of coxa 4, 1–3 small spines aligned vertically above the dorsal process of coxa 5–6, 15–20 small spines on the posterior margin of the pereon 7 and pleons 1–2, 3–5 antero-lateral spines on each side of the pleonites, sometimes with additional 1–3 tubercles (see Table 4).

Remarks: The *E. echinata* complex is polyphyletic on the molecular tree. ***E. spinosior* sp. nov.** forms a clade with ***E. maxima* sp. nov.** (see Fig. 2), but not with the specimens tentatively interpreted as *E. echinata*, *E.* aff. *echinata* 1 and *E.* aff. *echinata* 2.

Etymology: The name refers to the increased number of spines on the body of this species as compared to other species of the *E. echinata* complex. *Spinosior* is the comparative of the Latin adjective *spinosus*, whichs means thorny.

Echiniphimedia maxima sp. nov.

(Fig. 6)

urn:lsid:zoobank.org:act:4B64D5D9-863F-4AC5-A1F4-E3BE6EA9DFCA

Type material: Holotype: Female, 35 mm, CEAMARC, stn 9/675, Adélie Coast, 66° 32.09′ S, 141° 58.96′ E: MNHN-IU-2018-1706, *COI* GenBank PV738808 (J13), SCAN-ECH-ECH-09, Model 11. Paratypes: One specimen from ANT-XXVII/3, stn 308-1, Eastern Weddell Sea, 70° 51.30′ S, 10° 35.35′ W: RBINS INV.325031, SCAN-ECH-ECH-B. Five specimens from ANT-XXVII/3, stn 301-1, Eastern Weddell Sea, 70° 50.99′ S, 10° 35.23′ W: (1) RBINS INV.325032, SCAN-ECH-ECH-18, (2) RBINS INV.325033, SCAN-ECH-ECH-A, (3) RBINS INV.325034, SCAN-ECH-ECH-15, (4) RBINS INV.325035, SCAN-ECH-ECH-16, and (5) RBINS INV.325039, SCAN-ECH-ECH-17. Three specimens from ANT-XXVII/3, stn 292-2, Eastern Weddell Sea, 70° 50.69′ S, 10° 35.51′ W: (1) RBINS INV.325036, SCAN-ECH-ECH-14, (2) RBINS INV.325037, SCAN-ECH-ECH-21, and (3) RBINS INV.325040, SCAN-ECH-ECH-20. One specimen from ANT-XXVII/3, stn 291-1, Eastern Weddell Sea, 70° 50.50′ S, 10° 35.24′ W: RBINS INV.325038, SCAN-ECH-ECH-11. One specimen from CEAMARC, stn 1/2323, Adélie Coast, 66° 00.23′ S, 142° 18.83′ E: MNHN-IU-2018-1712, SCAN-ECH-ECH-23. One specimen from CEAMARC, 9/675, Adélie Coast, 66° 32.09′ S, 141° 58.96′ E: MNHN-IU-2018-1707, ·SCAN-ECH-ECH-27. One specimen from REVOLTA I, stn 002/002, Adélie Coast, 66° 39.80′ S, 139° 59.40′ E: MNHN-IU-2018-1708, SCAN-ECH-ECH-24. One specimen from TAN0402, stn 116, Ross Sea, 71° 17.93′ S, 170° 32.43′ E: NIWA 19100.

Distribution: Adélie Coast, Eastern Weddell Sea, Ross Sea.

Depth range: 30–520 m.

Diagnosis: ***Echiniphimedia maxima* sp. nov.** generally conforms to the description of *E. echinata* (Walker, 1906) by Coleman (2007), but differs but differs from related species of the *E. echinata* complex in the following characters. It differs from the specimens tentatively interpreted as the true *E. echinata*, *E.* aff. *echinata* 1, and *E.* aff. *echinata* 2, in the shape of the subantennal notch with the anterior lobe more than twice the length of the posterior, while the two lobes are subequal in the latter three species. It differs from ***E. spinosior* sp. nov.** in the following combination of characters: the anterior lobe of the subantennal notch is produced antero-ventrally and pointed, the posterior is rounded to slightly angular, coxa 2 is pointed, no tubercles below the posterior process of coxa 4, no spines above the dorsal process of coxa 5–6, 9–13 spines on the posterior margin of the pereonite 7 and pleonites 1–2, 2 antero-lateral spines on each side of pleonites 1–2, and 2 antero-lateral longer spines on pleonite 3, sometimes with an additional smaller one (see Table 4).

Remarks: The *E. echinata* complex is polyphyletic on the molecular tree. ***E. maxima* sp. nov.** forms a clade with ***E. spinosior* sp. nov** (see Fig. 2), but not with the specimens tentatively interpreted as *E. echinata*, *E.* aff. *echinata* 1, and *E.* aff. *echinata* 2.

Etymology: The name refers to the larger size that adult specimens of this species reach, as compared to other species of the *E. echinata* complex. *Maximus, -a, -um* (the biggest) is the superlative of the Latin adjective *magnus* (big).

Iphimediella ruffoi complex

Iphimediella ruffoi Coleman 1996

(Fig. 8)

Material examined: One specimen from CEAMARC, stn 11/2542, Adélie Coast, 66° 33.82′ S, 141° 15.34′ E: MNHN-IU-2023-675, *COI* GenBank PV738804 (H17), SCAN-IPH-RUF-H17, Model 14. One specimen from ANTXXVII-3, stn 265-2, Eastern Weddell Sea, 70° 47.34′ S, 10° 40.39′ W: RBINS INV.325047, SCAN-IPH-RUF-C.

Distribution: Adélie Coast, Eastern Weddell Sea.

Depth range: 170–357 m (present material).

Iphimediella longidentata sp. nov.

(Fig. 8)

urn:lsid:zoobank.org:act:BB73A5FB-82F5-4783-BC27-0CC611D65D10

Type material: Holotype: Female with juveniles in brood pouch, 19 mm, ANTXXIV-2, stn 48, Eastern Weddell Sea, 70° 23.94′ S, 08° 19.14′ W: RBINS INV.325048, *COI* GenBank PV738829 (N20), SCAN-IPH-RUF-N20, Model 15. Paratypes: Two specimens from ANTXXIV-2, stn 48, Eastern Weddell Sea, 70° 23.94′ S, 08° 19.14′ W: (1) RBINS INV.325049, SCAN-IPH-RUF-A, (2) RBINS INV.325050, SCAN-IPH-RUF-B. One specimen from ANTXXIII-8, stn 603-5, Eastern Weddell Sea, 70° 30.99′ S, 08° 48.08′ W: RBINS INV-122458, SCAN-IPH-RUF-E.

Distribution: Eastern Weddell Sea.

Depth range: 273–602 m.

Diagnosis: ***Iphimediella longidentata* sp. nov.** generally conforms to the description of *I. ruffoi* Coleman, 1996 by Coleman (2007), but differs from the specimens interpreted as the true *I. ruffoi* in the following combination of characters: the inferior process of the subantennal notch is a quarter longer than the superior one, the longer process of antenna 1 peduncular article 1 reaches the end of the 4th flagellar article, the rostrum reaches about two-thirds of antenna 1 peduncular article 1, the apex of coxa 1 is bifid, with two small teeth subequal in length, the coxa 5–7 are produced into a well-developed posteroventral tooth, the dorsal teeth on pereonite 7 and pleonites 1–2 reach well beyond the end of the following segment, the length of the basis of pereiopod 7 is about 1.5× its width, with a postero-ventral corner strongly produced (see Table 6).

Remarks: *Iphimediella longidentata* is smaller than *I. ruffoi*, with an adult size of 19 mm (against 26–29 mm for *I. ruffoi*).

Etymology: The species name (adjective *longidentatus*, -a, -um) refers to the longer dorsal processes, process of antenna 1 peduncular article 1, posteroventral teeth of coxa 5–7 and teeth on the posteroventral corner of basis of pereiopod 7, as compared to *I. ruffoi*.

Iphimediella rigida complex

Iphimediella rigida Barnard, 1930

(Fig. 9)

Material examined: One specimen from TAN0802, stn 17, Ross Sea, 73° 07.47′ S, 174° 19.23′ E: NIWA 35345, *COI* GenBank PV738788 (C22), SCAN-IPH-RIG-C22. One specimen from TAN0802, stn 31, Ross Sea, 74° 35.43′ S, 170° 16.54′ E: NIWA 35861, *COI* GenBank PV738787 (C21), SCAN-IPH-RIG-C21, Model 16.

Distribution: Ross Sea.

Depth range: 283–321 m (present material).

Iphimediella brachyodonta sp. nov.

(Fig. 9)

urn:lsid:zoobank.org:act:D67419ED-7EF5-4FD9-B32A-BA385DE199AE

Type material: Holotype: Female, 56 mm, ANTXXIX-3, stn 162-7, Weddell, Erebus, and Terror gulf, 63° 58.78′ S, 56° 46.24′ W: RBINS INV-122879, *COI* GenBank PV738826 (N17), SCAN-IPH-RIG-26, Model 17. Paratypes: Two specimens from ANTXXIX-3, stn 185-3, Bransfield Strait Central, 62° 57.22′ S, 58° 14.60′ W: (1) RBINS INV-122979, *COI* GenBank PV738772 (ANT3), SCAN-IPH-RIG-07 and (2) RBINS INV-122906, SCAN-IPH-RIG-25. One specimen from ANTXXIX-3, stn 193-8, Bransfield Strait Central, 62° 43.73′ S, 57° 29.04′ W: RBINS INV-122891, *COI* GenBank PV738774 (ANT4), SCAN-IPH-RIG-08. Seven specimens from ANTXXIX-3, stn 164-4, Peninsula Dundee Island, 63° 37.28′ S, 56° 9.11′ W: (1) RBINS INV.325051, *COI* GenBank PV738834 (O11), SCAN-IPH-RIG-22, (2) RBINS INV-122885, SCAN-IPH-RIG-A, (3) RBINS INV.325126, SCAN-IPH-RIG-06, (4) RBINS INV.325127, SCAN-IPH-RIG-03, (5) RBINS INV.325128, SCAN-IPH-RIG-01, (6) RBINS INV.325129, and (7) RBINS INV.325059, SCAN-IPH-RIG-04. Four specimens from ANTXXIX-3, stn 197-5, Bransfield Strait East, 62° 44.73′ S, 57° 26.79′ W: (1) RBINS INV-122880, SCAN-IPH-RIG-21, (2) RBINS INV.325052, SCAN-IPH-RIG-20, (3) RBINS INV.325055, SCAN-IPH-RIG-18, and (4) RBINS INV-325056, SCAN-IPH-RIG-19. One specimen from ANTXXIX-3, stn 217-6, Bransfield Strait East, 62° 53.45′ S, 58° 13.06′ W: RBINS INV-122877, SCAN-IPH-RIG-B. One specimen from ANTXXIX-3, stn 224-3, Bransfield Strait West, 63° 00.53′ S, 58° 35.67′ W: RBINS INV-122875, SCAN-IPH-RIG-09. Six specimens from ANTXXIX-3, stn 116-9, Bransfield Strait, North of Joinville, 62° 33.79′ S, 56° 27.81′ W: (1) RBINS INV-122875, SCAN-IPH-RIG-13, (2) RBINS INV-122881, SCAN-IPH-RIG-15, (3) RBINS INV.325053, SCAN-IPH-RIG-12, (4) RBINS INV.325054, SCAN-IPH-RIG-16, (5) RBINS INV.325057, SCAN-IPH-RIG-14, and (6) RBINS INV.325058, SCAN-IPH-RIG-11.

Distribution: Weddell (Erebus and Terror gulf), Peninsula (off Dundee Island), and Bransfield Strait.

Depth range: 102–431 m.

Diagnosis: ***Iphimediella brachyodonta* sp. nov.** conforms to the description of *I. rigida* Barnard, 1930 by Coleman (2007), but differs from the specimens interpreted as the true *I. rigida* in the following characters: the dorsal teeth on pereonite 7 and pleonites 1–3 do not reach half of the following segment, the postero-lateral margin of epimeral plate 1 is rounded to slightly angular, forming an obtuse angle, the postero-lateral margin of epimeral plate 2 is angular, forming an obtuse angle (see Table 7).

Etymology: The species name (adjective *brachyodontus*, *-a*, *-um*) derives from the Greek brachy- (short) and odon (tooth) and alludes to the size of its dorsal teeth, which are shorter than in the related *I. rigida*.

Iphimediella cyclogena complex

Iphimediella cyclogena

(Fig. 9)

Material examined: One female (44 mm) from TAN0402, stn 186, Ross Sea, 71° 30.72′ S, 171° 25.51′ E: NIWA 19072, *COI* GenBank PV738784 (C18), SCAN-IPH-CYC-C18, Model 18. Two specimens from TAN0402, stn 108, Ross Sea, 71° 16.31′ S, 170° 35.98′ E: (1) NIWA 20251, *COI* GenBank PV738790 (C35), SCAN-IPH-CYC-C35 and (2) NIWA 173687, *COI* GenBank PV738791 (C36), SCAN-IPH-CYC-C36. Three specimens from MD42, stn 22, Adélie Coast, 66° 57.42′ S, 72° 41.41′ E: (1) MNHN-IU-2014-4255, (2) MNHN-IU-2023-695, and (3) MNHN-IU-2023-696. One juvenile from TAN0402, stn 194, Ross Sea, 71° 31.80′ S, 170° 06.66′ E: NIWA 173684, SCAN-IPH-CYC-RS29.

Distribution: Ross Sea, Adélie Coast.

Depth range: 252–405 m.

Remarks: The anterior lobe appears somewhat longer on the illustrations of the holotype of *I. cyclogena* by K.H. Barnard (1930) than in the specimens examined here, but it is still distinctively shorter than the posterior lobe. As the type specimens also come from the Ross Sea, we interpret the present material as *I. cyclogena*. Coxa 1 also appears ‘truncate and excavate’ on the illustrations of the type specimen, with a pointed antero-inferior angle, while it is rounded in all specimens examined here (including ***I. longilobata* sp. nov**. specimens).

Iphimediella longilobata sp. nov.

(Fig. 9)

urn:lsid:zoobank.org:act:0DA971EC-7EF3-4AEA-88CA-3F349A53286C

Material examined: One specimen from ANTXXIX-3, stn 185-3, Bransfield Strait East, 63° 51.34' S, 55° 41.11' W: RBINS INV.325060, *COI* GenBank PV738773 (ANT30), SCAN-IPH-CYC-05, Model 19. One specimen from ANTXXIX-3, stn 116-9, Bransfield Strait North of Joinville, 62° 33.79' S, 56° 27.81' W: RBINS INV.325062, *COI* GenBank PV738856 (P14), SCAN-IPH-CYC-07. One specimen from ANTXXVII-3, stn 228-4, Peninsula Larsen A, 64° 55.58' S, 60° 33.37' W: RBINS INV.325064, *COI* GenBank PV738753 (A2), SCAN-IPH-CYC-07. One specimen from ANTXXIV-2, stn 48, Eastern Weddell Sea, 70° 23.94' S, 08° 19.14' W: RBINS INV.325061, *COI* GenBank PV738853 (O9), SCAN-IPH-CYC-20, Model 20.

Diagnosis: ***Iphimediella longilobata* sp. nov.** conforms to the description of *I. cyclogena* Barnard, 1930 by Coleman (2007), except for the shape of the subantennal notch: the anterior lobe is rounded to bluntly pointed and as long as or slightly longer than the posterior lobe in ***Iphimediella longilobata* sp. nov.**, whereas it is pointed and shorter than the posterior lobe in *Iphimediella cyclogena*.

Etymology: The species name (adjective *longilobatus, -a, -um*) refers to the only character by which this species can be distinguished from *I. cyclogena*, i.e. the longer anterior lobe of the subantennal notch.

Distribution: Bransfield Strait, Peninsula (Larsen A, B, C), Eastern Weddell Sea.

Depth: 248–602 m (present material).

Labriphimedia pulchridentata complex

Labriphimedia adeliae sp. nov.

(Fig. 10)

urn:lsid:zoobank.org:act:F3C31F56-97A8-4342-94A8-FB558E13F2F1

Type material: Holotype: Female with juveniles in brood pouch, 30 mm, CEAMARC, stn 86/3410, Adélie Coast, 65° 28.85′ S, 139° 24.18′ E: MNHN-IU-2014-4289, *COI* GenBank PV738860 (P18), SCAN-LAB-PUL-P18, Model 21. Paratype: One specimen from CEAMARC, stn 86/3410, Adélie Coast, 65° 28.85′ S, 139° 24.18′ E: MNHN-IU-2023-700, *COI* GenBank PV738861 (P19].

Distribution: Adélie Coast.

Depth range: 820 m.

Diagnosis: ***Labriphimedia adeliae* sp. nov.** conforms to the description of *L. pulchridentata* (Stebbing, 1883) by Coleman (2007), but differs from the original description of *L. pulchridentata* and ***L. anneninae* sp. nov.** in the following characters: the superior process of the subantennal notch is much broader than large, the second article of antenna 1 peduncle has two processes of subequal length, the coxa 1 is bifid, with two lobes of similar width, the coxa 2–3 are bifid and strongly concave, the coxa 4 is very narrow and deeply concave posteriorly, presence of dorsal teeth on pereonite 5, long bidentate teeth on pleonites, teeth on postero-ventral corner of pereonites 1–7, three dorso-lateral processes on pleonite 1 and long dorso-lateral process on pleonite 2, reaching more than half of the following segment (see Table 8).

Etymology: The species' name (genitive of the noun *adelia, -ae*) refers to the type locality, off the Adélie Coast.

Labriphimedia anneninae sp. nov.

(Fig. 10)

urn:lsid:zoobank.org:act:05144008-B7EA-468A-B9C4-C2383B1313CD

References: Lörz 2012

Type material: Holotype: Ovigerous female, 20 mm, TAN0802, stn 93, Macquarie Ridge, 55° 21.20′ S, 158° 26.21′ E: NIWA 40808, *COI* GenBank PV738795 (C44), SCAN-LAB-PUL-C44, Model 22. Paratype: One specimen from TAN0803, stn 98, Macquarie Ridge, 56° 14.78′ S, 158° 30.33′ E: P.87292 (Australian Museum), SCAN-LAB-PUL-C46.

Type locality: Macquarie Ridge.

Distribution: Macquarie Ridge.

Depth range: 605 m.

Diagnosis: ***Labriphimedia anneninae* sp. nov.** conforms to the description of *L. pulchridentata* (Stebbing, 1883) by Coleman (2007), but differs from the original description of *L. pulchridentata* and ***L. adeliae* sp. nov.** in the following characters: the superior process of the subantennal notch is as broad as long, the second article of antenna 1 peduncle has two processes with one much longer than the other, the coxa 1 is bifid, with the anterior lobe much broader than the posterior one, the coxa 2–3 are bifid and moderately concave, the coxa 4 is broad and weakly concave posteriorly, no dorsal teeth on pereonite 5, low bidentate carinae on pleonites, teeth on postero-ventral corner of pereonites 6–7, two dorso-lateral processes on pleonite 1 and short dorso-lateral process on pleonite 2, not reaching half of the following segment (see Table 8).

Etymology: This beautiful species is dedicated to Dr Anne-Nina Lörz, who published its discovery on the Macquarie Ridge (Lörz 2012) , and for her extensive work on Antarctic amphipods. The species name is the genitive of the noun *annenina, -ae*.

DISCUSSION

In the present study, we reconstructed a novel molecular phylogeny (*COI*, 28S, and *H3*) of the family Iphimediidae, comprising 29 of the 39 currently recognized Antarctic iphimediid species (south of the polar front). In the phylogenetic tree, the genera *Iphimediella*, *Gnathiphimedia*, and *Iphimedia* are polyphyletic. Through species delimitation methods based on *COI* sequence data and a thorough morphological analysis, we

discovered that 10 of the 29 species included in this study are, in fact, species complexes; 10 new species showing consistent morphological differences are formally described. We discuss the geographical distributions and potential evolutionary drivers of these iphimediid species complexes. In addition, we applied for the first time a 3D-geometric morphometrics approach to an amphipod species complex (*G. sexdentata s.l.*), which confirmed that *G. sexdentata* comprises at least two morphologically distinct species.

Genus-level systematics reveals convergent trophic adaptations

The genera *Iphimediella*, *Gnathiphimedia*, and *Iphimedia* appear polyphyletic on the molecular phylogeny. To date, the generic subdivision of Iphimediidae is only based on the mouthpart morphology (Coleman 2007). The general shape of the mandible, as well as the orientation and dentition of its incisor, are mainly used to distinguish genera. For instance, *Iphimediella* is characterized by an elongate and dentate incisor, oriented to cut in the transverse plane, whereas *Gnathiphimedia* has a broad and blunt incisor, to crush food in the frontal plane (Coleman 1989a). Such mandible shapes were interpreted as dietary adaptations (Watling 1993), e.g. *Iphimediella cyclogena* uses its mandibles to cut soft holothurian tissues, whereas *Gnathiphimedia mandibularis* crushes morsels of bryozoans with its stout mandibles (Coleman 1989a, Dauby *et al.* 2001, Nyssen *et al.* 2002, Michel *et al.* 2020). The genus *Iphimedia* mainly includes non-Antarctic species, with only five species out of 52 that are found in Antarctic and sub-Antarctic areas (https://www.marinespecies.org/, accessed on 27.03.2024). The present results show that *Iphimedia imparilabia,* collected in the sub-Antarctic magellanic region, does not form a clade with non-Antarctic *Iphimedia* species, but is nested among species of other (sub-)Antarctic genera in the Bayesian phylogeny. The monophyly of the genus *Iphimedia* has previously been questioned because of the high variability of its diagnostic characters (Watling and Holman 1981). *Iphimedia* is mainly distinguished by its elongated mandible with a narrow incisor, a 3-articulated palp of the maxilliped with an apicomedially produced article 2 (Rathke 1843, Coleman 2007). The polyphyly of *Iphimediella*, *Gnathiphimedia*, and *Iphimedia* suggests that similar trophic morphologies may have evolved several times independently during the evolutionary history of Iphimediidae. However, ancestral state reconstruction would be needed to formally test this hypothesis. Characters related to the feeding mode are likely to show convergent evolution, while species adapt to similar trophic niches, as has been observed for other Antarctic amphipods (Havermans *et al.* 2011, Michel *et al.* 2020). Altogether, these results highlight the need for a phylogenetically informed revision of the generic subdivision of Iphimediidae, as diagnostic mouthpart characters are shown to be highly homoplastic.

Iphimediidae species' diversity is greatly underestimated

The present study revealed that hidden diversity is present in 10 of the 29 nominal Antarctic Iphimediidae species included in our phylogenetic analyses. Each species complex contained between two to seven distinct species. Similarly, DNA and integrative research has uncovered species complexes in nearly every Antarctic animal group examined so far. Our results add to the growing evidence of hidden species' diversity within a wide variety of taxa (e.g. Held 2003, Linse *et al.* 2007, Mahon *et al.* 2008, Thornhill *et al.* 2008, Janosik and Halanych 2010, Allcock *et al.* 2011, Hemery *et al.* 2012, Brasier *et al.* 2016, Ruiz *et al.* 2020, Maroni *et al.* 2022).

For seven species complexes (*Stegopanoploea joubini*, *Maxilliphimedia longipes*, *Echiniphimedia echinata*, *Iphimediella ruffoi*, *Iphimediella cyclogena*, *Iphimediella rigida*, and *Labriphimedia pulchridentata*), the species' delimitations based on *COI* were supported by consistent morphological differences. In many cases, 'cryptic' species uncovered by genetic methods are likely to be readily separated by morphological variation that was overlooked, or previously assumed to be intraspecific (Sáez and Lozano 2005). Many studies combining DNA-based species' delimitation methods with more detailed morphological analyses uncovered diagnostic characters that had previously escaped detection (Dietz *et al.* 2015, Verheye *et al.* 2016, d'Udekem d'Acoz *et al.* 2018, Ruiz *et al.* 2020, Verheye and d'Udekem d'Acoz 2021). For instance, an integrative taxonomic study of Antarctic *Epimeria* revealed that most nominal species, in fact, consisted of multiple distinct species, exhibiting (small but) consistent morphological differences (Verheye *et al.* 2016, d'Udekem d'Acoz and Verheye 2017). The latter diagnostic characters were often in the shape and length of the dorsal teeth, the ornamentations on the antennae peduncles, coxae, bases of pereiopods, and epimeral plates, as well as in the shape of the ventrally positioned coxae 1–4 (d'Udekem d'Acoz and Verheye 2017).

Both *Echiniphimedia hodgsoni* and *Gnathiphimedia sexdentata* each comprise two clades (namely, 'hod. A' and 'hod. B' for *E. hodgsoni*, and 'sex. A' and 'sex. B' for *G. sexdentata* in Fig. 2) that show consistent morphological differences, while the putative species within the two clades do not. Hence, there are at least two species within *E. hodgsoni* and *G. sexdentata*, corresponding to the clades 'hod. A', 'hod. B', 'sex. A', and 'sex. B'. However, all three species' delimitation methods applied to the *COI* data suggest that there might be seven putative species in *E. hodgsoni* and six in *G. sexdentata*. Yet, as the sole use of *COI* data may lead to overestimations of species' diversity (Hupało *et al.* 2023), additional data are required to confirm this result.

While most of the species identified here were not truly cryptic, no consistent morphological differences were found within the *Anchiphimedia dorsalis* complex and the two clades of *E. hodgsoni* and *G. sexdentata*. Complete or partial reproductive isolation may result from differences in behavioural, ecological, or reproduction-related traits that have no (or few) morphological correlates, e.g. habitat preferences, auditory, or chemical mate recognition systems, courtship behaviour, reduced viability or fertility of the offspring, and gametic incompatibilities (Knowlton 1993). Moreover, body colour, which disappears with alcohol preservation, might be an important character for iphimediid species' identification (see Supporting Information, Table S2). Finally, it is possible that closely-related species may only be morphologically differentiated by minor variations in the shapes of certain structures; the latter may only be discernible through the application of quantitative geometric morphometric techniques (see, e.g. Malekmohammad *et al.* 2021, Layeghi *et al.* 2022), which we tested here on one species complex, *G. sexdentata*.

3D-geometric morphometrics as an additional tool for species' delimitation

We performed a 3D-geometric morphometrics (GM) analysis on the *G. sexdentata* complex to explore its potential in discriminating morphologically 'cryptic' species. Our 3D-GM analysis confirmed the existence of at least two morphologically distinct species within the *G. sexdentata* complex, as the two clades ('sex. A' and 'sex. B') are clearly differentiated by the shapes of their subantennal notch, coxa 4 and art. 1 ped. ant.1 (Figs 12, 14, 15). The putative species identified within those two clades by species' delimitation methods applied on *COI* data show variation in the shapes of the subantennal notch (*G. sexdentata* 4) and art. 1 ped. ant.1 (all species). However, as this variation is often continuous, larger numbers of specimens per putative species are needed to confirm our preliminary results and statistical tests for morphometric differences.

We observed here sexual dimorphism in Iphimediidae, in the form of a continuous, overlapping variation in the shapes of the subantennal notch, rostrum, and coxa 4 between the sexes (Figs 12–14). In gammaridean amphipods, sexual dimorphism is usually observed in body size, shape, and size of the gnathopods (Moore and Wong 1996) and antennae (Barnard 1971, McLaughlin 1980). Our results indicate that amphipod taxa, which do not display strong sexual dimorphism, may nevertheless show subtle variations between the two sexes in the shape of different structures.

Assessing shape variation through multivariate analyses enabled the distinction between sexual dimorphic and interspecific variation within the *G. sexdentata* complex, which would have been difficult to detect without quantitative tools. We demonstrated, for instance, that the rostrum shape cannot be used to differentiate species within *G. sexdentata s.l.*, as it only discriminated between sexes. Our results illustrate the potential of GM to provide additional diagnostic characters for species identification in Iphimediidae, as demonstrated for other amphipod taxa (Riedlecker *et al.* 2009, Malekmohammad *et al.* 2021, Layegui *et al.* 2022). Whether GM is efficient in identifying subtle variations between species that do not diverge in any other diagnostic characters (as shown for other crustaceans: Marchiori *et al.* 2014, Karanovic *et al.* 2016), such as the putative species within the *G. sexdentata* complex, merits further exploration with larger sample sizes from both sexes in a combined molecular–morphometric approach.

When a circum-Antarctic species comprises multiple regional species

The discovery of cryptic species complexes often changes the existing knowledge of species' realized distribution ranges. A species with a reported circumpolar distribution may, in fact, consist of multiple cryptic species with smaller distribution ranges. This has important implications for conservation as species distributed over narrower ranges are at higher extinction risks (Mace *et al.* 2008).

Prioritizing habitats for conservation often relies on estimates of species' richness and endemism (Bickford *et al.* 2007). The present revision of species' diversity within Antarctic Iphimediidae shows that most of the studied species, previously considered to be circum-Antarctic or geographically widespread (Coleman 2007; https://www.gbif.org/fr/occurrence/, accessed on 02/04/2024), consist, in fact, of multiple species with narrower geographical ranges, including only one or two adjacent biogeographical units [as defined by De Broyer and Jażdżewska (2014)]: *Echiniphimedia* aff. *echinata* 1–2 (as numbered on the phylogeny of Fig. 2), ***E. spinosior* sp. nov.,** *E. hodgsoni* 1–4, *E.* aff. *hodgsoni* 1–3, *Gnathiphimedia sexdentata* 1–4, *G.* aff. *sexdentata* 1–2. *Iphimediella rigida,* ***I. brachyodonta* sp. nov.**, ***I. longilobata* sp. nov.**, ***I. longidentata* sp. nov.**, ***Labriphimedia anneninae* sp. nov.**, ***L. adeliae* sp. nov.,** *Maxilliphimedia longipes,* ***M. acutilobata* sp. nov**, ***M. oliveri* sp. nov**., *Stegopanoploea joubini,* ***S. brevidentata* sp. nov.,** and *S.* cf. *bidentata*. For other nominal species, it remains to be investigated whether specimens from distant localities belong to the same species, as our dataset included only specimens from one or two adjacent areas (see Supporting Information, Table S12).

The distributional range of Antarctic shelf taxa depends on a number of correlated factors, linked to the biology of an organism and environmental features. Iphimediid species are strictly benthic, therefore stretches of >1000m deep are likely to constitute effective barriers to dispersal. This is exemplified by the *Labriphimedia pulchridentata* complex, as the specimens collected on the Macquarie Ridge, on the Kerguelen-Heard plateau, and the Antarctic shelf (Adélie Coast), separated by deep water, belong to three different species. As all amphipods are brooders, the mobility of the adults is probably determinant, as suggested by the wide distribution of some amphipod species whose adults are good swimmers (Havermans *et al.* 2013, Verheye and d'Udekem d'Acoz 2021). Observations of several species (*E. hodgsoni, E. scotti, G. mandibularis, I. cyclogena,* and *M. longipes*) in aquaria have shown that, most of the time, these iphimediids sit motionless on their host substrate or walk very slowly, but seldomly swim (De Broyer *et al.* 2001). Mobility also relates to trophic ecology, e.g. suspension-feeders are likely to be less mobile, while active predators and scavengers will be good swimmers (De Broyer *et al.* 2001, Lörz *et al.* 2009). Iphimediidae species typically inhabit the lower level of the epibenthic assemblages formed by sessile suspension-feeders (De Broyer *et al.* 2001). The family appears to be mostly composed of micropredatory browsers, specializing on a preferred prey within those epibenthic assemblages (Coleman 1989a, b, Dauby *et al.* 2001, Nyssen *et al.* 2002). The distribution of epibenthic communities is very patchy and unpredictable (Gutt and Piepenburg 2003, Raguá-Gil *et al.* 2004, Cummings *et al.* 2010, Gutt *et al.* 2013). Some continental shelf areas are permanently covered by floating ice shelves (Weddell and Ross embayments and, to a lesser extent, Amundsen and Bellingshausen seas) or perennial pack ice (western Weddell Sea). While diverse sessile suspension feeder communities may be sustained by the inflow of organic matter in undershelf areas that are relatively close to open water (observed at 100 km; Riddle *et al.* 2007), in more distant locations, the benthic fauna appears impoverished and mainly composed of grazers and detritus-feeders (Gutt *et al.* 2011, Post *et al.* 2013). Such areas are, therefore, likely to be important barriers to the dispersal of weakly mobile amphipods that are closely dependent on epibenthic assemblages, such as many iphimediids.

Although most Antarctic iphimediids appear to be weakly dispersive, some species might be able to range over longer distances. A few (putative) species still showed widespread

geographical distributions after the revision of species boundaries: the two putative species of the *A. dorsalis* complex (being found at the Peninsula, Eastern Weddell Sea, and Adélie Coast for one, and Peninsula and Ross Sea for the other), and *E.* aff. *echinata* 4 (Eastern Weddell Sea and Adélie Coast). *Iphimediella microdentata* was identified as a single species with a circum-Antarctic distribution (Eastern Weddell Sea, Adélie Coast, and Ross Sea; Supporting Information, Table S12). Ecological data are still lacking for many iphimediid species, and it is unknown if distinct species from a complex of closely related species may show distinct trophic preferences and behaviours (as in e.g. Klarner *et al.* 2013, Fišer *et al.* 2015), which could explain the observed differences in the extent of their distribution ranges.

Potential drivers of of iphimediid diversity

Plio-Pleistocene glacial–interglacial cycles probably acted as a 'diversity pump' (e.g. Clarke and Crame 1992, Rogers *et al.* 2007). During this period, grounded ice sheets extended over much of the continental shelf at glacial maxima (Pollard and DeConto 2009), erasing the shelf benthos (Clarke and Crame 1992, Thatje *et al.* 2005). Small populations isolated in glacial refugia may have gone through bottlenecks and diverged from each other by genetic drift, sometimes to the point of speciation (Allcock and Strugnell 2012). Strictly shelf species like iphimediid amphipods might have survived glacial cycles in continental shelf refugia (Convey *et al.* 2009, 2018). Current geological evidence suggests the existence of ice-free areas on the outer continental shelf, even during the extreme phases of glacial period in the Pleistocene (Golledge *et al.* 2012, Bentley *et al.* 2014). Possible persistence in sub-Antarctic refugia and subsequent re-colonization of the shelf should also be considered for iphimediids as a number of species (or species complexes) have distribution ranges that extend to sub-Antarctic areas or islands (e.g. *Labriphimedia pulchridentata* complex and *Iphimedia imparilabia*). Investigating demographic history, population connectivity, and lineage diversification across time might shed light on to how species survived glacial cycles (Clarke *et al.* 2004, Lau *et al.* 2020), and if glacial cycles were an important diversity driver in Antarctic Iphimediidae. The high variability in mouthpart shapes among species also suggests a potential ecological diversification into a variety of trophic niches (Watling and Thurston 1989, Coleman 2007). The benthic environment offers a large variety of habitats and opportunities for habitat specialization. The spatial fragmentation of suitable benthic habitats may lead to the genetic structuring of populations that are unable to cross intervening areas of unfavourable habitats (Wiens 2004, Rogers 2007).

CONCLUSION

While more than 8000 invertebrate species have been described in the Southern Ocean (De Broyer *et al.* 2014), it is estimated that as many as 17 000–20 000 species inhabit the Antarctic continental shelf (Gutt *et al.* 2004, De Broyer *et al.* 2011). In a rapidly changing Antarctic environment (Gutt *et al.* 2021), a baseline knowledge of biodiversity and species' distributional ranges is urgently needed to allow the assessing of change and implementing adequate conservation measures (Saucède *et al.* 2021). Integrative taxonomic studies are progressively reducing the knowledge gap in Antarctic marine biodiversity (De Broyer *et al.* 2011), and can now integrate advanced tools such as 3D-GM to clarify taxonomy in challenging groups (as in e.g. Burridge *et al.* 2019, Karanovic and Bláha 2019). Using a combination of DNA-based species' delimitations and morphological/morphometric analyses, we have identified 24 new species in Antarctic Iphimediidae amphipods, of which 10 are formally described, thereby increasing the number of nominal species from 39 to 49. The restricted distribution range of many of these species might increase their vulnerability to environmental changes (Powles *et al.* 2000). This study is a significant contribution to our knowledge of Antarctic shelf benthic diversity and distributions, which is essential to support conservation efforts.

SUPPLEMENTARY DATA

Supplementary data are available at *Zoological Journal of the Linnean Society* online.

ACKNOWLEDGEMENTS AND FUNDING

This work was supported by a CR FNRS fellowship (FNRS, Belgium) and a Wallonie-Bruxelles International (WBI) grant. The research programme led by Guillaume Lecointre, REVOLTA 1124, supported by the Institut polaire français Paul Emile Victor (IPEV) and the Muséum National d'Histoire Naturelle (MNHN), and the CAML-CEAMARC cruise of RSV *Aurora Australis* (IPY project no. 53), supported by the Australian Antarctic Division, the Japanese Science Foundation and the IPEV (project ICOTA), are acknowledged for providing extensive Antarctic material. The Melanesian specimens used in this study were collected during various deep-sea cruises, conducted, respectively, by MNHN and Institut de Recherche pour le Développement (IRD) as part of the Tropical Deep-Sea Benthos programme (Tropical Deep-Sea Benthos | MNHN). Funders and sponsors include the French Ministry of Foreign Affairs, the Total Foundation, Prince Albert II of Monaco Foundation, Stavros Niarchos Foundation, and Richard Lounsbery Foundation. We thank Laure Corbari (MNHN) for giving us access to this material. The travel expenses of two of the authors during ANT-XXIX/3 were funded by the Fonds Léopold III. We thank the Alfred-Wegener-Institut, Helmholtz-Zentrumfür Polar- und Meeresforschung (AWI) and the captain, crew, and chief scientists of various R.V. *Polarstern* expeditions for their efficiency, as well as present and past colleagues of the staff of the Royal Belgian Institute of Natural Sciences (RBINS), especially Henri Robert and Charlotte Havermans, for collecting specimens on board. We wish to thank the National Institute for Water and Atmospheric Research (NIWA, New Zealand) for giving us access to specimens from the Ross Sea, and especially Sadie Mills and Anne-Nina Lörz for their warm welcome and help with sorting the material. This publication is a contribution to the RECTO project (BELSPO, contract no. BR/154/A1/RECTO).

CONFLICT OF INTEREST

None declared.

DATA AVAILABILITY

The DNA sequence data underlying this article are available in the GenBank Nucleotide Database (at https://www.ncbi.nlm.nih.gov/genbank/) and can be accessed with the accession numbers in the Supporting Information, Table S1. The microCT meshes of whole

habitus used for the morphological study of Antarctic Iphimediidae, as well as meshes of the specific structures (head, coxa 4 and the first article of the antenna 1 peduncle) used in the morphometric analysis of *G. sexdentata,* are publicly available on Sketchfab at: https://sketchfab.com/mverheye

https://sketchfab.com/3d-models/gsexdentata-ant1-bb5e1619f4894432a0f97d77357629b5

https://sketchfab.com/3d-models/gsexdentata-coxa4-bab3d7aa43e644689bb80417a781343d

https://sketchfab.com/3d-models/gsexdentata-heads-d45433de7be6441888b1be2c8d619e45

https://sketchfab.com/3d-models/model-1-ste-jou-o28-stegopanoploea-joubini-63fcf683079e4e9d978ee4788839f99f

https://sketchfab.com/3d-models/model-2-ant17-stegopanoploea-brevidentata-775bf9155aa54ca59f9645dfaf1bdb8d

https://sketchfab.com/3d-models/model-3-ste-jou-j18-stegopanoploea-cf-bidentata-cd119b4a44844170a2b3113498910be5

https://sketchfab.com/3d-models/model-4-max-lon-rs33-maxilliphimedia-longipes-1fbcce7781494587b106925204e82ce7

https://sketchfab.com/3d-models/model-5-max-lon-06-maxilliphimedia-acutilobata-888367069227414e93ef81f519f5d0c3

https://sketchfab.com/3d-models/model-6-max-lon-02-maxilliphimedia-oliveri-ee02c78109854d6abd45ea1e5a92a32a

https://sketchfab.com/3d-models/model-7-ech-ech-a15-echiniphimedia-echinata-711f8112dbf44bf0bb2f207d63dfd360

https://sketchfab.com/3d-models/model-8-ech-06-echiniphimedia-aff-echinata-1-c4d11815ed174be49e40fb4f9310138a

https://sketchfab.com/3d-models/model-9-ech-10-echiniphimedia-aff-echinata-2-7ab857aa58fe49168cc0733464bfae13

https://sketchfab.com/3d-models/model-10-ech-ech-02-echiniphimedia-spinosior-568b1c6ee72a4361993e9e1b13c7acf8

https://sketchfab.com/3d-models/model-11-ech-ech-09-echiniphimedia-maxima-8605e0c5be9d4e0cb434e8060143730a

https://sketchfab.com/3d-models/model-12-ech-hod-02-echiniphimedia-hodgsoni-c827d8be0bb046cdabb60e7f666329cc

https://sketchfab.com/3d-models/model-13-ech-hod-03-echiniphimedia-aff-hodgsoni-cfdff51e7bf447e9b65593619bf1e672

https://sketchfab.com/3d-models/model-14-iph-ruf-h17-iphimediella-ruffoi-b54cec825e0b455e93dd79ead0ab387e

https://sketchfab.com/3d-models/model-15-iph-ruf-n20-iphimediella-longidentata-108dcc43c32a458194ad32ba0205258f

https://sketchfab.com/3d-models/model-16-iph-rig-c21-iphimediella-rigida-6647752cbbd94766a2b6471e15fe8b14

https://sketchfab.com/3d-models/model-17-iph-rig-26-iphimediella-brachyodonta-314dbdc418164d7cb4a0eb86e9fed923

https://sketchfab.com/3d-models/model-18-iph-cyc-c18-iphimediella-cyclogena-e852abfe3cd54cfcb61f39f76c5cae8f

https://sketchfab.com/3d-models/model-19-iph-cyc-05-iphimediella-longilobata-7de99a5237df41758ed4001750b570e6

https://sketchfab.com/3d-models/model-20-iph-cyc-20-iphimediella-longilobata-24a6aea72a794125b2903d1f64b3c486

https://sketchfab.com/3d-models/model-21-lab-pul-p18-labriphimedia-adeliae-a66c660b346a459d8b6eee90a5b41d52

https://sketchfab.com/3d-models/model-22-lab-pul-c44-labriphimedia-anneninae-782e5ec41518445daf94e9ac163135e8

https://sketchfab.com/3d-models/model-23-gna-sex-31-gnathiphimedia-sexdentata-31e0816f3c204154ac3f1318cd634dbe

https://sketchfab.com/3d-models/model-24-gna-sex-c27-g-aff-sexdentata-60b74555d2394d9a828a0191963ea4e9

https://sketchfab.com/3d-models/model-25-gna-sex-06-g-aff-sexdentata-79922417daca42a2873a38638d8836d3

REFERENCES

Adams DC, Otárola-Castillo E. geomorph: an R package for the collection and analysis of geometric morphometric shape data. *Methods in Ecology and Evolution* 2013;**4**:393–9. https://doi.org/10.1111/2041-210x.12035

Allcock AL, Strugnell JM. Southern Ocean diversity: new paradigms from molecular ecology. *Trends in Ecology & Evolution* 2012;**27**:520–8. https://doi.org/10.1016/j.tree.2012.05.009

Allcock AL, Barratt I, Eleaume M *et al.* Cryptic speciation and the circumpolarity debate: a case study on endemic Southern Ocean octopuses using the COI barcode of life. *Deep Sea Research Part II: Topical Studies in Oceanography* 2011;**58**:242–9. https://doi.org/10.1016/j.dsr2.2010.05.016

Amsler MO, Mcclintock JB, Amsler CD *et al.* An evaluation of sponge-associated amphipods from the Antarctic Peninsula. *Antarctic Science* 2009;**21**:579–89. https://doi.org/10.1017/s0954102009990356

Asochakov IA. Technique for measuring body length of amphipods. *Hydrobiological Journal* 1994;**30**:107.

Barnard KH. Amphipoda. *British Antarctic (Terra Nova) Expedition 1910, Natural History Reports* 1930;**5**:1–326. https://doi.org/10.5962/bhl.part.27664

Barnard KH. Amphipoda. *Discovery Reports* 1932;**5**:1–326. https://doi.org/10.5962/bhl.part.27664

Barnard JL. *Keys to the Hawaiian Marine Gammaridea, 0-30 Meters*, Vol. **58**. Washington: Smithsonian Contributions to Zoology, 1971.

Bellan-Santini D. Invertébrés marins des XIIème et XVème Expéditions Antarctiques Françaises en Terre Adélie. 10. Amphipodes Gammariens. *Tethys* 1972;**4**:157–238.

Bentley MJ, Cofaigh CO, Anderson JB *et al.* A community-based geological reconstruction of Antarctic Ice Sheet deglaciation since the Last Glacial Maximum. *Quaternary Science Reviews* 2014;**100**:1–9.

Blanco-Bercial L, Cornils A, Copley N *et al.* DNA barcoding of marine copepods: assessment of analytical approaches to species identification. *PLoS Currents* 2014;**6**:ecurrents.tol.cdf8b74881f87e3b01d56b43791626d2. https://doi.org/10.1371/currents.tol.cdf8b74881f87e3b01d56b43791626d2

Bookstein FL. *Morphometric Tools for Landmark Data: Geometry and Biology*. Cambridge: Cambridge University Press, 1991.

Botton-Divet L, Cornette R, Fabre AC *et al.* Morphological analysis of long bones in semi-aquatic mustelids and their terrestrial relatives. *Integrative and Comparative Biology* 2016;**56**:1298–309. https://doi.org/10.1093/icb/icw124

Brandão SN, Sauer J, Schön I. Circumantarctic distribution in Southern Ocean benthos? A genetic test using the genus *Macroscapha* (Crustacea, Ostracoda) as a model. *Molecular Phylogenetics and Evolution* 2010;**55**:1055–69. https://doi.org/10.1016/j.ympev.2010.01.014

Brasier MJ, Wiklund H, Neal L *et al.* DNA barcoding uncovers cryptic diversity in 50% of deep-sea Antarctic polychaetes. *Royal Society Open Science* 2016;**3**:1–19.

Burridge AK, Van Der Hulst R, Goetze E *et al.* Assessing species boundaries in the open sea: an integrative taxonomic approach to the pteropod genus *Diacavolinia*. *Zoological Journal of the Linnean Society* 2019;**187**:1016–40. https://doi.org/10.1093/zoolinnean/zlz049

Carstens BC, Pelletier TA, Reid NM *et al.* How to fail at species' delimitation. *Molecular Ecology* 2013;**22**:4369–83. https://doi.org/10.1111/mec.12413

Chen Y, Ye W, Zhang Y *et al.* High speed BLASTN: an accelerated MegaBLAST search tool. *Nucleic Acids Research* 2015;**43**:7762–8. https://doi.org/10.1093/nar/gkv784

Chevreux E. Diagnoses d'amphipodes nouveaux. Deuxième expédition dans l'Antarctique, dirigée par le Dr. Charcot, 1908-1910. *Bulletin du Muséum National d'Histoire Naturelle* 1912;**18**:208–18.

Chevreux E. Amphipodes. Deuxième Expédition Antarctique Française (1908–1910). *Sciences Naturelles: Documents Scientifiques* 1913;**77**:186.

Clarke A, Crame JA. The Southern Ocean benthic fauna and climate change: a historical perspective. *Philosophical Transactions of the Royal Society of London, Series B: Biological Sciences* 1992;**338**:299–309.

Clarke A, Johnston NM. Antarctic marine benthic diversity. In: Gibson RN, Atkinson RJA (eds), *Oceanography and Marine Biology*. London and New York: Taylor & Francis, 2003, 47–114.

Clarke A, Aronson RB, Crame JA *et al.* Evolution and diversity of the benthic fauna of the Southern Ocean continental shelf. *Antarctic Science* 2004;**16**:559–68. https://doi.org/10.1017/s0954102004002329

Clement M, Posada D, Crandall KA. TCS: a computer program to estimate gene genealogies. *Molecular Ecology* 2000;**9**:1657–9. https://doi.org/10.1046/j.1365-294x.2000.01020.x

Coleman CO. On the nutrition of two Antarctic Acanthonotozomatidae (Crustacea: Amphipoda): gut contents and functional morphology of mouthparts. *Polar Biology* 1989a;**9**:287–94. https://doi.org/10.1007/bf00287425

Coleman CO. *Gnathiphimedia mandibularis* KH Barnard 1930, an Antarctic amphipod (Acanthonotozomatidae, Crustacea) feeding on Bryozoa. *Antarctic Science* 1989b;**1**:343–4. https://doi.org/10.1017/s0954102089000519

Coleman OC. Synopsis of the Amphipoda of the Southern Ocean. *Bulletin de l'Institut Royal des Sciences Naturelles de Belgique* 2007;**77**:1–134.

Constable AJ, Melbourne-Thomas J, Corney SP *et al.* Climate change and Southern Ocean ecosystems I: how changes in physical habitats directly affect marine biota. *Global Change Biology* 2014;**20**:3004–25. https://doi.org/10.1111/gcb.12623

Convey P, Peck LS. Antarctic environmental change and biological responses. *Science Advances* 2019;**5**:1–16.

Convey P, Bindschadler R, Di Prisco G *et al.* Antarctic climate change and the environment. *Antarctic Science* 2009;**21**:541–63.

Convey P, Bowman V, Chown SL, *et al.* Ice bound Antarctica: biotic consequences of the shift from a temperate to a polar climate. In: Hoorn C, Perrigo A, Antonelli A (eds), *Mountains, Climate and Biodiversity*. Oxford UK: John Wiley & Sons, 2018, 355–73.

Corrigan LJ, Horton T, Fotherby H *et al.* Adaptive evolution of deep-sea amphipods from the superfamily Lysiassanoidea in the North Atlantic. *Evolutionary Biology* 2014;**41**:154–65. https://doi.org/10.1007/s11692-013-9255-2

Cummings VJ, Thrush SF, Chiantore M *et al.* Macrobenthic communities of the north-western Ross Sea shelf: links to depth, sediment characteristics and latitude. *Antarctic Science* 2010;**22**:793–804. https://doi.org/10.1017/s0954102010000489

Dauby P, Scailteur Y, De Broyer C. Trophic diversity within the eastern Weddell Sea amphipod community. *Hydrobiologia* 2001;**443**:69–86.

De Broyer C. Recherches sur la systématique et l'évolution des crustacés amphipodes gammarides antarctiques et subantarctiques. D.Phil. Thesis, Université Catholique de Louvain, 1983.

De Broyer C, Danis B. How many species in the Southern Ocean? Towards a dynamic inventory of the Antarctic marine species. *Deep Sea Research Part II: Topical Studies in Oceanography* 2011;**58**:5–17. https://doi.org/10.1016/j.dsr2.2010.10.007

De Broyer C, Jażdżewska A. Biogeographic patterns of Southern Ocean benthic amphipods. In: De Broyer C, Koubbi P *et al.* (ed.), *Biogeographic Atlas of the Southern Ocean.* Cambridge: Scientific Committee on Antarctic Research, 2014, 155–65.

De Broyer C, Scailteur Y, Chapelle G *et al.* Diversity of epibenthic habitats of gammaridean amphipods in the eastern Weddell Sea. *Polar Biology* 2001;**24**:744–53. https://doi.org/10.1007/s003000100276

De Broyer C, Jazdzewski K, Dauby P. Chapter 32. Biodiversity patterns in the Southern Ocean: lessons from Crustacea. In: Huiskes AHL, Gieskes WWC, Rozema J *et al.* (eds), *Antarctica in a Global Context*. Leiden: Backhuys, 2003, 201–14.

Dellicour S, Flot JF. The hitchhiker's guide to single-locus species' delimitation. *Molecular Ecology Resources* 2018;**18**:1234–46. https://doi.org/10.1111/1755-0998.12908

De Queiroz K. Species concepts and species' delimitation. *Systematic Biology* 2007;**56**:879–86. https://doi.org/10.1080/10635150701701083

Dietz L, Arango CP, Dömel JS *et al.* Regional differentiation and extensive hybridization between mitochondrial clades of the Southern Ocean giant sea spider *Colossendeis megalonyx*. *Royal Society Open Science* 2015;**2**:140424–15. https://doi.org/10.1098/rsos.140424

Ezard T, Fujisawa T, Barraclough TG. *splits: SPecies' LImits by Threshold Statistics. R Package v.1.0-14/r31*, 2009. Vienna, Austria: R-Forge. Available at: https://r-forge.r-project.org/projects/splits/

Fišer Z, Altermatt F, Zakšek V *et al.* Morphologically cryptic amphipod species are 'ecological clones' at regional but not at local scale: a case study of four *Niphargus* species. *PLoS One* 2015;**10**:e0134384. https://doi.org/10.1371/journal.pone.0134384

Fujisawa T, Barraclough TG. Delimiting species using single-locus data and the Generalized Mixed Yule Coalescent approach: a revised method and evaluation on simulated data sets. *Systematic Biology* 2013;**62**:707–24. https://doi.org/10.1093/sysbio/syt033

Funk DJ, Omland KE. Species-level paraphyly and polyphyly: frequency, causes, and consequences, with insights from animal mitochondrial DNA. *Annual Review of Ecology, Evolution, and Systematics* 2003;**34**:397–423. https://doi.org/10.1146/annurev.ecolsys.34.011802.132421

Golledge NR, Fogwill CJ, Mackintosh AN *et al.* Dynamics of the last glacial maximum Antarctic ice-sheet and its response to ocean forcing. *Proceedings of the National Academy of Sciences of the United States of America* 2012;**109**:16052–6. https://doi.org/10.1073/pnas.1205385109

Graeve M, Dauby P, Scailteur Y. Combined lipid, fatty acid and digestive tract content analyses: a penetrating approach to estimate feeding modes of Antarctic amphipods. *Polar Biology* 2001;**24**:853–62.

Grant RA, Griffiths HJ, Steinke D *et al.* Antarctic DNA barcoding; a drop in the ocean? *Polar Biology* 2011;**34**:775–80. https://doi.org/10.1007/s00300-010-0932-7

Griffiths HJ. Antarctic marine biodiversity—what do we know about the distribution of life in the Southern Ocean? *PLoS One* 2010;**5**:e11683. https://doi.org/10.1371/journal.pone.0011683

Gunz P, Mitteroecker P, Bookstein FL. Semilandmarks in three dimensions. In: Slice DE, (ed.), *Modern Morphometrics in Physical Anthropology*. New York: Kluwer Academic/Plenum Publishers, 2005, 73–98.

Gutt J, Piepenburg D. Scale-dependent impact on diversity of Antarctic benthos caused by grounding of icebergs. *Marine Ecology Progress Series* 2003;**253**:77–83. https://doi.org/10.3354/meps253077

Gutt J, Sirenko BI, Smirnov IS *et al.* How many macrozoobenthic species might inhabit the Antarctic shelf? *Antarctic Science* 2004;**16**:11–6. https://doi.org/10.1017/s0954102004001750

Gutt J, Barratt I, Domack E *et al.* Biodiversity change after climate-induced ice-shelf collapse in the Antarctic. *Deep Sea Research Part II: Topical Studies in Oceanography* 2011;**58**:74–83. https://doi.org/10.1016/j.dsr2.2010.05.024

Gutt J, Barnes DK, Lockhart SJ *et al.* Antarctic macrobenthic communities: a compilation of circumpolar information. *Nature Conservation* 2013;**4**:1–13. https://doi.org/10.3897/natureconservation.4.4499

Gutt J, Isla E, Xavier JC *et al.* Antarctic ecosystems in transition—life between stresses and opportunities. *Biological Reviews* 2021;**96**:798–821.

Havermans C, Nagy ZT, Sonet G *et al.* DNA barcoding reveals new insights into the diversity of Antarctic species of *Orchomene sensu lato* (Crustacea: Amphipoda: Lysianassoidea). *Deep Sea Research Part II: Topical Studies in Oceanography* 2011;**58**:230–41. https://doi.org/10.1016/j.dsr2.2010.09.028

Havermans C, Sonet G, d'Udekem d'Acoz C *et al.* Genetic and morphological divergences in the cosmopolitan deep-sea amphipod *Eurythenes gryllus* reveal a diverse abyss and a bipolar species. *PLoS One* 2013;**8**:e74218. https://doi.org/10.1371/journal.pone.0074218

Held C. Molecular evidence for cryptic speciation within the widespread Antarctic crustacean *Ceratoserolis trilobitoides* (Crustacea, Isopoda). In: Huiskes AHL, Gieskes WWC, Rozema J *et al.* (eds), *Antarctic Biology in a Global Context*. Leiden: Backhuys, 2003, 135–9.

Hemery LG, Eléaume M, Roussel V *et al.* Comprehensive sampling reveals circumpolarity and sympatry in seven mitochondrial lineages of the Southern Ocean crinoid species *Promachocrinus kerguelensis* (Echinodermata). *Molecular Ecology* 2012;**21**:2502–18. https://doi.org/10.1111/j.1365-294X.2012.05512.x

Hou Z, Fu J, Li S. A molecular phylogeny of the genus *Gammarus* (Crustacea: Amphipoda) based on mitochondrial and nuclear gene sequences. *Molecular Phylogenetics and Evolution* 2007;**45**:596–611. https://doi.org/10.1016/j.ympev.2007.06.006

Hupało K, Copilaș-Ciocianu D, Leese F *et al.* Morphology, nuclear SNPs and mate selection reveal that COI barcoding overestimates species' diversity in a Mediterranean freshwater amphipod by an order of magnitude. *Cladistics* 2023;**39**:129–43.

ICZN. *International Code of Zoological Nomenclature*, 4th edn. London: The International Trust for Zoological Nomenclature 1999 c/o. The Natural History Museum, 1999, 1–124.

Jackson DA. Stopping rules in principal components analysis: a comparison of heuristical and statistical approaches. *Ecology* 1993;**74**:2204–14. https://doi.org/10.2307/1939574

Janosik AM, Halanych KM. Unrecognized Antarctic biodiversity: a case study of the genus *Odontaster* (Odontasteridae; Asteroidea). *Integrative and Comparative Biology* 2010;**50**:981–92. https://doi.org/10.1093/icb/icq119

Joly S, Stevens MI, Van Vuuren BJ. Haplotype networks can be misleading in the presence of missing data. *Systematic Biology* 2007;**56**:857–62. https://doi.org/10.1080/10635150701633153

Kapli P, Lutteropp S, Zhang J *et al.* Multi-rate Poisson tree processes for single-locus species' delimitation under maximum likelihood and Markov chain Monte Carlo. *Bioinformatics* 2017;**33**:1630–8. https://doi.org/10.1093/bioinformatics/btx025

Karanovic T, Bláha M. Taming extreme morphological variability through coupling of molecular phylogeny and quantitative phenotype analysis as a new avenue for taxonomy. *Scientific Reports* 2019;**9**:2429. https://doi.org/10.1038/s41598-019-38875-2

Karanovic T, Djurakic M, Eberhard SM. Cryptic species or inadequate taxonomy? Implementation of 2D geometric morphometrics based on integumental organs as landmarks for delimitation and description of copepod taxa. *Systematic Biology* 2016;**65**:304–27. https://doi.org/10.1093/sysbio/syv088

Katoh K, Standley DM. MAFFT multiple sequence alignment software version 7: improvements in performance and usability. *Molecular Biology and Evolution* 2013;**30**:772–80. https://doi.org/10.1093/molbev/mst010

King RA, Leys R. The Australian freshwater amphipods *Austrochiltonia australis* and *Austrochiltonia subtenuis* (Amphipoda: Talitroidea: Chiltoniidae) confirmed and two new cryptic Tasmanian species revealed using a combined molecular and morphological approach. *Invertebrate Systematics* 2011;**25**:171–96. https://doi.org/10.1071/is10035

Klages M, Gutt J. Comparative studies on the feeding behaviour of high Antarctic amphipods (Crustacea) in laboratory. *Polar Biology* 1990;**11**:73–9.

Klarner B, Maraun M, Scheu S. Trophic diversity and niche partitioning in a species rich predator guild–Natural variations in stable isotope ratios (13C/12C, 15N/14N) of mesostigmatid mites (Acari, Mesostigmata) from Central European beech forests. *Soil Biology and Biochemistry* 2013;**57**:327–33. https://doi.org/10.1016/j.soilbio.2012.08.013

Knowlton N. Sibling species in the sea. *Annual Review of Ecology and Systematics* 1993;**24**:189–216. https://doi.org/10.1146/annurev.ecolsys.24.1.189

Lanfear R, Calcott B, Ho SY *et al.* PartitionFinder: combined selection of partitioning schemes and substitution models for phylogenetic analyses. *Molecular Biology and Evolution* 2012;**29**:1695–701. https://doi.org/10.1093/molbev/mss020

Lau SC, Wilson NG, Silva CN *et al.* Detecting glacial refugia in the Southern Ocean. *Ecography* 2020;**43**:1639–56.

Layeghi Y, Momtazi F, Yazdi AB *et al.* An integrated taxonomic approach, using geometric morphometric methods, reveals the cryptic diversity of *Parhyale darvishi* Momtazi & Maghsoudlou, 2016 (Crustacea: Amphipoda: Hyalidae). *Zoologischer Anzeiger* 2022;**299**:96–105. https://doi.org/10.1016/j.jcz.2022.05.009

Linse K, Cope T, Lörz AN *et al.* Is the Scotia Sea a centre of Antarctic marine diversification? Some evidence of cryptic speciation in the circum-Antarctic bivalve *Lissarca notorcadensis* (Arcoidea: Philobryidae). *Polar Biology* 2007;**30**:1059–68. https://doi.org/10.1007/s00300-007-0265-3

Loerz A, Maas E, Linse K *et al.* Do circum-Antarctic species exist in peracarid Amphipoda? A case study in the genus *Epimeria* Costa, 1851 (Crustacea, Peracarida, Epimeriidae). *ZooKeys* 2009;**18**:91–128. https://doi.org/10.3897/zookeys.18.103

Luo A, Ling C, Ho SY *et al.* Comparison of methods for molecular species' delimitation across a range of speciation scenarios. *Systematic Biology* 2018;**67**:830–46.

Mace GM, Collar NJ, Gaston KJ *et al.* Quantification of extinction risk: IUCN's system for classifying threatened species. *Conservation Biology* 2008;**22**:1424–42. https://doi.org/10.1111/j.1523-1739.2008.01044.x

Mahon AR, Arango CP, Halanych KM. Genetic diversity of *Nymphon* (Arthropoda: Pycnogonida: Nymphonidae) along the Antarctic Peninsula with a focus on *Nymphon australe* Hodgson 1902. *Marine Biology* 2008;**155**:315–23. https://doi.org/10.1007/s00227-008-1029-5

Malekmohammad K, Khalaji-Pirbalouty V, Oraei H *et al.* Identifying closely related species of the genus *Gammarus* (Crustacea, Amphipoda) using geometric morphometrics. *Iranian Journal of Animal Biosystematics* 2021;**17**:137–46.

Marchiori AB, Bartholomei-Santos ML, Santos S. Intraspecific variation in *Aegla longirostri* (Crustacea: Decapoda: Anomura) revealed by geometric morphometrics: evidence for ongoing speciation? *Biological Journal of the Linnean Society* 2014;**112**:31–9. https://doi.org/10.1111/bij.12256

Maroni PJ, Baker BJ, Moran AL *et al.* One Antarctic slug to confuse them all: the underestimated diversity of *Doris kerguelenensis*. *Invertebrate Systematics* 2022;**36**:419–35. https://doi.org/10.1071/is21073

McLaughlin PA. *Comparative Morphology of Recent Crustacea*. San Francisco: W.H. Freeman, 1980, 1–177.

Michel LN, Danis B, Dubois P *et al.* Increased sea ice cover alters food web structure in East Antarctica. *Scientific Reports* 2019;**9**:8062. https://doi.org/10.1038/s41598-019-44605-5

Michel LN, Nyssen FL, Dauby P *et al.* Can mandible morphology help predict feeding habits in Antarctic amphipods? *Antarctic Science* 2020;**32**:496–507. https://doi.org/10.1017/s0954102020000395

Miller MA, Pfeiffer W, Schwartz T. Creating the CIPRES Science Gateway for inference of large phylogenetic trees. In: *2010 Gateway Computing Environments Workshop (GCE)*. IEEE, 2010, 1–8.

Misof B, Misof K. A Monte Carlo approach successfully identifies randomness in multiple sequence alignments: a more objective means of data exclusion. *Systematic Biology* 2009;**58**:21–34. https://doi.org/10.1093/sysbio/syp006

Monaghan MT, Wild R, Elliot M *et al.* Accelerated species inventory on Madagascar using coalescent-based models of species delineation. *Systematic Biology* 2009;**58**:298–311. https://doi.org/10.1093/sysbio/syp027

Moore PG, Wong YM. Observations on the life history of *Orchomene nanus* (Krøyer) (Amphipoda: Lysianassoidea) at Millport, Scotland as deduced from baited trapping. *Journal of Experimental Marine Biology and Ecology* 1996;**195**:53–70. https://doi.org/10.1016/0022-0981(95)00094-1

Mutanen M, Pretorius E. Subjective visual evaluation vs. traditional and geometric morphometrics in species' delimitation: a comparison of moth genitalia. *Systematic Entomology* 2007;**32**:371–86. https://doi.org/10.1111/j.1365-3113.2006.00372.x

Nicholls E. The Amphipoda Gammaridea. Australasian Antarctic Expedition 1911–14. *Scientific Reports. Series C. Zoology and Botany* 1938;**2**:1–145.

Nyssen F, Brey T, Lepoint G *et al*. A stable isotope approach to the eastern Weddell Sea trophic web: focus on benthic amphipods. *Polar Biology* 2002;**25**:280–7. https://doi.org/10.1007/s00300-001-0340-0

Nyssen F, Brey T, Dauby P *et al*. Trophic position of Antarctic amphipods—enhanced analysis by a 2-dimensional biomarker assay. *Marine Ecology Progress Series* 2005;**300**:135–45. https://doi.org/10.3354/meps300135

Otto JC, Wilson KJ. Assessment of the usefulness of ribosomal 18S and mitochondrial COI sequences in Prostigmata phylogeny. In: *Acarology: Proceedings of the 10th International Congress*. Melbourne: CSIRO Publishing, 2001.

Padial JM, Miralles A, De la Riva I *et al*. The integrative future of taxonomy. *Frontiers in Zoology* 2010;**7**:16–4. https://doi.org/10.1186/1742-9994-7-16

Paradis E, Claude J, Strimmer K. APE: analyses of phylogenetics and evolution in R language. *Bioinformatics* 2004;**20**:289–90. https://doi.org/10.1093/bioinformatics/btg412

Parzen E. Extraction and detection problems and reproducing kernel Hilbert spaces. *Journal of the Society for Industrial and Applied Mathematics, Series A: Control* 1962;**1**:35–62. https://doi.org/10.1137/0301004

Peck LS. Antarctic marine biodiversity: adaptations, environments and responses to change. *Oceanography and Marine Biology: An Annual Review* 2018;**56**:2–133.

Pilar Cabezas M, Cabezas P, Machordom A *et al*. Hidden diversity and cryptic speciation refute cosmopolitan distribution in *Caprella penantis* (Crustacea: Amphipoda: Caprellidae). *Journal of Zoological Systematics and Evolutionary Research* 2013;**51**:85–99. https://doi.org/10.1111/jzs.12010

Pollard D, DeConto RM. Modelling West Antarctic ice sheet growth and collapse through the past five million years. *Nature* 2009;**458**:329–32. https://doi.org/10.1038/nature07809

Pons J, Barraclough TG, Gomez-Zurita J *et al*. Sequence-based species' delimitation for the DNA taxonomy of undescribed insects. *Systematic Biology* 2006;**55**:595–609. https://doi.org/10.1080/10635150600852011

Post E, Bhatt US, Bitz CM *et al*. Ecological consequences of sea-ice decline. *Science* 2013;**341**:519–24. https://doi.org/10.1126/science.1235225

Powles H, Bradford MJ, Bradford RG *et al*. Assessing and protecting endangered marine species. *ICES Journal of Marine Science* 2000;**57**:669–76.

Puillandre N, Lambert A, Brouillet S *et al*. ABGD, Automatic Barcode Gap Discovery for primary species' delimitation. *Molecular Ecology* 2012;**21**:1864–77. https://doi.org/10.1111/j.1365-294X.2011.05239.x

Raguá-Gil JM, Gutt J, Clarke A *et al*. Antarctic shallow-water megaepibenthos: shaped by circumpolar dispersion or local conditions? *Marine Biology* 2004;**144**:829–39.

Rambaut A, Drummond AJ, Xie D *et al*. Posterior summarization in Bayesian phylogenetics using Tracer 1.7. *Systematic Biology* 2018;**67**:901–4. https://doi.org/10.1093/sysbio/syy032

Rannala B, Yang Z. *Species Delimitation*. Self published, 2020.

Rathke H. Beiträge zur Fauna Norwegens. *Nova Acta Academiae Caesareae Leopoldino-Carolinae Naturae Curiosorum, Breslau & Bonn* 1843;**20**:1–264.

Raupach MJ, Malyutina M, Brandt A *et al*. Molecular data reveal a highly diverse species flock within the munnopsoid deep-sea isopod *Betamorpha fusiformis* (Barnard, 1920) (Crustacea: Isopoda: Asellota) in the Southern Ocean. *Deep Sea Research Part II: Topical Studies in Oceanography* 2007;**54**:1820–30. https://doi.org/10.1016/j.dsr2.2007.07.009

Riddle MJ, Craven M, Goldsworthy PM *et al*. A diverse benthic assemblage 100 km from open water under the Amery Ice Shelf, Antarctica. *Paleoceanography* 2007;**22**:PA204.

Riedlecker EI, Ashton GV, Ruiz GM. Geometric morphometric analysis discriminates native and non-native species of Caprellidae in western North America. *Journal of the Marine Biological Association of the United Kingdom* 2009;**89**:535–42. https://doi.org/10.1017/s0025315408002452

Rogers AD. Evolution and biodiversity of Antarctic organisms: a molecular perspective. *Philosophical Transactions of the Royal Society of London, Series B: Biological Sciences* 2007;**362**:2191–214. https://doi.org/10.1098/rstb.2006.1948

Rohlf FJ, Slice D. Extensions of the Procrustes method for the optimal superimposition of landmarks. *Systematic Zoology* 1990;**39**:40–59. https://doi.org/10.2307/2992207

Ronquist F, Huelsenbeck JP. MrBayes 3: Bayesian phylogenetic inference under mixed models. *Bioinformatics* 2003;**19**:1572–4. https://doi.org/10.1093/bioinformatics/btg180

Ruane S. Using geometric morphometrics for integrative taxonomy: an examination of head shapes of milksnakes (genus *Lampropeltis*). *Zoological Journal of the Linnean Society* 2015;**174**:394–413. https://doi.org/10.1111/zoj.12245

Ruiz MB, Taverna A, Servetto N *et al*. Hidden diversity in Antarctica: molecular and morphological evidence of two different species within one of the most conspicuous ascidian species. *Ecology and Evolution* 2020;**10**:8127–43. https://doi.org/10.1002/ece3.6504

Sáez AG, Lozano E. Body doubles. *Nature* 2005;**433**:111. https://doi.org/10.1038/433111a

Saucède T, Eléaume M, Jossart Q *et al*. Taxonomy 2.0: computer-aided identification tools to assist Antarctic biologists in the field and in the laboratory. *Antarctic Science* 2021;**33**:39–51. https://doi.org/10.1017/s0954102020000462

Schellenberg A. Die Gammariden der deutschen Südpolar-Expedition 1901–1903. *Deutsche Sudpolar-Expedition 1901-1903* 1926;**18**:235–414.

Schlager S. Morpho and Rvcg—shape analysis in R: R-packages for geometric morphometrics, shape analysis and surface manipulations. In: Zheng G, Li S, Székely G (eds), *Statistical Shape and Deformation Analysis*. Amsterdam: Elsevier, 2017, 217–56.

Schlick-Steiner BC, Steiner FM, Seifert B *et al*. Integrative taxonomy: a multisource approach to exploring biodiversity. *Annual Review of Entomology* 2010;**55**:421–38. https://doi.org/10.1146/annurev-ento-112408-085432

Sheather SJ, Jones MC. A reliable data-based bandwidth selection method for kernel density estimation. *Journal of the Royal Statistical Society: Series B (Methodological)* 1991;**53**:683–90.

Tamura K, Stecher G, Peterson D *et al*. MEGA6: molecular evolutionary genetics analysis version 6.0. *Molecular Biology and Evolution* 2013;**30**:2725–9. https://doi.org/10.1093/molbev/mst197

Thatje S. Effects of capability for dispersal on the evolution of diversity in Antarctic benthos. *Integrative and Comparative Biology* 2012;**52**:470–82. https://doi.org/10.1093/icb/ics105

Thatje S, Hillenbrand CD, Larter R. On the origin of Antarctic marine benthic community structure. *Trends in Ecology & Evolution* 2005;**20**:534–40. https://doi.org/10.1016/j.tree.2005.07.010

Thornhill DJ, Mahon AR, Norenburg JL *et al*. Open-ocean barriers to dispersal: a test case with the Antarctic Polar Front and the ribbon worm *Parborlasia corrugatus* (Nemertea: Lineidae). *Molecular Ecology* 2008;**17**:5104–17. https://doi.org/10.1111/j.1365-294X.2008.03970.x

Trathan PN, Agnew D. Climate change and the Antarctic marine ecosystem: an essay on management implications. *Antarctic Science* 2010;**22**:387–98. https://doi.org/10.1017/s0954102010000222

Turner J, Bindschadler R, Convey P, *et al*. *Antarctic Climate Change and the Environment*. Cambridge, UK: Scientific Committee on Antarctic Research Scott Polar Research Institute, 2009.

d'Udekem d'Acoz C, Verheye ML. *Epimeria* of the Southern Ocean with notes on their relatives (Crustacea, Amphipoda, Eusiroidea). *European Journal of Taxonomy* 2017;**359**:1–553.

d'Udekem d'Acoz C, Schön I, Robert H. The genus *Charcotia* Chevreux, 1906 in the Southern Ocean, with the description of a new species

(Crustacea, Amphipoda, Lysianassoidea). *Belgian Journal of Zoology* 2018;**148**:31–82.

Vaidya G, Lohman DJ, Meier R. SequenceMatrix: concatenation software for the fast assembly of multi-gene datasets with character set and codon information. *Cladistics* 2011;**27**:171–80. https://doi.org/10.1111/j.1096-0031.2010.00329.x

Verheye ML, Backeljau T, d'Udekem d'Acoz C. Looking beneath the tip of the iceberg: diversification of the genus *Epimeria* on the Antarctic shelf (Crustacea, Amphipoda). *Polar Biology* 2016;**39**:925–45. https://doi.org/10.1007/s00300-016-1910-5

Verheye ML, D'Udekem D'Acoz C. Integrative taxonomy of giant crested *Eusirus* in the Southern Ocean, including the description of a new species (Crustacea: Amphipoda: Eusiridae). *Zoological Journal of the Linnean Society* 2021;**193**:31–77.

Walker AO. Preliminary descriptions of new species of Amphipoda from the 'Discovery' Antarctic Expedition, 1902–1904. *Annals and Magazine of Natural History, (Ser. 7)* 1906;**17**:452–8.

Walker AO. Crustacea. III. Amphipoda. *National Antartic Expedition 1901–1904. Natural History* 1907;**3**:1–39.

Watanabe A. How many landmarks are enough to characterize shape and size variation? *PLoS One* 2018;**13**:e0198341. https://doi.org/10.1371/journal.pone.0198341

Watling L. Functional morphology of the amphipod mandible. *Journal of Natural History* 1993;**27**:837–49. https://doi.org/10.1080/00222939300770511

Watling L, Holman H. Additional acanthonotozomatid, paramphitoid, and stegocephalid Amphipoda from the Southern Ocean. *Proceedings of the Biological Society of Washington* 1981;**94**:181–227.

Watling L, Thurston MH. Antarctica as an evolutionary incubator: evidence from the cladistic biogeography of the amphipod family Iphimediidae. *Geological Society, London, Special Publications* 1989;**47**:297–313. https://doi.org/10.1144/gsl.sp.1989.047.01.22

Wiens JJ. What is speciation and how should we study it? *The American Naturalist* 2004;**163**:914–23. https://doi.org/10.1086/386552

Wiens JJ. Species' delimitation: new approaches for discovering diversity. *Systematic Biology* 2007;**56**:875–8. https://doi.org/10.1080/10635150701748506

Zapata F, Jiménez I. Species' delimitation: inferring gaps in morphology across geography. *Systematic Biology* 2012;**61**:179–94. https://doi.org/10.1093/sysbio/syr084

Zhang J, Kapli P, Pavlidis P *et al.* A general species' delimitation method with applications to phylogenetic placements. *Bioinformatics*2013;**29**:2869–76.https://doi.org/10.1093/bioinformatics/btt499

Zwickl DJ. Genetic algorithm approaches for the phylogenetic analysis of large biological sequence datasets under the maximum likelihood criterion. D.Phil. Thesis, The University of Texas, 2006.

Witt JDS, Threloff DL, Hebert PDN. DNA barcoding reveals extraordinary cryptic diversity in an amphipod genus: implications for desert spring conservation. *Molecular Ecology* 2006;**15**:3073–3082. doi:https://doi.org/10.1111/j.1365-294X.2006.02999.x

Powell JR. Accounting for uncertainty in species delineation during the analysis of environmental DNA sequence data. *Methods in Ecology and Evolution* 2011;**3**:1–11. doi:https://doi.org/10.1111/j.2041-210X.2011.00122.x

Garcia Sanz M, Constant E, Goussard F *et al.* Imaging methodologies in natural sciences: The AST-RX Platform (Accès Scientifique à la Tomographie à Rayons X) of the Muséum national d'Histoire naturelle. Paris. *UVX 2012* 2013;**01001**:1–7. doi:https://doi.org/10.1051/uvx/201301001

Ren X, Huang L. Studies on Gammaridea and Caprellidea (Crustacea: Amphipoda) from the northwest waters off the Antarctic Peninsula. *Studia Marina Sinica* 1991;**32**:185–323.

Coleman CO. Two new amphipod species (Crustacea) *Iphimediella ruffoi* and *Iphimediella dominici* from the Antarctic Ocean. *Boll. Mus. civ. St. nat. Verona* 1996;**20**:117–133.

Lörz A. First records of Epimeriidae and Iphimediidae (Crustacea, Amphipoda) from Macquarie Ridge, with description of a new species and its juveniles. *Zootaxa* 2012;**3200**:49–60.

Bickford D, Lohman DJ, Sohdi NS *et al.* Cryptic species as a window on diversity and conservation. *Trends in Ecology and Evolution* 2007;**22**:148–155.